Computational simulation of physiological blood flow through arterial stenosis for measuring the effects of stenotic shapes on various flow parameters

KHAIRUZZAMAN MAMUN

Mechanical Engineering Department

Iwate University, Morioka, Japan

15 September, 2020

A thesis

On

Computational simulation of physiological blood flow through arterial stenosis for measuring the effects of stenotic shapes on various flow parameters

By

Khairuzzaman Mamun

Supervisor

Prof. Dr. Ken-ichi Funazaki

The thesis is submitted for the partial fulfillment of the
degree of Doctor of Philosophy in the Department of Mechanical Engineering
Iwate University, Morioka, Japan

15 September, 2020

DEDICATION

This thesis is dedicated to my beloved

Parents

ABSTRACT

The aim of this study is to investigate the flow behavior of physiological blood flow through arterial stenosis for measuring the effects of stenotic Shapes on various physiological parameters. This is to provide a basic understanding of the effects of stenotic shapes. The blood is assumed to be incompressible, homogeneous and Non-Newtonian, while artery is assumed to be a rigid wall but in some part of this study artery is considered to be elastic. Since the blood flow is to be fully developed at inlet region of the arterial tube, so the inlet velocity profile is taken as parabolic and spiral. Moreover, the time-dependent pressure profile has been taken for outlet boundary condition. The physiological velocity profile have been imposed at inlet for unsteady condition. Reynolds number at the inlet has been ranged approximately from 86 to 966 for the investigation. As the heat transfer in the blood flow process is not considered, therefore energy equation is not solved. Pressure based solver, and finite volume method are used for calculations. Due to constriction blood passes through the throat and post stenotic region with high velocity, the flow velocity at post stenotic region increases but pressure of that region decreases. So, moderate and severe arterial stenosis can produce highly disturbed flow regions with turbulent flow characteristics. For this reason Low Reynolds number $k-\omega$ model is used as governing equation. Though, in some parts of this study laminar model has been taken.

Arterial elasticity has become avital predictor of cardiovascular diseases in the past few of years, so numerical simulations have been done for a comparative study of blood flow through elastic stenotic artery with rigid stenotic artery. The wall of the vessels is considered to be rigid as well as elastic. Young's modulus and Poisson's ratio of the elastic wall of the artery are 1.08 MPa and 0.49 respectively. The deformation of the arteries was modeled as two-way fluid–structure interaction (FSI) using the ANSYS package. Comparative results from the arteries of rigid and elastic wall have been presented by graphical representations. Blood velocity, pressure and wall shear stress have been taken as the numerical parameters. Thus, differences between rigid and deformed walls were checked based on Blood velocity, pressure and wall shear stress for different time steps.

In addition, the investigations have been carried out to characterize the flow behavior of blood through carotid arteries. The numerical results have been presented in terms of wall shear stress distributions, streamlines contours and axial velocity contours. However, highest wall shear stress has been observed in the bifurcation area. Unexpectedly, transient or unstable flow has created flow disturbance regions in the arteries. Moreover, the disturbance of flow has risen as the severity of stenosis in the artery has been increased.

For a statistical analysis to investigate the effect of stenotic shapes and spiral flows on wall shear stress in the stenotic arteries, 120 simulations have been performed for getting the statistical data from the numerical results. Actually, the numerical results of wall shear stress have been taken for the statistical analysis. The simulations and the statistical analysis have been performed by using ANSYS - 18.1 and SPSS respectively. The cases for WSS_{max}, WSS_{min}, WSS_{ave}, $Pressure_{max}$, $Pressure_{drop}$, $Velocity_{max}$ and $Velocity_{ave}$ are statistically significant as p-value are less than 0.05. Besides, 73.4%, 55.6%, 63.6%, 61.4%, 66%, 82.1% and 78.7% of the variation of the WSS_{max}, WSS_{min}, WSS_{ave}, $Pressure_{max}$, $Pressure_{drop}$, $Velocity_{max}$ and $Velocity_{ave}$ respectively can be explained by the stenotic severity, eccentricity, and length and flow spirality. However, $Velocity_{min}$, can't be explained by the stenotic severity, eccentricity, length and flow spirality because the p-value of $Velocity_{min}$ is greater than 0.05. The severity is the most influencing factor for WSS_{max}, but flow spirality has no influence on the WSS_{max}. Thus, the WSS_{max} has been influenced by the stenotic severity, eccentricity and length, whereas the WSS_{min} has been influenced by the stenotic severity and flow spirality. The stenotic length has an influence on the WSS_{max}, $Pressure_{max}$, $Velocity_{max}$ and $Velocity_{ave}$ whereas the stenotic severity has an influence on all of the dependent variables. The $Pressure_{max}$, $Velocity_{max}$ and $Velocity_{ave}$ have been influenced by the stenotic severity and length, so, stenotic eccentricity and flow spirality have no

influence on them. The $Pressure_{drop}$ has been influenced only by the stenotic severity. However, the stenotic shape and flow spirality haven't any influence on the $Velocity_{min}$.

In short, the stenotic severity and length are very important influential factors for the shape of the arterial stenosis because of having the impacts on physiological parameters. On the other hand, stenotic eccentricity is not a very important influential factor for the shape of the arterial stenosis. Moreover, flow spirality is not at all an influencing factor for flow parameters as it has only an impact on the WSS_{min}.

AUTHOR'S DECLARATION

I, Khairuzzaman Mamun, student of Iwate University, Iwate, Japan declare that the research work carried out within this study for the Doctor of Philosophy degree is entirely developed by me. To the best of my knowledge and belief, no other work or material by other people or parties have been used without due reference within the text. Moreover, it has not been submitted to elsewhere for the award of any degree or diploma in home or aboard.

Khairuzzaman Mamun

Department of Mechanical Engineering,
Iwate University, Morioka, Iwate, Japan

CERTIFICATE

It is my pleasure to certify that the Ph.D. thesis entitled "Computational simulation of physiological blood flow through arterial stenosis for measuring the effects of stenotic shapes on various flow parameters" submitted by Khairuzzaman Mamun in partial fulfillment of the requirement for the degree of Doctor of Philosophy in Mechanical Engineering, Iwate University, Morioka, Iwate, Japan has been completed under my supervision. This research work is a novel one and it has not been submitted elsewhere for any kind of degree.

I wish him a bright future and every success in life.

Professor Dr. Funazaki ken-ichi

Department of Mechanical Engineering
Iwate University, Morioka, Iwate, Japan

ACKNOWLEDGEMENT

From the core of my heart I would like to convey my earnest admiration, loyalty and reverence to the almighty Allah, the most merciful, for keeping everything in order and enabling me to complete this thesis successfully.

First let me express my profound gratitude to my research supervisor, **Prof. Dr. Funazaki ken-ichi**, for his guidance and inspiration. It would be impossible for me to finish this research without his patience, enthusiasm, motivation, and direction. It has also been a pleasure to have worked with him. His support, supervision and assistance are always greatly appreciated.

I am grateful to Prof. Dr. Most. Nasrin for providing me encouragement and mental support during my research work.

I express my gratitude to all of my other teachers for their kind help and valuable suggestion. I am also thankful to Iwate University, Morioka, Iwate, Japan and generally thank to the office staff for their collaboration.

Finally, I stretch out my heartiest love to my beloved mother, father, wife, sister and brother during the progress of the thesis paper for their direct and indirect co-operation without which this study would be impossible.

CONTENTS

LIST OF FIGURE

LIST OF TABLE

VOCABULARY

Symbol	Meaning
LDL	Lower Density Lipoprotein
HDL	Higher Density Lipoprotein
MRI	Magnetic Resonance Imaging
CT	Computed Tomography
CFD	Computational Fluid Dynamics
3D	Three Dimensional
RBC	Red Blood Cell
WBC	White Blood Cell
ASVD	Arteriosclerotic Vascular Disease
CE	Cholesteryl Ester
CMV	Cytomegalovirus
PDE	Partial Differential Equation
FDM	Finite Difference Method
FVM	Finite Volume Method
FEM	Finite Element Method
UDF	User Defined Function
EFD	Experimental Fluid Dynamics
EI	Eccentricity Index

NOMENCLATURE

Symbol	Meaning
D	Diameter of the healthy artery
r	Radial location of the flow field
R	Radius of the healthy artery
L	Length of the Artery
t	Instant of time
T	Time period of the inlet flow cycle
g	Acceleration due to gravity
u	Instantaneous velocity
U	Average velocity
x	Axial location of the flow field
Re	Reynolds number
τ	Shearing stress
ρ	Density of the fluid
μ	Viscosity of the fluid
μ_0	Blood viscosity for zero shear rates
μ_∞	Blood viscosity for high shear rates
ν	Kinematic viscosity of the fluid
$\emptyset$	The shear strain angle
γ	Shear rate
γ_c	reference shear rate
$\dot{\gamma}$	instantaneous shear rate
k	Turbulent kinetic energy
f	Frequency of the cardiac cycle
ε	Dissipation of turbulent kinetic energy
ω	Specific dissipation rate
c	Intensity of the flow Spirality
WSS	Wall Shear Stress
WSS_{max}	Maximum Wall Shear Stress
WSS_{min}	Minimum Wall Shear Stress
WSS_{ave}	Average Wall Shear Stress
$Pressure_{max}$	Maximum Pressure
$Pressure_{drop}$	Pressure Drop
$Velocity_{max}$	Maximum Velocity
$Velocity_{min}$	Minimum Velocity
$Velocity_{ave}$	Average Velocity

Chapter 1

Introduction

1.1 Introduction

The physiology of the cardiovascular system was studied step by step through many years. The role of the blood vessels has already been identified, when it was realized that the arteries and veins have different roles. Arteries carry blood with oxygen red blood cells, oxygen, white blood cells, nutrients, and other vital substances that the body requires from heart out to body. On the other hand, veins carry blood with carbon dioxide and various devoid of substance from body to heart. Arteries are strong, flexible blood vessels that are able to expand and contract. They expand as heart beats, and contract between heartbeats. In other word, arteries are strong and flexible blood vessels that can expand and contract with heartbeats. Veins are less flexible than arteries. Arteries contain endothelium, a thin layer of cells that keeps the artery smooth and allows blood to flow easily. Atherosclerosis starts when the endothelium becomes damaged, allowing Lower Density Lipoprotein (LDL) cholesterol to accumulate in the artery wall. The body sends macrophage white blood cells to clean up the cholesterol, but sometimes the cells get stuck there at the affected site. Over time this results in plaque being built up, consisting of bad cholesterol (LDL cholesterol) and macrophage white blood

cells. This can cause severe diseases such as the development of atherosclerosis. Atherosclerosis, which means the hardening of arteries, is caused by a plaque over the artery walls. In a natural manner, arteries are normally smooth to allow for easy transportation of red blood cells, oxygen, white blood cells, nutrients, and other vital substances that the body requires, but cholesterols have been found to promote the formation of plaque on artery walls and over time it affects the blood flow path. However, the plaque hardens of the arterial walls, which loses its flexibility as well as tends to cause a narrowing of the arterial passage. As a result the arterial wall loses its elastic property which limits the area of blood flow. This narrowing of the artery is called arterial stenosis.

1.2 Backgrounds and literature review

Recently there has been a significant amount of research done on blockage arteries which are caused by atherosclerosis or stenosis because, a stenosed artery is now very significant topic to the biomedical researcher for focusing of numerous research efforts. The cardiovascular system actually maintains blood flow to all cells such as the artery, capillary and vain in the body. Thus, cardiovascular diseases are the types of disease that involve heart or blood vessels. Stenosis is one of the most devastating cardiovascular diseases which are formed by depositing

fatty substances on the wall of the blood vessels because, it may lead to total vessel blockage in some instances and therefore poses a serious medical problem.

Now a days research on carotid arteries are also increasing because it is a very important artery in the body which are located on both side of the neck, the blood vessels that carry oxygenated blood to the head, brain and face. Actually, they supply essential oxygenated blood to the large front part of the brain which controls thought, speech, personality as well as our sensory (our ability to feel) and motor (our ability to move) functions. Besides, the brain survives on a continuous supply of oxygen and glucose carried by blood through it. Thus, Carotid artery disease such as stenosis in the carotid artery can cause cerebral disturbance.

The initial research conducted on the physics of atherosclerosis incorporated mostly experimental techniques into visualizing the flow. Many of these experiments provided important information. Thus, numerous experiments have been conducted focusing on the clinical aspects of the disease of the arteries to study the geometry and fluid effects on the condition as well as to understand the physics involved with the disease itself, including the cause and possible methods of treating it. Although, these studies have provided valuable data, there are limitations with these experimental techniques that need to be investigated further using other methods.

Further insights into flow recirculation and flow separation had been generated through other visualization techniques such as dye tracing. However, it was not feasible to probe the entire flow region. The recent use of laser Doppler anemometry has allowed for more accurate acquisition of flow velocities and has provided very useful visualizations of the flow behavior. Some flow characteristics, such as the wall shear stress, can be provided poor results near the wall region even by the more advanced experimental methods. On the other hand, computational methods have shown a strong capability in modeling flow behavior and can provide good results near the wall region, which can be specified according to realistic conditions. As a result, computer simulations have been, recently, seen as an excellent method of studying flow within stenosed vessels. Computational simulations have the benefit of being economical in comparison to experimental methods. These simulations can provide virtually any information such as flow velocities, pressures, wall shear stresses that may be beneficial to medical practitioners. Blood flow velocity determines the amount of blood passing through the artery to supply necessary nutrients. Variations in artery's geometry can adversely affect the flow path and cause regions to receive less nutrients or life-sustaining materials. Conversely, it can also increase the accumulation of harmful materials. Therefore, it is important to study blood flow velocities to understand the flow behavior. Pressure within the artery determines the resistance

against the flow in the artery. A large pressure drop across the artery promotes forward flow. Wall shear stresses on vessel walls have been difficult to acquire precise and numerous measurements experimentally but have a strong link with the formation of arterial stenosis. Therefore, it is preferable to acquire precise results from computational simulations. It is clear that computer-aided simulations are more preferable for analyzing the behavior of blood in arteries. They can provide a complete and accurate visualization of the fluid and solid behavior. This can be easily interpreted and benchmarked with the available experimental results.

1.3 Early Studies of Blood Flow within Stenosed Arteries

Studies of stenosis can be helpful to understand the biomechanics of vascular diseases. In general, the blood flow does not face any obstacles on the way and the flow is regular and smooth. However, sometimes due to presence of cholesterol, calcium and other substance in blood, a fatty substance called plaque develops near the inner wall of the artery. As the time passes this plaque grows resulting in hardening the arterial wall and narrowing the blood vessels. This can cause severe diseases such as the development of atherosclerosis. As a result the arterial wall loses its elastic property which limits the area of blood flow. Therefore, the flow turns to be abnormal in the reduced cross sectional area of the artery stated by Khader and Shenoy [1]. One of the studies in this area suggested

that pulsatile blood flow through arterial vessel implicate in several types of hemodynamic forces which can impact in vessel wall structure. These forces are also the cause of development of vascular pathologies and important factors in atherosclerosis. The regions of high shear stress, which implicates in a direct mechanical harm of the vessel wall, are regions where atherosclerosis occurs. Therefore, the vessel with steady blood flow and low shear stress becomes comparatively disease free that was investigated by Li et al. [2].

At present, there is no standard procedure to measure the physical severity of the stenosis. Doctors often judge the severity based on a patient's physical symptoms as well as growth rate, constriction size and pressure drop often at high risk to patient's lives as stated by Chua, and Shread [3]. But the results of numerical simulation can be better than MRI, CT and Ultrasound techniques in analyzing the severity of stenosis. Further the comparison of stenosed flow behavior with the normal one can provide the proper understanding of underlying mechanism behind the development of atherosclerosis. The flow behavior in the stenosed artery is quite different in comparison to the normal one. Stress and resistance to flow are much higher in stenosed artery than one in the normal artery. Chua and Shread [3] proved that the flow through the constricted tube is characterized by high velocity jet generated in constricted region. Khader and Shenoy [1] found the results from numerical simulation which demonstrated that

velocity and stenotic jet length increases during increasing the severity of stenosis. Their results also demonstrated that the 3D stenotic CFD model is capable to predict the changes in flow behavior for increased severity of stenosis. Young et al. [4] also studied the wall shear stress and pressure gradient in the stenosis and evaluated the cause of plaque rupture. The authors founded pulsatile blood flow through the stenosis with elastic wall to observe the lumen movement. According to their study the peak WSS occurred just before minimum lumen position. Pinto et al. [5] conducted numerical simulation assuming a physiological pulsatile flow through different models of stenosis. In case of subject-specific anatomically realistic stenosed carotid bifurcation subjected to pulsatile inlet condition, the simulation results demonstrated the rapid fluctuation of velocity and pressure in post-stenotic region by S. Lee and S. Lee [6]. Ahmed and Giddens [7] studied both steady and pulsatile flow through 25%, 50% and 75% constriction of a rigid tube where Reynolds number ranged from 500 to 2000. Lorenzini and Casalena [8] did another study, the stenosis having different geometric profiles like trapezium; semi-ellipse and triangle were analyzed considering the Non-Newtonian behavior. The authors investigated that the length of flow disturbance is due to stenotic shape and height, downstream disturbance is due to stenotic walls and peak velocity depends on the shape and height of stenosis.

There are some locations in the artery where blood flow has low Reynolds number or shear rate. However, it has been described that Newtonian behaviour to blood flow is only valid when shear rates is greater than 100s-1, which tends to occur only in larger arteries, according to Pedley [9]. Besides, if the shear rate is high, the blood behaves like a Newtonian fluid whose viscosity be 0.00345Pa.s, according to Berger and Jou [10]. However, if the shear rate of blood flow falls down, the blood flow exhibits Non-Newtonian property. In addition, blood exhibits remarkable Non-Newtonian properties in some diseased condition like severe myocardial infarction, cerebrovascular diseases and hypertension, described by Chien [11]. Thus, non-Newtonian blood models would provide a more accurate representation of blood flow behaviour within the arteries. However, in some diseased conditions, blood flow is Non-Newtonian regardless. Studies had documented three types of Non-Newtonian blood properties: thixotropy, viscoelasticity and shear thinning. Thixotropy is a transient property of blood, which is exhibited at low shear rates and has a fairly long time scale. Mandal [12] suggested that this indicates a secondary importance in physiological blood flow. Mandal further explained, based on the research by Thurston [13, 14], that blood contains a number of particles and cells suspended within the flow that interact with each other significantly as to complicate two-phase modeling. Blood therefore exhibits significant viscoelastic properties, which is also a transient condition at the

frequency range of common physiological condition. This has attracted significant research interest trying to determine useful mechanical properties to be employed in analytical calculations and simulations. Mandal [12], noted that the viscoelastic property of blood diminishes vary rapidly as shear rate rises. At physiological hematocrit values, which is the volume fraction of red blood cells in whole blood, this effect is not significant, suggesting that this Non-Newtonian behavior is of secondary importance for normal pulsatile blood flow. This leaves shear thinning, which is a property of blood that is not transient in nature and therefore exhibited in normal blood flow at all shear rates up to 100s-1, whereby flow becomes Newtonian in nature. Mandal [12] therefore concluded that shear thinning is the dominant characteristic of blood. Studies had therefore attempted to fit experimentally measured blood flow behavior to shear thinning equations with modifications to take into account the hematocrit values in Cho and Kensey [15]; Walawender et al [16]; Cokelet et al [17]; Powell and Eyring [18]. A common property of these shear thinning equations was that the effective viscosity of the blood drops in regions of high shear rates and vice versa. From these studies several models were derived and validated against experimentally derived blood flow properties.

Johnston et al [19] studied the application of different Non-Newtonian models onto a steady flow, and later a transient flow, by Johnston et al [20], within

an artery model obtained via angiography. These models were the Power Law model, Walburn- Schneck model, Casson model, Carreau model and Generalized Power Law model by Johnston. For instance, the Walburn-Schneck model can be simplified to the Power Law model by Johnston et al [19]. These models have a tendency to predict decreasing viscosity at regions of high strain rate, including regions, which should have Newtonian fluid behavior. Therefore, Cho and Kensey [15] used the Power Law model which has a constant viscosity at strain rate above $226.5s^{-1}$. The Power Law model in itself was a very popular model due to the simplicity of the equation and because it tended to yield significant Non-Newtonian behavior according to Perktold et al [21]. The Carreau model, as used by Cho and Kensey [15] and Johnston et al [19] had been seen to provide close approximations to experimental blood flow conditions. Gijsen et al. [22] studied the impact of Non-Newtonian properties of blood on the velocity distribution. They made a comparison between the Non- Newtonian fluid model and a Newtonian fluid at different Reynolds numbers. Comparison revealed that the character of flow of the Non-Newtonian fluid was simulated quite well by using the appropriate Reynolds number. As an initial study, Formaggia et al. [23] and Lee and Xu [24] analyzed the blood flow behavior in non-stenotic vessels or a normal artery. A great number of theoretical studies related to blood flow through stenosed arteries have been carried out recently. In most of the studies carried out

so far, the presence of "mild" (or single stenosis) was considered. Chakravarty and Mandal [25], noted that the problem becomes more acute in the presence of an "overlapping" stenosis (two or more stenosis one after the other) in the artery instead of having a "mild" stenosis.

The initial research on blood flow within stenosed arteries concentrated on experimental simulations. Numerous experimental studies have been carried out in animals, stenosis models, and humans by Giddens et al. [26]; Saad and Giddens [27]; and strandness et al. [28]. Clark [29] and Saad and Giddens [27] showed that transitional flow or turbulence can be expected distal to the constriction even with relatively mild stenoses. However, numerical simulation of blood flow can help to obtain detailed flow patterns, such as wall shear stress distributions which are very difficult to obtain experimentally. Thus, numerical modelling of stenotic blood flow has been being popular day by day. However, moderate and severe stenoses may create a highly disturbed flow region in the downstream area of the stenotic artery. These disturbed flows may either remain laminar or may undergo transition to turbulent flow depending upon the flowrate through the stenotic geometry. Besides, turbulence represents an abnormal flow condition, which is related to several vascular disorders such as post-stenotic dilatation described by Cassanova and Giddens [30]. Thus, the development of turbulent flow has important clinical consequences. It may also significantly decrease in pressure and abnormally

increase wall shear stresses in the artery, which may result in haemolysis and the activation of platelets.

Smith [31] conducted extensive studies of steady flows through an axisymmetric stenosed artery using an analytical approach where he described that the resulting flow patterns were highly dependent on geometry of the stenosis and the overall Reynolds number of the flow. Deshpande et al [32] analysed the finite difference scheme to solve the flow through an axisymmetric stenosis under steady flow and arrived at similar conclusions. Besides, Young and Tsai [33] conducted experimental analysis on steady flow through stenosed arteries with varying severity, stenosis length, axisymmetric and asymmetric conditions, and with a range of Reynolds numbers from laminar to turbulent flows. Talukder et al. [34] investigated the effects of double stenoses and the influence of the distance between stenoses on pressure drops in steady and Newtonian flows through the solid artery and found that the pressure drop is linearly related to the number of stenoses. Kumar and awasthi [35] analytically examined the laminar and Newtonian blood flows in a solid artery with multiple stenoses. They also studied the effect of haematocrit percentage on pressure drop and wall shear stress. Stenosis eccentricity is another important key characteristic of stenosis that contributes to the extent of physiological disturbance, according to Falk et al. [36]. Javadzadegan et al., [37, 38] have found the significant roles of stenotic severity

and eccentricity in coronary hemodynamic. Besides, the presence of a helical spiral type blood flow with varying direction of rotation within the aorta has been well confirmed [39-42] and has been shown by several CFD studies to be beneficial for reducing hemodynamic anxiety in human arteries [43-48]. In addition to these computational studies, several experimental investigations have also confirmed the beneficial impacts of aortic spiral flow in the cardiovascular system [49-51].

Wall shear stress (WSS) is the frictional force generated by the blood flow in the blood vessels. It is one of the main hemodynamic forces to influence vascular endothelial cells, which plays avital role in the development and progression of atherosclerotic plaques and arterial aneurysms, according to Barbara et al. [52]. Besides, it works directly on the endothelium as a biological stimulator by controlling the cellular function [53, 54]. However, high wall shear stress in normal arteries is believed to have protective roles to form stenosis, but it enhances platelet activation and subsequent aggregation and even plaque rupture in stenotic arteries [55, 56]. In addition to high WSS, regions of relatively low WSS in normal arteries are also believed to have a higher propensity to form the stenosis [57, 58]. Thus, stenosis can be formed for both in high and low wall shear stress in the arteries.

A new area in fluid mechanics, studying the fluid dynamics of biological fluids in the presence of magnetic fields, is bio-magnetic fluid dynamics. Many

researchers are very interested to investigate the effect of magnetic field on the blood flow. However, bio-magnetic fluid dynamics was developed by Haik et al. [59], the biological fluids are treated as electrically non-conducting magnetic fluids known as ferrofluids. Ferrofluids are used in the medicines, anti-cancer drug carrier, and micro-valve application etc. The investigation of basic bio-magnetic fluid dynamics flow problems attracts the researcher's interest due to the numerous proposed applications in bioengineering and medical sciences. Among them is the development of magnetic devices for cell separation, targeted transport of drugs using magnetic particles as drug carriers, magnetic wound treatment and cancer tumor treatment causing magnetic hyperthermia, reduction of bleeding during surgeries and provocation of occlusion of the feeding vessels of cancer tumors and development of magnetic tracers, according to Voltairas et al. [60]. Chemotherapy application is another important application of these fluids. In the application the drug is placed on the magnetic nanoparticles and is injected near the tumor. The drug is absorbed by the tumor through a high gradient magnetic field, which is concentrated near the tumor center. This approach reduces the side effect of anti-cancer drug. This method has been mostly applied experimentally to small animals. Recently some researchers have reported the application of such method for human therapy where the tumor is near the skin, according to Arnold et al. [61].

The main problem of chemotherapy is not the lack of efficient drugs, but the inability to precisely deliver and concentrate these drugs in affected areas. Neighboring tissues of the tumors are affected due to the failure of separation of targeted areas for an increase of toxic. Magnetic drug delivery is a promising method to accomplish precise targeting. Here, the drug is injected into the bloodstream with a magnetic compound. The targeted areas are surrounded by an external magnetic field that is able to affect the blood stream by reducing its flow rate. In these regions the drug is slowly released. Consequently, relatively small amounts of the drug magnetically targeted to the tumor, which can replace large amounts of the freely circulating drug. At the same time, drug concentrations at the tumor will be significantly higher compared to the ones delivered by systemic delivery methods. However, the particle size and the intensity of the magnetic field are two important factors for delivery of drug to the tumor. For instance, strong magnetic field and large particles size intensity may clog up the blood vessel while a weak magnetic field may not be able to deliver the drug to the tumor.

Very encouraging findings have been recently reported by Alexiou et al. [62] from their experiments with rabbits with artificially initiated limb tumors. It is described that treatments using only 20% of the standard drug amount with an active magnetic targeting showed full recovery of treated limbs. Drug concentration measurements in different organs showed that treatment resulted in

26 time's higher local concentrations in tumor areas, and significant reduction of drug presence in healthy organs such as liver, heart, brain, and kidney. In contrast to that, attempts with the standard (systemic) approach using 50% of normal amount were not successful.

In addition, the magnetic drug targeting is a comprehensive mathematical model for analysis of blood flow when subjected to strong magnetic fields. It can be very useful to understand the effects of a magnetic resonance imaging (MRI) scanner with a magnetic field strength between 1.5 and 4 T on blood behavior. Many patients exposed to 1.5–4 T MRI scanning experienced sensations of nausea, vertigo, metallic taste or sleepiness during the treatments, reported by Schenck et al. [63]. Yamamoto et al. [64] observed in their in vitro experiments that the blood viscosity can be significantly increased even in a 1.5 T MRI scanner.

Sud and Sekhon [65] conducted numerical investigation to study the effects of the interactions between an imposed magnetic field and blood flow through the human arterial system. Their model was based on an analytical expression for the flow rate in multi-branching arterial configuration subjected to a transversal magnetic field. They got results which demonstrate that the rate of blood flow through the system was reduced. Kinouchi et al. [66] included the Lorentz force into the Navier–Stokes equations in their theoretical analysis of the interaction between magnetic field and aortic blood flow. A solution of these extended

Navier–Stokes equations was obtained by the finite element technique for blood flow through aortic vessels in the presence of a magnetic field. The resulting Lorentz force led to a reduction of 5– 10% blood volume flow at high intensities of applied magnetic fields.

Bali and Awasthi [67] studied the effects of the imposed magnetic field on the resistance to blood flow velocities in an idealized stenotic artery. They considered a steady two-dimensional axisymmetric laminar flow of a non-Newtonian fluid subjected to a transversal magnetic field. The Lorentz force was included in the momentum equations. Results were presented for different values of the Hartmann number.

Haik et al. [68] proposed a concept in analogy with the fluid dynamics of Ferro fluids for a model that describes the blood behavior in presence of gradients of an external magnetic field. In contrast to previous studies, the Lorentz force was neglected and a magnetization force was introduced. Khashan and Haik [69] applied the same model in a recent study where numerical simulations of laminar blood flow over a two-dimensional eccentric stenotic orifice subjected to a permanent magnet were performed. Papadopoulos and Tzirtzilakis [70] also applied Haik's model where a blood flow in a curved square duct under the influence of a magnetic field was studied by a finite-difference numerical method. The numerical simulations described that both axial velocity and the secondary

flow at the transversal plane were significantly influenced by a strong magnetic field. Tzirtzilakis [71] presented similar results where a blood flow in a straight rectangular duct under the influence of a uniform and a non-uniform magnetic field was numerically studied. In this model, the magnetization force and the Lorentz force was accounted for too.

An extended bio-magnetic fluid dynamics model, which includes the initial bio-magnetic fluid dynamics model of Haik et al. [68], was developed by Tzirtzilakis [71]. According to this bio-magnetic fluid dynamics model, a bio-fluid is considered as a Newtonian, homogeneous, incompressible and electrically conducting fluid and the flow is considered as laminar. One other difference with the initial model of Haik et al. [68] is that the bio-fluid is not considered isothermal and the temperature distribution is studied in the flow field. According to the bio-magnetic fluid dynamics model of Tzirtzilakis [71] the bio-fluid flow under the influence of a magnetic field is consistent with the principles of Ferro hydrodynamics (FHD) [72] and magneto hydrodynamics (MHD) [73] and the dominant forces in the flow field are those of the magnetization and the Lorentz force [71]. These principles were adopted due to the fact that blood behaves like an electrically conducting fluid which simultaneously exhibits magnetization in strong magnetic fields [71].

Due to the fact that the above mentioned bio-magnetic fluid dynamics models are consistent with the principles of FHD, the flow simulations of bio-magnetic fluid dynamics with a modification of the dimensionless parameters could be applied for a Ferro fluid. In an experimental study of Ferro fluid flow, Ganguly et al. [74] verified the existence of the vortex as a consequence of the application of the magnetic field. One of the most common methodologies for the numerical treatment of incompressible fluid flow problems is the adoption of the stream function–vorticity formulation. Such a treatment was used by Loukopoulos and Tzirtzilakis [75] for the numerical investigation of the steady bio-magnetic fluid dynamics channel flow under the influence of a spatially varying magnetic field. In that study the matrix of the unknowns is diagonally dominant where a finite differences technique was also adopted in order to assure that in the algebraic system arising after discretization. This technique was first presented by Loukopoulos et al. [76].

The role of the form of the magnetic field gradient applied in bio-magnetic fluid dynamics flow problems is an important factor investigated in [71]. For the bio-magnetic fluid dynamics channel flow problem of [76], where a sharp magnetic field gradient is applied, the only dominant force is that of the magnetization [71] and the determinative parameter of the flow field is the arising non-dimensional magnetic number. In some cases the magnetization and

consequently the magnetic number can take very high values. This increment of the magnetization can be achieved either by adding artificially created nanoparticles or by decreasing the Reynolds number. Clearly, the magnetic number expresses the ratio of the magnetization forces to the viscous forces when the Reynolds number is decreased, the magnetic number is increased [71].Thus, the numerical solution is not a trivial task for high magnetic numbers requiring the adoption of robust techniques [76]. The development of a more stable and simpler in the application numerical methodology for bio-magnetic fluid dynamics problems was presented by Tzirtzilakis [77]. This methodology is based on the development of a semi-implicit numerical technique for the estimation of the solution. Moreover, it's a new methodology for the construction of the boundary condition for the vorticity equation on the solid walls [77]. It is believed that experimental study as well as numerical simulations can significantly contribute to further advancements of various applications of bio-magnetic fluid dynamics problems. Thus various studies on bio-magnetic fluid dynamics problems have been reviewed and some important results have been presented in the chapter of recommendation for further studies.

Fluid-structural interaction is a relatively new applied methodology to understand the impact of the flow on structures as well as to learn the interaction between fluid flow and its surrounding. This interaction cannot be neglected in

blood flow, according to Zhao et al [78]. Although it was originally applied to solve aero elasticity problems for aerodynamic research interests, it has increasingly been used in biomechanical simulations, including those involving blood flows through stenosed arteries. It is taken as a vital progress in research on blood flows, since it lead to a better understanding of the structural change of both the blood flow and the arteries. Tang et al [79] performed a FSI analysis on many types of stenosed arteries and provided analysis on wall deformation, stress distribution and flow characteristics. They studied the wall deformation, flow structures and stress distribution and pointed out that the blood vessel is possible to collapse in this part and totally suspense the flow of blood. They have shown that a low pressure exists around the stenosed region. However, due to the thickness of the wall at that location there is sufficient structural stiffness to avoid collapse. The cross-sectional area of the flow in the non-stenosed regions was increased by applying FSI into the simulation, which leads to a decrease of the velocity profile and enlarges the flow recirculation effects, according to Chan et al [80]. More specifically, the wall shear stress (WSS) was reduced by applying FSI simulation and the maximum stress appeared at the shoulder of the constricted part [80]. Oscuii et al. [81] also applied FSI modelling to learn the interaction between the blood flow and the elastic blood vessel. It is found that fluid-structural interaction modelling with pressure boundary conditions supplies an appropriate simulation of

wall circumferential stress and hemodynamic shear stress. The existence of a constricted part in a blood vessel has been assumed to cause a very low pressure of an area especially in a high constricted blood vessel. Besides of this kind of stenotic collapse, the large variations of pressure also lead to an acceleration of the fatigue around the stenosed region, suspected by McCord and Ku [82]. As a consequence, the likelihood of plaque rupture could be enhanced [82]. An extensive study on blood flow through a stenosis vessel with sharp transitions was done by Lee and Xu [24]. The geometry and the results of this study were based on a previous experiment by Ohja et al [83]. They investigated pulsatile flow through a constricted tube of geometry and fluid characteristics similar to that used by Lee and Xu [24]. Actually, they used a linear elastic vessel wall to represent the artery walls and Newtonian fluid to represent the blood. They used commercially available software, which has an iterative method to couple the fluid and structural portions depends on geometric displacements. It is found that the result of their study is similar to the result of the previous experimental results, which validates the techniques used in their study. It is observed from their results that the expansion of the arteries caused by internal pressure, which is responsible for a maximum stress around the shoulders of the constricted zone and slower flow velocity. An interesting note was that the fluid velocity and structural displacements were out of phase with each other, because a time-dependent

sinusoidal flow was used in this study. Tang et al [79] used viscoelastic artery wall instead of using isotropic elastic solids. Moreover, they selected a method of time-varying pressure difference between the inlet and outlet of the artery, which is similar to the diastolic and systolic phases of realistic blood flow, instead of a specified flow rate through the stenosis. They observed similar results of the study of Lee and Xu [24] that high shear stresses and artery expansion near the stenosis throats. Extensive studies on blood flow in a deformable tapered stenotic artery have done by Chakravaty and Mandal [84] to validate the proposed method of coupling wall deformations with fluid flow. After that, Mandal [12] conducted the simulation using the previously established methods with similar conditions while setting the fluid to have a Generalized Power Law non-Newtonian model. The results in terms of fluid characteristics such as fluid velocity, wall shear stress and pressure gradients were excellent. 'Simple pulsatile flows through a smooth stenosis of reasonably small severity using the SIMPLER algorithm' has been studied by Zendehbudi and Moayeri [85]. Besides, 'both numerical and experimental analyses for comparison and validation' has been conducted by Deplano and Siouffi [86]. An Impressive research with FSI model has been conducted by Li and Kleinstreuer [87], where the blood was set to have non-Newtonian properties following the Quemada model. This study gave a three-dimensional view of the critical stresses resulting from different flow pressures.

1.4 Motivation and aims

Recently there have been a significant number of researches done on stenosed arteries. Some studies available at present focus on the clinical aspects of the disease. There has been a great attempt to understand the physics involved with the disease itself, including the cause and possible methods of treating it. Numbers of experimental studies have been done to investigate the geometry and fluid effects on the condition. These studies provided valuable data for further researches. Recently, computational techniques have strong ability to demonstrate the flow behavior within stenosed arteries of varying geometry and conditions that can be specified according to realistic conditions. This method is economical, fast and provides better results which are helpful to understand the cause of disease.

In the present study, we planned to simulate blood flow in carotid arteries with stenosis using the low-Reynolds number k-w turbulence model. The Cross model has been implemented in the simulation to approximate the non-Newtonian flow. Numerical simulation of blood flow offers detailed flow patterns, such as wall shear stress distributions, which are very difficult to obtain experimentally. Thus, wall shear stress distributions, streamlines contours and axial velocity contours have been presented to analyze the flow characteristics.

The above mentioned previous experimental and computational results made the analysis on the Newtonian and Non-Newtonian blood flow through elastic

stenotic artery or rigid body stenotic artery including a detailed observation. Apart from this, an attempt has been made for a comparative study of blood flow through elastic stenotic artery with rigid body stenotic artery in this present studies. Detailed investigation of flow parameters like pressure, Wall Shear stress and velocity distributions have been graphically presented for the comparison between the results getting from the elastic stenotic artery and rigid body stenotic artery.

Although the individual effects of aortic spiral blood flow as well as stenotic severity, stenotic length and stenotic eccentricity on the wall shear stress and on other hemodynamic parameter has been investigated, combinational effects of them are unknown. Therefore, the present study investigates to find out the effects of flow spirality and stenotic shape on the hemodynamic parameters such as velocities, pressure and wall shear stress.

1.5 Problem statement

Numerus studies has been done on arterial stenosis, but no one has done any study on measuring the effects of stenotic shapes using statistical technique. The main purpose of this study is to investigate the effect of arterial stenotic shapes on various flow parameters. Blood flow through carotid artery has been studied for demonstrating the flow behavior to understand the effect of carotid artery on the flow parameters. A statistical analysis has been performed for finding the effects of

stenotic eccentricity, severity and stenotic length on the hemodynamic parameters such as velocities, pressure and wall shear stress.

1.6. Objectives: The main objectives of this study are:

[1] To understand the blood dynamics in carotid arteries.

[2] To analyze the wall shear stress, velocity, streamline and pressure distributions of stenosed carotid arteries of different severities.

[3] To demonstrate the significant changes of flow behaviour through arterial stenosis.

[4] To check the comparison of pressure, velocity and wall shear stress distributions of elastic wall and rigid wall artery for different stenotic severities.

[5] To analyze the effects of stenosis for different stenotic eccentricity, severities, and length.

[6] To investigate the influences of stenotic severities, eccentricity, and length on the hemodynamic parameters such as velocities, pressure and wall shear stress.

1.7. Methodology

Mathematical modeling of blood flows in the arteries is an important and challenging problem. The numerical simulations are performed by well-known software ANSYS Fluent 18.1. A pressure based algorithm is chosen as the solver type. This solver is generally selected for an incompressible fluid. As there is no heat transfer in the blood flow process, energy equation is not solved. In solution methods, the SIMPLE algorithm is selected for pressure-velocity coupling. First Order Upwind scheme is employed as a numerical scheme for discretization of the momentum equation.

The steps of the study are as follows:

[1] All geometries of artery are modeled by using ANSYS design module of Workbench.

[2] Mesh generation are accomplished by using ANSYS mashing of Workbench too.

[3] The governing equations of the blood flow through arterial stenosis are solved by using ANSYS FLUENT 18.1.

[4] Non-Newtonian model (cross model) is performed by using user defined function.

[5] Blood properties and Boundary conditions are programmed by using programming language C++.

[6] Two way FSI system coupling has been used for modeling the artery as elastic.

[7] Statistical data are collected from the results of 120 numerical simulations.

[8] Regression analysis has been done by using popular statistical software SPSS.

[9] The results are shown in contours, graphs and table presentations by utilizing the ANSYS Post processing software.

1.8. Thesis Layout:

Chapter 1 provides motivation, background, methodology, objective and methodology of the thesis.

Chapter 2 describes the arterial stenosis and its related issues.

Chapter 3 describes the Navier- Stokes equations with their derivation and a brief discussion on statistics such as regression analysis and regression models.

Chapter 4 provides the description of geometry, boundary conditions, and validations.

Chapter 5 provides the results and discussions.

Chapter 6 provides the conclusions.

Chapter 7 provides the recommendations for further studies.

Chapter 2

An overview of arterial stenosis and its related issues

Overview

This chapter discusses the blood, heart, blood circulatory system, artery structure, atherosclerosis and stenosis as well as the physical properties of blood flow.

2.1 Blood

Blood is a bodily fluid that delivers necessary substances such as nutrients and oxygen to the cells and transports metabolic waste products away from those same cells. It is composed of blood cells suspended in blood plasma. Plasma, which constitutes 55% of blood fluid, is mostly water (92% by volume), and contains dissipated proteins, glucose, mineral ions, hormones and blood cells themselves. The blood cells are mainly red blood cells (also called RBCs or erythrocytes) and white blood cells, including leukocytes and platelets.

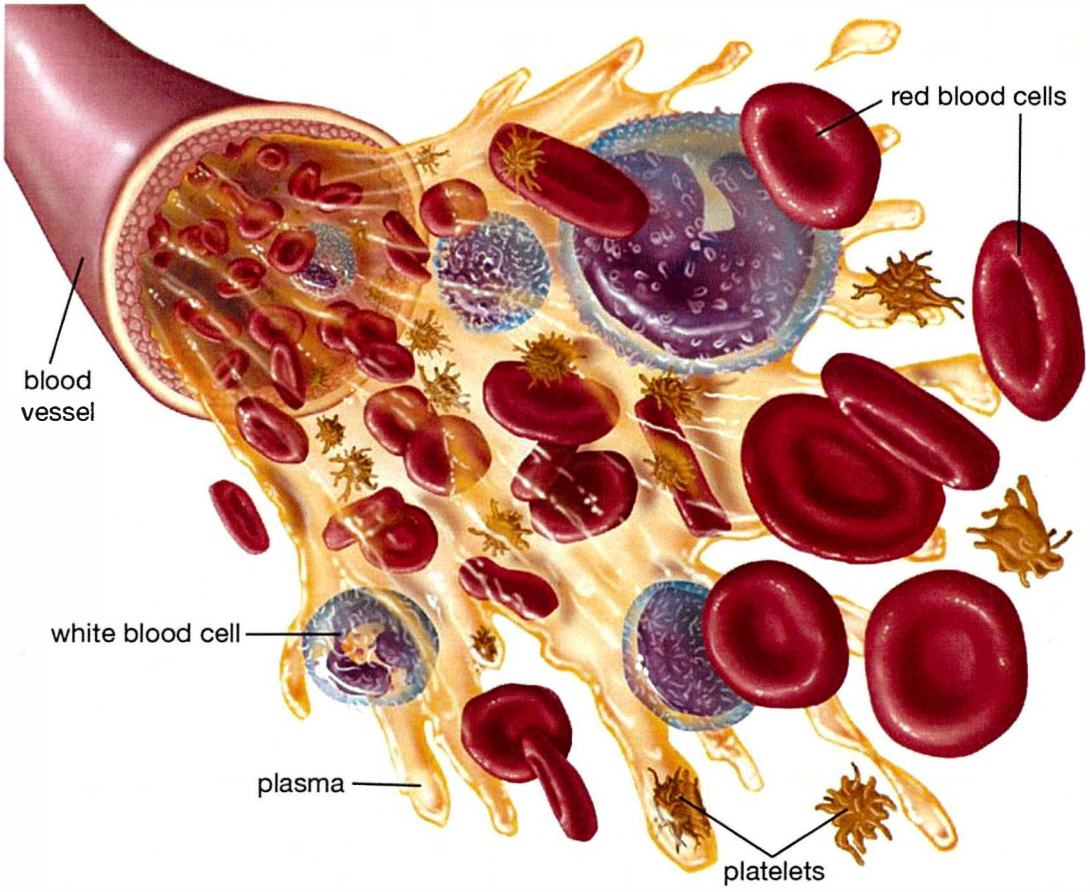

Figure 2.1: Blood into a blood vessel [95].

2.2 Blood flow

The heart functions as a pump and acts as a double pump in the cardiovascular system to provide a continuous circulation of blood throughout the body. This circulation includes the systemic circulation and the pulmonary circulation. Both circuits transport blood but they can also be seen in terms of the gases they carry. The pulmonary circulation collects oxygen from the lungs and

delivers carbon dioxide for exhalation. The systemic circuit transports oxygen to the body and returns relatively deoxygenated blood and carbon dioxide to the pulmonary circuit. Blood flows through the heart in one direction, from the atria to the ventricles, and out through the pulmonary artery into the pulmonary circulation, and the aorta into the systemic circulation.

2.3 Blood vessel

The blood vessels are the part of the circulatory system that transports blood throughout the human body. There are three major types of blood vessels: the arteries, which carry the blood away from the heart; the capillaries, which enable the actual exchange of water and chemicals between the blood and the tissues; and the veins, which carry blood from the capillaries back toward the heart.

Arteries is a blood vessel that takes blood away from the heart to all parts of the body (tissues, lungs, etc.). Most arteries carry oxygenated blood; the two exceptions are the pulmonary and the umbilical arteries, which carry deoxygenated blood to the organs that oxygenate it.

Arteries have a blood pressure higher than other parts of the circulatory system. The pressure in arteries varies during the cardiac cycle. It is highest when the heart contracts and lowest when heart relaxes. The variation in pressure

produces a pulse, which can be felt in different areas of the body, such as the radial pulse. After travelling from the aorta, blood travels through peripheral arteries into smaller arteries called arterioles, and eventually to capillaries. Arterioles help in regulating blood pressure by the variable contraction of the smooth muscle of their walls, and deliver blood to the capillaries. Arterioles have the greatest collective influence on both local blood flow and on overall blood pressure.

The aorta is the root systemic artery, which is the main artery in the body. It receives blood directly from the left ventricle of the heart via the aortic valve. As the aorta branches, and these arteries branch in turn, they become successively smaller in diameter, down to the arterioles. The very first branches off of the aorta are the coronary arteries, which supply blood to the heart muscle itself. These are followed by the branches off the aortic arch, namely the brachiocephalic artery, the left common carotid, and the left subclavian arteries.

The brachiocephalic artery or brachiocephalic trunk or innominate artery is an artery of the mediastinum that supplies blood to the right arm and the head and neck. It is the first branch of the aortic arch, and soon after it emerges, the brachiocephalic artery divides into the right common carotid artery and the right subclavian artery. There is no brachiocephalic artery for the left side of the body. The left common carotid, and the left subclavian artery, come directly off the aortic arch. The left and right common carotid arteries (carotids) are arteries that

supply the head and neck with oxygenated blood; they divide in the neck to form the external and internal carotid arteries. The subclavian arteries are paired major arteries of the upper thorax, below the clavicle. They receive blood from the aortic arch. The left subclavian artery supplies blood to the left arm and the right subclavian artery supplies blood to the right arm, with some branches supplying the head and thorax.

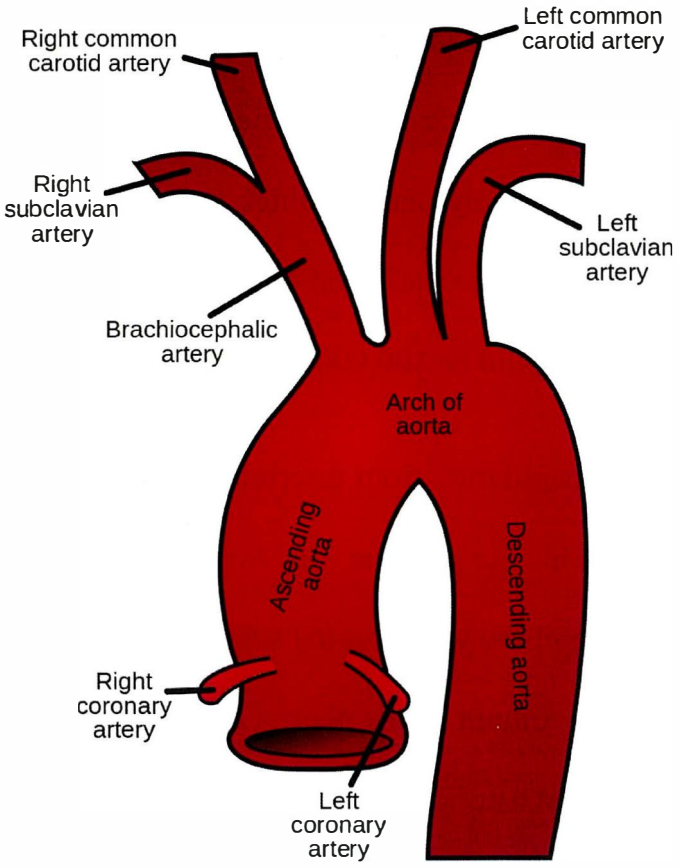

Figure 2.2: Ascending aorta, arch of aorta and descending aorta [96].

Veins have valves which stop the blood from flowing backward. Compared to the arteries, pressure in the veins is very low. The blood is being pushed through the arteries as the heart squeezes the blood out. This is not true for the veins. Blood is pushed through the veins when body muscles contract and squeeze the veins. In this way the blood moves.

2.4 Capillaries

Capillaries are small blood vessels acting as veins and arteries. They surround the body cells at the ends of the arteries and at the beginning of the veins. The walls of capillaries are only one cell thick so substances (Food or cells) can easily get through them and into the blood or out. If all the capillaries of the body were set end to end they would be 100,000 km long!

As blood enters capillaries from arterioles (small arteries), it slows down. This allows substances in the plasma, as well as O2 from red blood cells, to diffuse through the capillary wall into the surrounding tissues (the capillary wall is thin and permeable). Liquid in the plasma also passes out. This forms tissue fluid, bathing the cells. Waste products from the cells, e.g. CO2, diffuse back through the capillary walls into the plasma. Some of the tissue fluid also passes back.

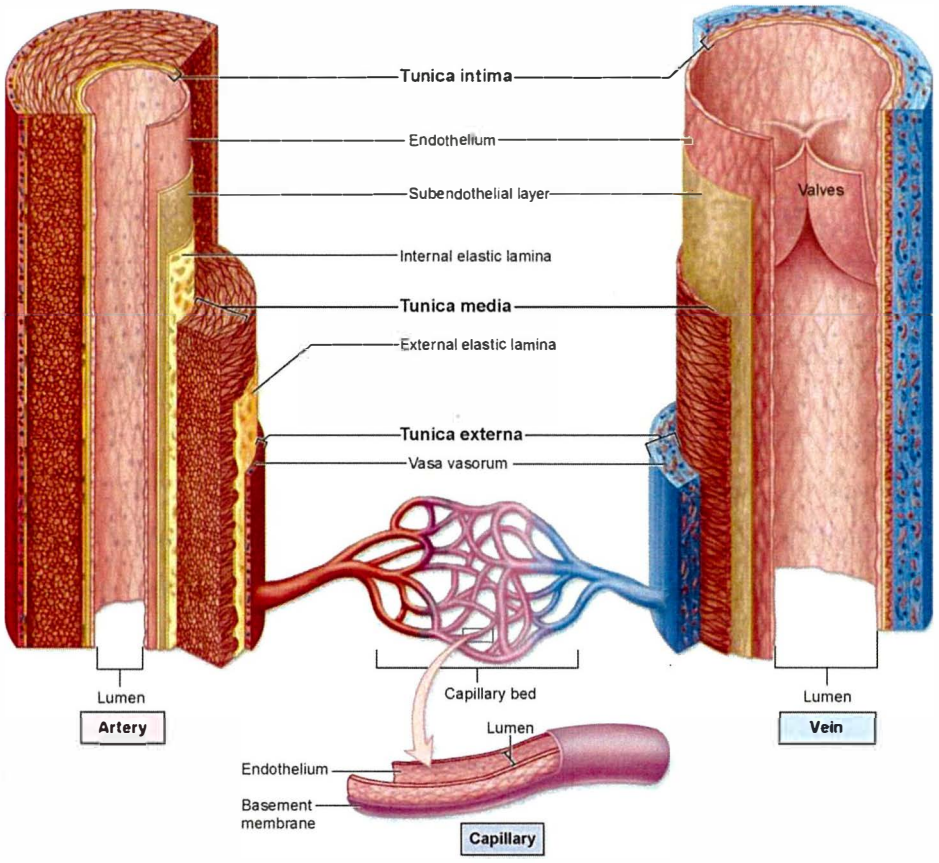

Figure 2.3: The structure of the artery, vein and capillary [97].

Table 2.1: difference between artery, capillary and vein.

	Arteries	Capillaries	Veins
Function	Carry blood away from the heart at high pressure.	- Supply all cells with their requirements. - Take away waste products.	Return blood to the heart at low pressure.
Structure of wall	- Thick and strong. - Contain muscles, elastic fibers and fibrous tissue.	Very thin, only one cell thick.	- Thin. - Mainly fibrous tissue. - Contain far less muscle and elastic tissue than arteries.

Lumen	- Narrow. - Varies with heartbeat (increases as a pulse of blood passes through).	- Very narrow. - Just wide enough for a red blood cell to pass through.	Wide.
Valves	No valve is in the artery.	No valve is in the Capillary.	Valve prevents backflow.
How structure fits function	- Strength and elasticity needed to withstand the pulsing of the blood, prevent bursting and maintain pressure wave. - Helps to maintain high blood pressure, preventing blood flowing backwards.	- No need for strong walls, as most of the blood pressure has been lost. - Thin walls and narrow lumen bring blood into close contact with body tissue, allowing diffusion of materials between capillary and surrounding tissues. - White blood cells can squeeze between cells of the wall.	- No need for strong walls, as most of the blood pressure has been lost. - Wide lumen offers less resistance to blood flow.

2.4 Heart

The heart is located slightly to the left of the centre of your chest between the two lungs. It is made of cardiac muscle and is surrounded by a double membrane called the pericardium. There is a fluid between these two membranes called pericardial fluid. This fluid helps to reduce friction when the heart beats. The heart is about the size of a clenched fist. It is also called power house of the body.

The human heart is primarily a shell. There are four cavities, or open spaces, inside the heart that fill with blood. Two of these cavities are called atria. The other two are called ventricles. The two atria form the curved top of the heart. The ventricles meet at the bottom of the heart to form a pointed base which points toward the left side of your chest. The left ventricle contracts most forcefully, so you can best feel your heart pumping on the left side of your chest.

The left side of the heart houses one atrium and one ventricle. The right side of the heart houses the others. A wall, called the septum, separates the right and left sides of the heart. A valve connects each atrium to the ventricle below it. The bicuspid valve connects the left atrium with the left ventricle. The tricuspid valve connects the right atrium with the right ventricle. The semilunar valves allow the blood to flow out of the heart into the two main arteries (aorta and pulmonary artery). They prevent blood from returning to the heart.

The top of the heart connects to a few large blood vessels. The largest of these is the aorta, or main artery, which carries nutrient-rich blood away from the heart. Another important vessel is the pulmonary artery which connects the heart with the lungs as part of the pulmonary circulation system. The two largest veins that carry blood into the heart are the superior vena cava and the inferior vena cava. They are called "vena cava" because they are the "heart's veins." The

superior is located near the top of the heart. The inferior is located beneath the superior.

The heart's structure makes it an efficient, never-ceasing pump. From the moment of development through the moment of death, the heart pumps. The heart, therefore, has to be strong. The average heart's muscle, called cardiac muscle, contracts and relaxes about 70 to 80 times per minute without you ever having to think about it. As the cardiac muscle contracts it pushes blood through the chambers and into the vessels. Nerves connected to the heart regulate the speed with which the muscle contracts.

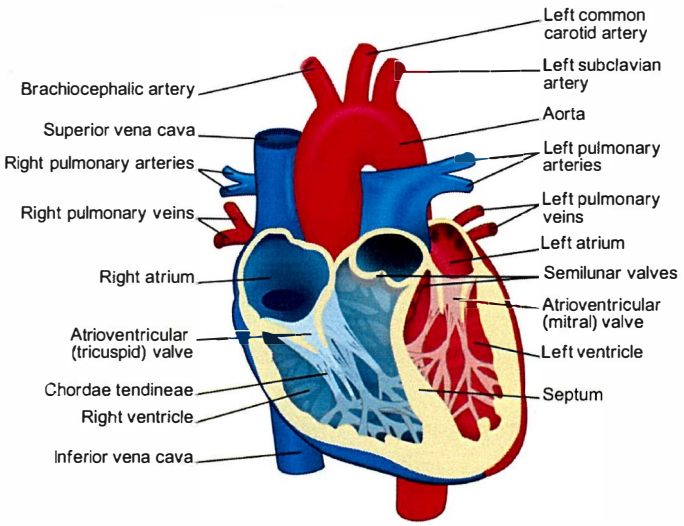

Figure 2.4: An anterior view of heart [98].

Considering how much work it has to do, the heart is surprisingly small. The average adult heart is about the size of a clenched fist and weighs about 11 ounces (310 grams). Located in the middle of the chest behind the breastbone, between the lungs, the heart rests in a moistened chamber called the pericardial cavity which is surrounded by the ribcage. The diaphragm, a tough layer of muscle, lies below. As a result, the heart is well protected.

2.5 Human Circulatory System

The human circulatory system pumps five litres of blood through a complex network of passages that passes through the vital organs of the human body.

The circulatory system, also called the cardiovascular system, is an organ system that permits blood to circulate and transport nutrients (such as amino acids and electrolytes), oxygen, carbon dioxide, hormones, and blood cells to and from cells in the body to nourish it and help to fight diseases, stabilize body temperature and pH, and to maintain homeostasis. The heart is responsible for providing the driving push to move all this blood whereas the lungs allow for the exchange of gasses: providing oxygen to be carried to the vital and peripheral organs and taking away the carbon dioxide build-up. Therefore, the circulatory system itself can be separated into three distinct portions: the pulmonary system, encompassing the lungs; the coronary system, encompassing the heart and the systemic system,

which covers the rest of the system. It is common to combine both the pulmonary system with the coronary system to a system by itself called the cardiopulmonary system.

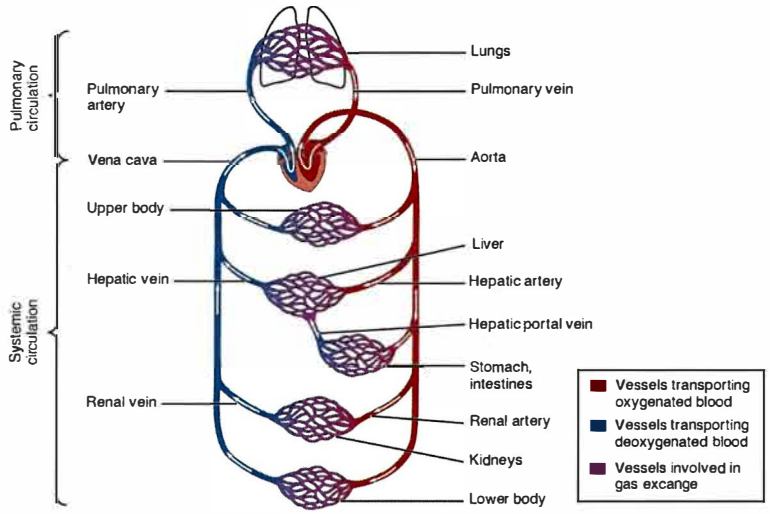

Figure 2.5: Representation of the human circulatory system showing both the pulmonary circulation and the systemic circulation [99].

Cardiopulmonary circulation involves the movement of blood from heart to lungs and back again and is important for removing waste gasses and saturating the blood with oxygen prior to being pumped from the heart to other portions of the body. The veins bring in blood rich in waste materials, particularly carbon dioxide which results from the combustion processes necessary to generate energy carried out throughout the body. This enters the right atrium of the heart (lower chamber) via two large veins called the vena-cavae, which then contracts (systole) and

pushes the blood into the right ventricle (upper chamber) via a one-way valve. The right ventricle then contracts to force the fluids out through the pulmonary artery into the lungs, whereby the aforementioned exchange of gasses occurs. This blood, now rich in oxygen is further pumped into the left atrium via the pulmonary vein, which is pumped into the left ventricle of the heart and expelled through the aorta, the largest artery in the body (to withstand the high pressures), to the other portions of the body. It is important to note that there are a series of valves within the heart and within the veins around the body that prevent backflow from occurring by sealing off the vessels when the heart is expanding (diastole), causing a lower pressure upstream.

The systemic circulation covers the blood flow immediately after it leaves the heart to circulate around the body, depositing oxygen and nutrients while collecting waste products, to when it returns back into the heart. Within this flow, the blood will absorb nutrients attained from the digestion process, which is then used to provide fuel for energy as well as for cell growth and storage. The blood will deposit any unnecessary waste through the liver within this circulation as well, which will be expelled from the body. All the vessel walls are smooth to allow for ease of flow and strong enough to withstand the varying pulses of the flow.

Within the systemic circulation, it can be seen how the arteries, which transfer oxygen rich blood, become veins that take away the waste gasses. Where this transfer occurs, the relatively large arteries branch up into arterioles which branch further into capillaries. These small branches allow for the maximum transfer of materials carried within the blood to the parts of the body that need them. Capillaries have extremely thin walls to allow for this transfer, and they eventually come together to form venules. Venules join together to form veins. Veins are notably smaller in diameter than arteries as they need not withstand as high pressures and do not transfer as much materials, but they do have valves along the vessel to prevent flow reversal. Figure 2.5 provides a comparison of the blood flow characteristics along these different vessels.

2.6 Atherosclerosis and stenosis

Atherosclerosis (or arteriosclerotic vascular disease) is a condition where the arteries become narrowed and hardened due to an excessive buildup of plaque around the artery wall. The disease disrupts the flow of blood around the body, posing serious cardiovascular complications. Arteries contain an endothelium, a thin layer of cells that keeps the artery smooth and allows blood to flow easily. Atherosclerosis starts when the endothelium becomes damaged, allowing LDL cholesterol to accumulate in the artery wall. The body sends macrophage white

blood cells to clean up the cholesterol, but sometimes the cells get stuck there at the affected site. Over time this results in plaque being built up, consisting of bad cholesterol (LDL cholesterol) and macrophage white blood cells. The plaque clogs up the artery, disrupting the flow of blood around the body. This potentially causes blood clots that can result in life-threatening conditions such as heart attack, stroke and other cardiovascular diseases. The condition can affect the entire artery tree, but mainly affects the larger high-pressure arteries.

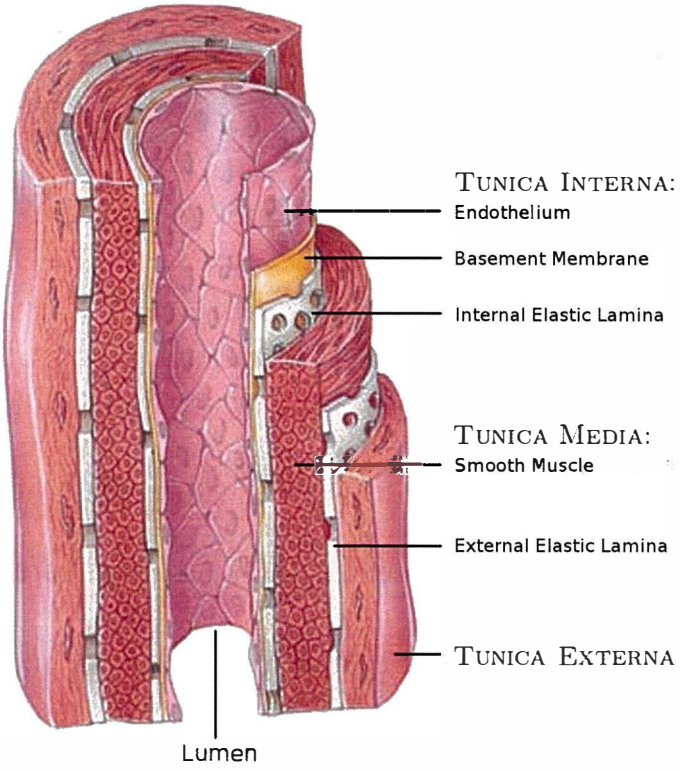

Figure 2.6: Diagram of a typical artery detailing the layers of tissue that constitutes the artery wall [100].

Atherosclerosis (also known as arteriosclerotic vascular disease or ASVD) is a specific form of arteriosclerosis in which an artery wall thickens as a result of invasion and accumulation of White Blood Cells (WBCs). The accumulation of the WBCs is termed "fatty streaks" early on because of appearance being similar to that of marbled steak. These accumulations contain living, active WBCs (producing inflammation) and remnants of dead cells, including cholesterol and triglycerides. The remnants eventually include calcium and other crystallized materials, within the outer-most and oldest plaque. The "fatty streaks" reduce the elasticity of the artery walls. However, they do not affect blood flow for decades, because the artery muscular wall enlarges at the locations of plaque. The wall stiffening may eventually increase pulse pressure; widened pulse pressure is one possible result of advanced disease within the major arteries.

Atherosclerosis is therefore a syndrome affecting arterial blood vessels due to a chronic inflammatory response of WBCs in the walls of arteries. This is promoted by Low-Density Lipoproteins (LDL, plasma proteins that carry cholesterol and triglycerides) without adequate removal of fats and cholesterol from the macrophages by functional High-Density Lipoproteins (HDL). It is commonly referred to as a "hardening" or furring of the arteries. It is caused by the formation of multiple atheromatous plaques within the arteries.

The atherosclerotic process is not fully understood. Atherosclerosis is initiated by inflammatory processes in the endothelial cells of the vessel wall in response to retained LDL particles.

Lipoproteins in the blood vary in size. Some data suggests that small dense LDL (sdLDL) particles are more prone to pass between the endothelial cells, going behind the cellular monolayer of endothelium. LDL particles and their content are susceptible to oxidation by free radicals, and the risk is higher while the particles are in the wall than while in the bloodstream. However, LDL particles have a half-life of only a couple of days, and their content (LDL particles typically carry 3,000 to 6,000 fat molecules, including: cholesterol, phospholipids, cholesteryl esters, triglycerides & all other fats in the water outside cells, to the tissues of the body) changes with time.

Once inside the vessel wall, LDL particles can become more prone to oxidation. Endothelial cells respond by attracting monocyte white blood cells, causing them to leave the blood stream, penetrate into the arterial walls and transform into macrophages. The macrophages' ingestion of oxidized LDL particles triggers a cascade of immune responses which over time can produce an atheroma if HDL removal of fats from the macrophages does not keep up. The immune system's specialized white blood cells (macrophages and T-lymphocytes)

absorb the oxidized LDL, forming specialized foam cells. If these foam cells are not able to process the oxidized LDL and recruit HDL particles to remove the fats, they grow and eventually rupture, leaving behind cellular membrane remnants, oxidized materials, and fats (including cholesterol) in the artery wall. This attracts more white blood cells, resulting in a snowballing progression that continues the cycle, inflaming the artery. The presence of the plaque induces the muscle cells of the blood vessel to stretch, compensating for the additional bulk, and the endothelial lining thickens, increasing the separation between the plaque and lumen. This somewhat offsets the narrowing caused by the growth of the plaque, but it causes the wall to stiffen and become less compliant to stretching with each heartbeat. However, some researchers believe that atherosclerosis may be caused by an infection of the vascular smooth muscle cells. Chickens, for example, develop atherosclerosis when infected with the Marek's disease herpesvirus. Herpesvirus infection of arterial smooth muscle cells has been shown to cause Cholesteryl Ester (CE) accumulation, which is associated with atherosclerosis. Cytomegalovirus (CMV) infection is also associated with cardiovascular diseases.

While doctors recommend a healthy diet and exercise to reduce the effects of stenosis, there are currently available several methods to remove the plaque formation on the arterial walls. One of this is medication, in which the patient ingests either antiplatelet or anticoagulants. Both of these medications seek to

prevent the material from clumping together to cause the blockage along the artery. The other methods involve surgery and include balloon angioplasty, laser angioplasty or urethrectomy. Balloon angioplasty involves feeding a catheter from a main artery into the coronary artery with a balloon tip, which is inflated at the site of the stenosis. This pushes the stenotic portion into the artery wall and hopefully increase the cross sectional area of the region. A stent, which is a wired mesh, may also be inserted later via the catheter to hold the artery wall in place. Laser angioplasty also relies on having a catheter fed to the coronary artery with a laser tip to destroy the built-up plaque with pulsing bursts of light.

The last method, urethrectomy, involves having a drill tip on the catheter and is used where the plaque build-up is too hard to be removed via the other two methods. The drill cuts up the plaque and some types are capable of removing the bits that fall off in order to prevent the fatty material from flowing further downstream. In the more severe cases, though, it may be necessary to perform a bypass graft, whereby healthy blood vessels are harvested from other parts of the body and sewed onto the coronary arteries to that blood can be routed past the blockage. This form of open-heart surgery, although risky, is highly effective in restoring blood flow into the heart.

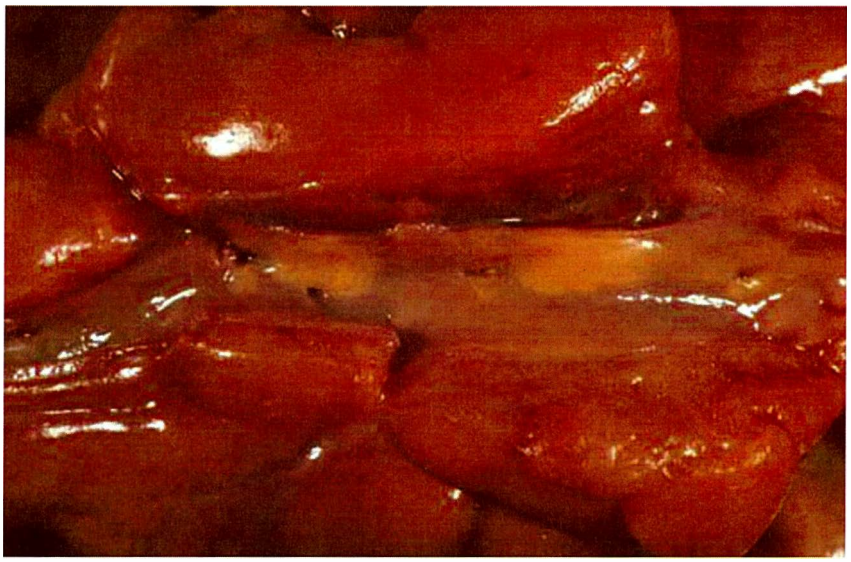

Figure 2.7: Mild atherosclerosis within a coronary artery. The formation of yellow plaque can be seen to traverse a significant length of the section, although this is still insufficient to cause disease [101].

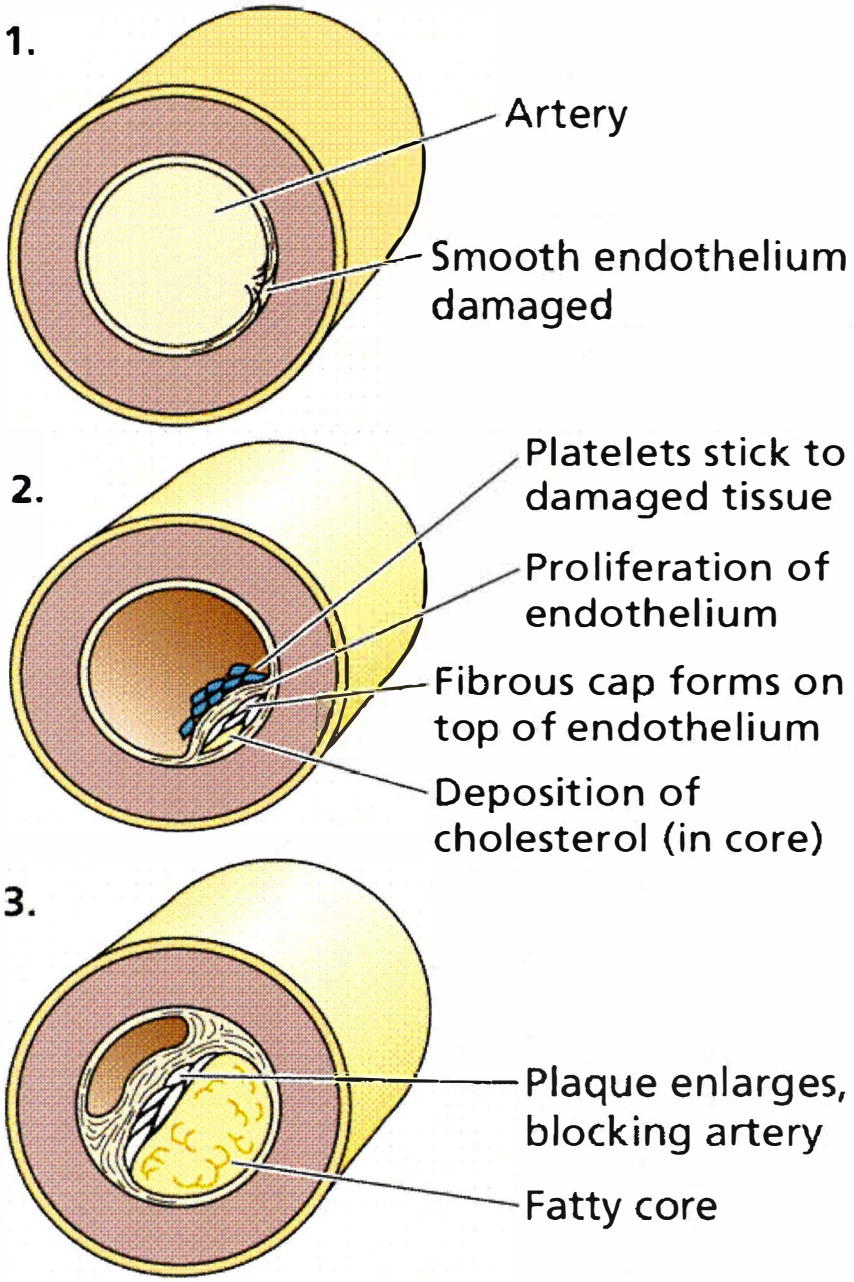

Figure 2.8: Diagrams of the growth of stenosis within an artery, Purves et al [92].

Chapter 3

An overview of Navier-Stokes equation and Statistical details

Overview

This chapter presents the Navier- Stokes equations with their derivation and statistical details such as regression analysis and regression models.

3.1 Navier-Stokes equations

The Navier-Stokes equations, developed by Claude-Louis Navier and George Gabriel Stokes in 1822, are equations which can be used to determine the velocity vector field that applies to a fluid, given some initial conditions. They arise from the application of Newton's second law in combination with a fluid stress (due to viscosity) and a pressure term. For almost all real situations, they result in a system of nonlinear partial differential equations; however, with certain simplifications they can sometimes be reduced to linear differential equations. Usually, however, they remain nonlinear, which makes them difficult or impossible to solve; this is what causes the turbulence and unpredictability in their results.

Derivation of the Navier-Stokes equations: the Navier-Stokes equations can be derived from the basic conservation and continuity equations applied to

properties of fluid. In order to derive the equations of fluid motion, we must first derive the continuity equation (which dictates conditions under which things are conserved), apply the equation to conservation of mass and momentum, and finally combine the conservation equations with a physical understanding of what a fluid is.

Continuity equation: The basic continuity equation is an equation which describes the change of an intensive property. An intensive property is something which is independent of the amount of material you have. For instance, temperature would be an intensive property; heat would be the corresponding extensive property. The continuity equation derived can later be applied to mass and momentum. Continuity equation or conservation of mass states that the fluid mass cannot change.

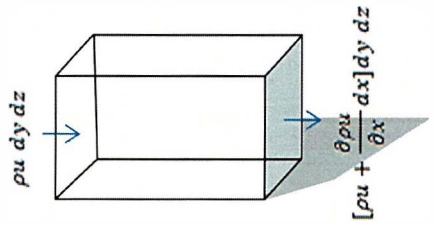

Figure 3.1: Elemental Cartesian fixed control volume showing the inlet and outlet mass flows.

We choose an infinitesimal fixed control volume (*dx, dy, dz*), as in Figure 3.1. The flow through each side of the element is approximately one-dimensional, so the appropriate mass conservation relation to use here is,

$$\int_{cv} \frac{\partial p}{\partial t} d\vartheta + \sum_i (\rho_i A_i v_i)_{out} - \sum_i (\rho_i A_i v_i)_{in} = 0 \qquad (3.1)$$

The element is so small that the volume integral simply reduces to a differential term: $\int_{cv} \frac{\partial p}{\partial t} dV \approx \frac{\partial p}{\partial t} dxdydz.$

The mass flow terms occur on all six faces, three inlets and three outlets. For mass conservation, if ρu is known on the left face, the value of this product on the right face is $\rho u + \frac{\partial}{\partial x}(\rho u)dx$. The Figure 3.1 shows only the mass flows on the x or left and right face. The flows on the y or bottom and top, and the z (back and front) faces have been omitted to avoid cluttering up the drawing. We can list all these six flows as follows in table 3.1.

Table 3.1: The mass flows on six faces

Face	Inlet mass flow	Outlet mass flow
X	$\rho u\, dy\, dz$	$[\rho u + \frac{\partial}{\partial x}(\rho u)dx]dy\, dz$
Y	$\rho v\, dx\, dz$	$[\rho v + \frac{\partial}{\partial y}(\rho v)dy]dx\, dz$
z	$\rho w\, dx\, dy$	$[\rho w + \frac{\partial}{\partial z}(\rho w)dz]dx\, dy$

Introduce these terms into Equation (3.1) and we have:

$$\frac{\partial \rho}{\partial t} dx\, dy\, dz + \frac{\partial}{\partial x}(\rho u) dx\, dy\, dz + \frac{\partial}{\partial y}(\rho v) dy\, dx\, dz + \frac{\partial}{\partial z}(\rho w) dz\, dx\, dy = 0.$$

The element volume cancels out of all terms, leaving a partial differential equation involving the derivatives of density and velocity:

$$\frac{\partial \rho}{\partial t} + \frac{\partial}{\partial x}(\rho u) + \frac{\partial}{\partial y}(\rho v) + \frac{\partial}{\partial z}(\rho w) = 0, or\ \frac{\partial \rho}{\partial t} + \nabla.(\rho V) = 0 \qquad (3.2)$$

This is the desired result. That is the flow may be steady or unsteady, viscous or frictionless, compressible or incompressible. If the flow is steady then the equation be $\nabla.(\rho V) = 0$; if the flow is incompressible then the equation be $\nabla.V = 0$.

Now we use the same elemental control volume as in Figure 3.1, for which the appropriate form of the linear momentum relation is:

$$\sum F = \frac{\partial}{\partial t}(\int_{cv} V \rho d\vartheta) + \sum_i (\dot{m}_i V_i)_{out} - \sum_i (\dot{m}_i V_i)_{in} \qquad (3.3)$$

Again the element is so small that the volume integral simply reduces to a derivative term:

$$\frac{\partial}{\partial t}(V\rho d\vartheta) \approx \frac{\partial}{\partial t}(\rho V)dxdy\,dz \tag{3.4}$$

The momentum fluxes occur on all six faces, three inlets and three outlets. Referring again to Figure 3.1, we can form a table (3.2) of momentum fluxes by exact analogy with the discussion that led up to the equation for net mass flux.

Table 3.2: The momentum fluxes on six faces

Face	Inlet momentum flux	Outlet momentum flux
X	$\rho uV\,dy\,dz$	$[\rho uV + \frac{\partial}{\partial x}(\rho uV)dx]dy\,dz$
Y	$\rho vV\,dx\,dz$	$[\rho vV + \frac{\partial}{\partial y}(\rho vV)dy]dx\,dz$
z	$\rho wV\,dx\,dy$	$[\rho wV + \frac{\partial}{\partial z}(\rho wV)dz]dx\,dy$

Introduce these terms and Equation (3.4) into equation (3.3), and get this intermediate result:

$$\sum F = dx\,dy\,dz\left[\frac{\partial}{\partial t}(\rho V) + \frac{\partial}{\partial x}(\rho uV) + \frac{\partial}{\partial y}(\rho vV) + \frac{\partial}{\partial z}(\rho wV)\right] \tag{3.5}$$

A simplification occurs if we split up the term in brackets as follows:

$$\frac{\partial}{\partial t}(\rho V)+\frac{\partial}{\partial x}(\rho uV)+\frac{\partial}{\partial y}(\rho vV)+\frac{\partial}{\partial z}(\rho wV)=V\left[\frac{\partial \rho}{\partial t}+\nabla.(\rho V)\right]+\rho\left(\frac{\partial V}{\partial t}+u\frac{\partial V}{\partial x}+v\frac{\partial V}{\partial y}+w\frac{\partial V}{\partial z}\right) \quad (3.6)$$

The term in brackets on the right-hand side is seen to be the equation of continuity, Equation (3.2), which vanishes identically. The long term in parentheses on the right-hand side is seen from Equation (3.5) to be total acceleration of a particle that instantaneously occupies the control volume:

$$\frac{\partial V}{\partial t}+u\frac{\partial V}{\partial x}+v\frac{\partial V}{\partial y}+w\frac{\partial V}{\partial z}=\frac{dV}{dt} \quad (3.7)$$

Thus we have now reduced Equation (3.5) to,

$$\sum F=\rho\frac{dV}{dt}\,dx\,dy\,dz \quad (3.8)$$

These forces are of two types, body forces and surface forces. Body forces are due to external fields (gravity, magnetism, electric potential) that act on the entire mass within the element. We consider only the body force is gravity. The gravity force on the differential mass $\rho\,dx\,dy\,dz$ within the control volume is,

$$dF_{grav}=\rho g\,dx\,dy\,dz \quad (3.9)$$

The surface forces are due to the stress on the side of the control surface. These stresses are the sum of hydrostatic pressure plus viscous stresses τ_{ij} that arises from motion with velocity gradients:

$$\sigma_{ij} = \begin{vmatrix} -p + \tau_{xx} & \tau_{yx} & \tau_{zx} \\ \tau_{xy} & -p + \tau_{yy} & \tau_{zy} \\ \tau_{xz} & \tau_{yz} & -p + \tau_{zz} \end{vmatrix} \tag{3.10}$$

It is not these stresses but their gradient, or differences, which cause a net force on the differential control surface. This is seen by referring to Figure 3.2, which shows only the x-directed stresses to avoid cluttering up the drawing. For example, the leftward force $\sigma_{xx} dy\, dz$ on the left face is balanced by the rightward force $\sigma_{xx} dy\, dz$ on the right face, leaving only the net rightward force $\frac{\partial \sigma_{xx}}{\partial x} dx\, dy\, dz$ on the right face. The same thing happens on the other four faces, so that the net surface force in the x direction is given by:

$$dF_{x,surf} = \left[\frac{\partial \sigma_{xx}}{\partial x} + \frac{\partial \sigma_{yx}}{\partial y} + \frac{\partial \sigma_{zx}}{\partial z}\right] dx\, dy\, dz \tag{3.11}$$

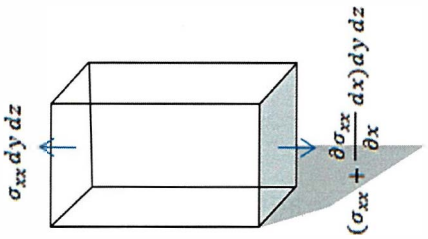

Figure 3.2: Elemental Cartesian fixed control volume showing the surface forces in the x direction only.

We see that this force is proportional to the element volume. Notice that the stress terms are taken from the top row of the array in Equation (3.10). Splitting this row into pressure plus viscous stresses, we can rewrite Equation (3.11) as,

$$\frac{dF_x}{d\vartheta} = -\frac{\partial p}{\partial x} + \frac{\partial \tau_{xx}}{\partial x} + \frac{\partial \tau_{yx}}{\partial y} + \frac{\partial \tau_{zx}}{\partial z} \tag{3.12}$$

In exactly similar manner, we can drive the y and z forces per unit volume on the control surface:

$$\frac{dF_y}{d\vartheta} = -\frac{\partial p}{\partial y} + \frac{\partial \tau_{xy}}{\partial x} + \frac{\partial \tau_{yy}}{\partial y} + \frac{\partial \tau_{zy}}{\partial z} \tag{3.13}$$

$$\frac{dF_z}{d\vartheta} = -\frac{\partial p}{\partial z} + \frac{\partial \tau_{xz}}{\partial x} + \frac{\partial \tau_{yz}}{\partial y} + \frac{\partial \tau_{zz}}{\partial z} \tag{3.14}$$

From the Equation (3.12), (3.13), and (3.14) we get net vector surface force:

$$\left(\frac{dF}{d\vartheta}\right)_{surf} = -\nabla p + \left(\frac{dF}{d\vartheta}\right)_{viscous} \tag{3.15}$$

Where viscous force has total nine terms:

$$\left(\frac{dF}{d\vartheta}\right)_{viscous} = i\left(\frac{\partial \tau_{xx}}{\partial x} + \frac{\partial \tau_{yx}}{\partial y} + \frac{\partial \tau_{zx}}{\partial z}\right) + j\left(\frac{\partial \tau_{xy}}{\partial x} + \frac{\partial \tau_{yy}}{\partial y} + \frac{\partial \tau_{zy}}{\partial z}\right) + k\left(\frac{\partial \tau_{xz}}{\partial x} + \frac{\partial \tau_{yz}}{\partial y} + \frac{\partial \tau_{zz}}{\partial z}\right).$$

$$\text{or, } \left(\frac{dF}{d\vartheta}\right)_{viscous} = \nabla . \tau_{ij} \tag{3.16}$$

Where, $\tau_{ij} = \begin{bmatrix} \tau_{xx} & \tau_{yx} & \tau_{zx} \\ \tau_{xy} & \tau_{yy} & \tau_{zy} \\ \tau_{xz} & \tau_{yz} & \tau_{zz} \end{bmatrix}$ is the viscous stress tensor acting on the element. The surface force is thus the sum of the pressure gradient vector and the divergence of the viscous stress tensor. Substituting into the Equation (3.8) and utilizing (3.9), we have basic differential momentum equation for an infinitesimal element:

$$\rho g - \nabla p + \nabla . \tau_{ij} = \rho \frac{dV}{dt} \tag{3.17}$$

For a Newtonian fluid, the viscous stresses are proportional to the element strain rates and the coefficient of viscosity. For incompressible flow,

$$\tau_{xx} = 2\mu\left(\frac{\partial u}{\partial x} - \frac{1}{3}\nabla . V\right), \tau_{yy} = 2\mu\left(\frac{\partial v}{\partial y} - \frac{1}{3}\nabla . V\right), \tau_{zz} = 2\mu\left(\frac{\partial w}{\partial z} - \frac{1}{3}\nabla . V\right), \tau_{xy} = \tau_{yx} = \mu\left(\frac{\partial u}{\partial y} + \frac{\partial v}{\partial x}\right), \tau_{xz} = \tau_{zx} = \mu\left(\frac{\partial u}{\partial z} + \frac{\partial w}{\partial x}\right), \tau_{zy} = \tau_{yz} = \mu\left(\frac{\partial w}{\partial y} + \frac{\partial v}{\partial z}\right) \tag{3.18}$$

Substitution of these equations into the Equation (3.17) gives the equation:

$$\rho \frac{dV}{dt} = \rho g - \nabla p + \mu \Delta V + \frac{1}{3}\mu \nabla . (\nabla . V) \tag{3.19}$$

For incompressible fluid $\nabla . V = 0$, then the above equation will be,

$$\rho \frac{dV}{dt} = \rho g - \nabla p + \mu \Delta V \tag{3.20}$$

This is the Navier-Stokes equation.

The Navier-Stokes equation makes a surprising amount of intuitive sense given the complexity of what it is modeling. The left hand side of the equation, $\rho \frac{dV}{dt}$, is the force on each fluid particle. The equation states that the force is composed of three terms:

$-\nabla p$: A pressure term (also known as the volumetric stress tensor) which prevents motion due to normal stresses. The fluid presses against itself and keeps it from shrinking in volume.

$\mu \Delta V + \frac{1}{3}\mu \nabla . (\nabla . V)$: A stress term (known as the stress deviator tensor) which causes motion due to horizontal friction and shear stresses. The shear stress causes turbulence and viscous flows - if you drag your hand through a liquid, you

will note that the moving liquid also causes nearby liquid to start moving in the same direction. Turbulence is the result of the shear stress.

$\boldsymbol{\rho g}$**:** is the force term which is acting on every single fluid particle.

This intuitively explains turbulent flows and some common scenarios. For example, if water is sitting in a cup, the force (gravity) ρg is equal to the pressure term because $\frac{d}{dz}(\rho g z) = \rho g$ Thus, since gravity is equivalent to the pressure, the fluid will sit still, which is indeed what we observe when water is sitting in a cup.

Assuming that the flow is incompressible, both the continuity equation and the Navier- Stokes equations reduce to,

$$\frac{\partial u_i}{\partial x_i} = 0 \tag{3.21}$$

$$\frac{\partial u_i}{\partial t} + u_j \frac{\partial u_i}{\partial x_j} = -\frac{1}{\rho}\frac{\partial p}{\partial x_i} + \frac{\mu}{\rho}\frac{\partial^2 u_i}{\partial x_j^2} \tag{3.22}$$

Where x_i, u_i, p, ρ, $\frac{\mu}{\rho}$, and t respectively are position, velocity, pressure, density, kinematic viscosity, and time. We decompose the flow quantities, f_i into

$$f_i(x,t) = F_i(x) + f_i'(x,t) \tag{3.23}$$

Where $F_i(x)$ is the time average and $f_i'(x,t)$ is the fluctuating part of the quantity. The time average of the quantity and the time average of the fluctuating part of the quantity are defined respectively by,

$$F_i(x) = \lim_{T\to\infty} \frac{1}{T} \int_{t_0}^{t_0+T} f_i(x,t)dt \tag{3.24}$$

and

$$\overline{f_i'(x,t)} = \lim_{T\to\infty} \frac{1}{T} \int_{t_0}^{t_0+T} (f_i(x,t) - F_i(x))dt = 0 \tag{3.25}$$

In this problem $f_i(x,t)$ is either the velocity u_i or the pressure p. Introducing (3.23) into (3.21) and time averaging using the definition (3.24) and (3.25), we get,

$$\overline{\frac{\partial u_i}{\partial x_i}} = 0 \; or, \frac{\overline{\partial (U_i+u_i')}}{\partial x_i} = 0 \; or, \frac{\overline{\partial U_i}}{\partial x_i} + \frac{\overline{\partial u_i'}}{\partial x_i} = 0 \; or, \frac{\partial U_i}{\partial x_i} = 0 \tag{3.26}$$

Now inserting (3.23) into (3.22), and time averaging we get,

$$\overline{\frac{\partial (U_i+u_i')}{\partial t}} + \overline{(U_j + u_j')\frac{\partial (U_i+u_i')}{\partial x_j}} = -\overline{\frac{1}{\rho}\frac{\partial (P+p')}{\partial x_i}} + \overline{\frac{\mu}{\rho}\frac{\partial^2 (U_i+u_i')}{\partial x_j^2}} \tag{3.27}$$

The second term on the left hand side leads to the product,

$$\overline{u_j' \frac{\partial u_i'}{\partial x_j}} \tag{3.28}$$

This, due to continuity, can be rewritten as:

$$\frac{\partial \overline{u_j' u_i'}}{\partial x_j} \tag{3.29}$$

Except from this, all terms involving fluctuating parts of the flow parameters vanish. Therefore the Reynolds-Average Navier-Stokes equation can be expressed as:

$$\frac{\partial U_i}{\partial t} + U_j \frac{\partial U_i}{\partial x_j} = -\frac{1}{\rho}\frac{\partial P}{\partial x_i} + \frac{\partial}{\partial x_j}\left(\frac{\mu}{\rho}\frac{\partial U_i}{\partial x_j} - \overline{u_j' u_i'}\right) \tag{3.30}$$

The term $\overline{u_j' u_i'}$ is a result of the non linear convective terms, and is referred to as the Reynolds stresses. We need to model this term in order to solve the Equation (3.30).

The full Reynolds stress tensor is symmetric, and consequently it contains six new unknowns. Deriving transport equations for $\overline{u_j' u_i'}$ from the Navier-Stokes equations gives rise to third order products of the fluctuating velocities. As a consequence, the number of unknowns compared to the number of equations cannot be reduced this way. The latter is unknown as the closure problem. The problem is circumvented applying the Boussinesq approximation, in which we assume proportionality between the Reynolds stress tensor and the strain rate tensor.

$$-\overline{u_j' u_i'} = \frac{\mu_t}{\rho}\left(\frac{\partial U_i}{\partial x_j} + \frac{\partial U_j}{\partial x_i}\right) - \frac{2}{3}k\delta_{ij} \tag{3.31}$$

Which defines the eddy viscosity $\frac{\mu_t}{\rho}$. By the dimensional analysis the eddy viscosity can be modeled as

$$\mu_t = \rho C_\mu f_\mu \frac{k^2}{\varepsilon} \tag{3.32}$$

Where C_μ is found empirically to be 0.09 from the condition of equilibrium flow, f_μ is a damping function used to compensate for low Reynolds number effects in near wall regions, k is turbulent kinetic energy, and ε is dissipation of turbulent kinetic energy. The divergence of the Reynolds stress Tensor (3.31) is

$$-\frac{\partial \overline{u_j' u_i'}}{\partial x_j} = \frac{\partial}{\partial x_j}\left(\frac{\mu_t}{\rho}\frac{\partial U_i}{\partial x_j}\right) - \frac{\partial}{\partial x_j}\left(\frac{2}{3}k\delta_{ij}\right) \tag{3.33}$$

Here, δ_{ij} is Kronecker delta.

Which we insert in (3.30), and finally obtain

$$\frac{\partial U_i}{\partial t} + U_j\frac{\partial U_i}{\partial x_j} = -\frac{1}{\rho}\frac{\partial\left(P+\frac{2}{3}\rho k\right)}{\partial x_i} + \frac{\partial}{\partial x_j}\left(\frac{1}{\rho}(\mu+\mu_t)\frac{\partial U_i}{\partial x_j}\right) \tag{3.34}$$

This is the eddy viscosity model.

However, for low Reynold's number *k-w* turbulent model the k equation is -

$$\rho u_j \frac{\partial k}{\partial x_j} = \frac{\partial}{\partial x_j}\left[\left(\mu + \frac{\mu_t}{\sigma_k}\right)\frac{\partial k}{\partial x_j}\right] + G - \rho\omega k \quad (3.35)$$

and the ω equation -

$$\rho u_j \frac{\partial \omega}{\partial x_j} = \frac{\partial}{\partial x_j}\left[\left(\mu + \frac{\mu_t}{\sigma_\omega}\right)\frac{\partial \omega}{\partial x_j}\right] + c_1 \frac{\omega}{k} G - c_2 \rho \omega^2 \quad (3.36)$$

Where σ - closure coefficient, ω - specific dissipation rate, turbulent viscosity $\mu_t = c_\mu \rho \frac{k}{\omega}$, and

The generation rate of turbulence kinetic energy, $G = \mu_t \left(\frac{\partial u_i}{\partial x_j} + \frac{\partial u_j}{\partial x_i}\right)\frac{\partial u_i}{\partial x_j}$ (3.37)

The values of the Wilcox model constants were:

$c_1 = 0.555,\ c_2 = 0.8333,\ c_\mu = 0.09,\ \sigma_k = 2$ and $\sigma_\omega = 2$.

3. 2 Statistical details

3. 2. 1 Statistics

Statistics concerns the collection, organization, analysis, interpretation and presentation of data. Statistics deals with every aspect of data, including the planning of data collection in terms of the design of surveys and experiments. Statisticians collect data by developing specific experiment designs and survey samples. Representative sampling assures that inferences and conclusions can reasonably extend from the sample to the population as a whole.

An experimental study involves taking measurements of the system under study, manipulating the system, and then taking additional measurements using the same procedure to determine if the manipulation has modified the values of the measurements. Two main statistical methods are used in data analysis and descriptive statistics. Data analysis is a process of inspecting, cleansing, transforming and modeling data with the goal of discovering useful information, informing conclusion and supporting decision making. Descriptive statistics summarize data from a sample using indexes such as the mean or standard deviation, and inferential statistics, which draw conclusions from data that are subject to random variation such as observational errors, sampling variation. Descriptive statistics are most often concerned with two sets of properties of a distribution such as central tendency and dispersion. Central tendency or location seeks to characterize the distribution's central or typical value. On other hand, dispersion or variability characterizes the extent to which members of the distribution depart from its center and each other. Inferences on mathematical statistics are made under the framework of probability theory, which deals with the analysis of random phenomena. A standard statistical procedure involves the test of the relationship between two statistical data sets. A hypothesis is proposed for the statistical relationship between the two data sets. Then the hypothesis is compared as an alternative to a null hypothesis of no relationship between two data

sets. Rejecting the null hypothesis is a method for using statistical tests in which the null can be proven false. However, two basic forms of error are recognized for a null hypothesis. For example, null hypothesis is falsely rejected giving a "false positive" and null hypothesis fails to be rejected and an actual relationship between populations is missed giving a "false negative". Thus, multiple problems have come to be associated with these errors.

3. 2. 2 Test statistic

A test statistic is used in statistical hypothesis testing. In general, a test statistic is defined in such a way as to quantify behaviors that would distinguish the null hypothesis. An important property of a test statistic is that its sampling distribution under the null hypothesis must be calculable, either exactly or approximately, which allows p-values to be calculated. Two widely used test statistics are the t-statistic and the F-test. A t-test is appropriate for comparing means under relaxed conditions. Tests of proportions are analogous to tests of means. F-tests are commonly used when deciding whether groupings of data by category are meaningful. If the variance of test scores of the left-handed in a class is much smaller than the variance of the whole class, then it may be useful to study lefties as a group.

3. 2. 3 Regression analysis

It is a set of statistical processes for estimating the relationships between a dependent variable which is often called the 'outcome variable' and one or more independent variables which is often called 'predictors', 'covariates', or 'features'. The most common form of regression analysis is linear regression, in which a researcher finds the line or a more complex linear combination that most closely fits the data according to a specific mathematical criterion. It allows the researcher to estimate the conditional expectation or population average value of the dependent variable when the independent variables take on a given set of values. Regression analysis is primarily used for two distinct purposes. First, regression analysis is widely used for prediction and forecasting, where its use has substantial overlap with the field of machine learning. Second, in some situations regression analysis can be used to infer relationships between the independent and dependent variables. Importantly, regressions by themselves only reveal relationships between a dependent variable and a collection of independent variables in a fixed dataset. To use regressions for prediction or to infer the relationships, respectively, a researcher can justify why existing relationships have predictive power for a new context or why a relationship between two variables has a causal interpretation. The latter is especially important when researchers hope to estimate causal relationships using observational data.

3. 2. 4 Regression Model

Researchers first select a model what they would like to estimate and then use their chosen method to estimate the parameters of that model. Regression models involve the following components,

1. The unknown parameters, often denoted as a scalar or vector β.
2. The independent variables, which are observed in data and are often denoted as a vector X_i (where i denotes a row of data).
3. The dependent variable, which are observed in data and often denoted using the scalar Y_i.
4. The error terms, which are not directly observed in data and are often denoted using the scalar e_i.

In various fields of application, different terminologies are used in place of dependent and independent variables. Most regression models propose that Y_i is a function of X_i and β, with e_i representing an additive error term that may stand in for un-modeled determinants of Y_i or random statistical noise: $Y_i = f(X_i, \beta) + e_i$. The researchers' goal is to estimate the function $f(X_i, \beta)$ that most closely fits the data. To carry out regression analysis, the form of the function f must be specified.

In linear regression, the model specification is that the dependent variable, Y_i is a linear combination of the parameters (but need not be linear in the independent variables). For example, in simple linear regression for modelling n data points there is one independent variable: X_i, and two parameters, β_0 and β_1: Straight line: $Y_i = \beta_0 + \beta_1 X_i + e_i$. Where, i=1, 2, 3…n.

In multiple linear regression, there are several independent variables or functions of independent variables. Adding a term in X_i^2 to the preceding regression gives: Parabola: $Y_i = \beta_0 + \beta_1 X_i + \beta_2 X_i^2 + e_i$. Where, i=1, 2, 3…n.

This is still linear regression. Although, the expression on the right hand side is quadratic in the independent variable X_i, it is linear in the parameters β_0, β_1 and β_2. In both cases, e_i is an error term and the subscript i indexes a particular observation.

Regression models predict a value of the Y variable given known values of the X variables. Prediction within the range of values in the dataset used for model-fitting is known informally as interpolation. Prediction outside this range of the data is known as extrapolation. Performing extrapolation relies strongly on the regression assumptions. The further the extrapolation goes outside the data, the more room there is for the model to fail due to differences between the assumptions and the sample data or the true values.

Chapter 4

Geometry, Fluid properties, and Boundary conditions

Overview

This chapter describes the geometries, fluid properties, selection of governing equations and boundary conditions of this study.

4.1 Geometry

Three idealized Carotid arteries have been used as geometry for investigating the blood flow through the carotid arteries, shown in Fig. 4.1. One healthy and two stenotic Carotid arteries (with different severities such as 65% and 85% stenosis) have been investigated where stenoses are located before the bifurcation of the arteries. The wall is considered to be rigid. However, the model divided into three parts such as Common Carotid Artery (the zone just before the bifurcation), Internal Carotid artery (the right bifurcated part) and External Carotid Artery (left bifurcated part). The length (L) of the models is 72 mm. Moreover, the diameter of the inlet of the model, end of ICA and end of ECA are 6 mm, 3.75 mm and 2.5 mm respectively.

For the comparative study of blood flow through elastic stenotic artery with rigid body stenotic artery, three dimensional idealized stenotic arteries have been

used as the geometric model. These models have been differentiated by only their stenotic severity such as 45%, 55%, 65% and 75% (by area). The diameter, D, of the models is 6 mm. The geometric models have been divided by three parts such as pre stenotic length (4D), stenotic length (2D) and post stenotic length (6D). Wall has been taken as rigid as well as elastic for the arteries.

For a statistical analysis to investigate the effect of stenotic shapes and spiral flows on wall shear stress in the stenotic arteries, 120 simulations have been performed for getting the statistical data from the numerical results. Thus, one hundred twenty idealized stenotic arteries have been used as the geometric model for this study; whereas only four among them have been shown in the Figure 4.2. However, Figure 4.3 shows the cross-sectional views of the middle of the stenosis of 70% severity when eccentricity are 0, 0.2, 0.6, 0.8 and 0.9.

The models have been differentiated by their stenotic shape such as Stenotic severity, eccentricity and length; which are changed with model to model. Various stenotic severities (by area), which were changed from 25% to 85%, have been randomly selected for the models in the study. Stenotic eccentricity has been quantified by the eccentricity index (EI) ranging from 0 to 0.9 where EI of 0 corresponds to a concentric stenosis whereas EI of 0.9 corresponds to a highly eccentric stenosis. Besides, stenotic lengths 1D, 1.5D, 2D, 2.5D and 3D have been

taken in the models where D means diameter of the artery. The diameter of the models is 6 mm. The geometry of generated models have been divided by three parts such as pre stenotic length (4D), stenotic length isn't fixed and has been changed from 1D to 3D for different models and post stenotic length (6D). The wall is considered to be rigid.

These arteries are modeled by using ANSYS Workbench. However, the flow field meshing nodes and elements number are different for the different models, because the shape and size of the stenosis are not the same.

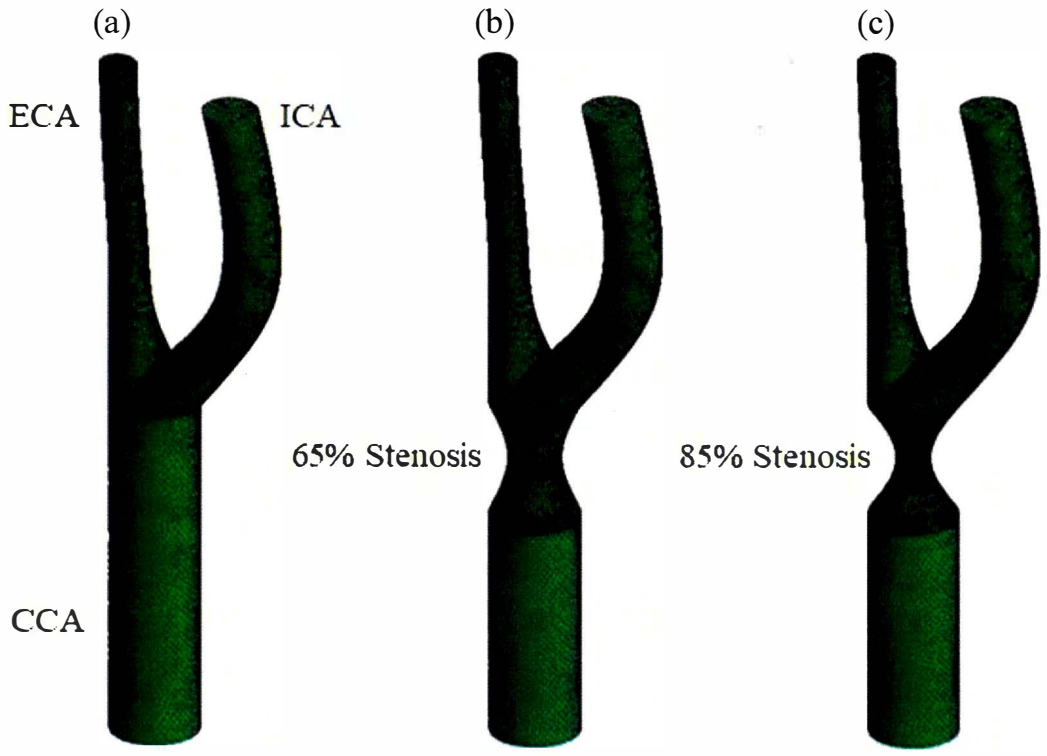

Fig. 4.1: (a) Healthy Carotid Artery, (b) 65% stenotic Carotid Artery and (C) 85% stenotic Carotid Artery.

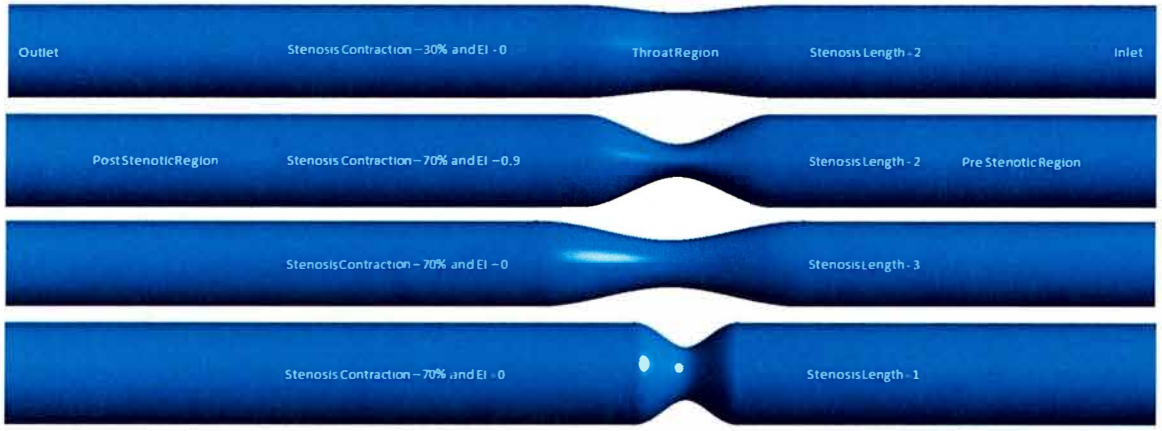

Fig. 4.2: Different stenotic arteries with the different stenosis's shapes.

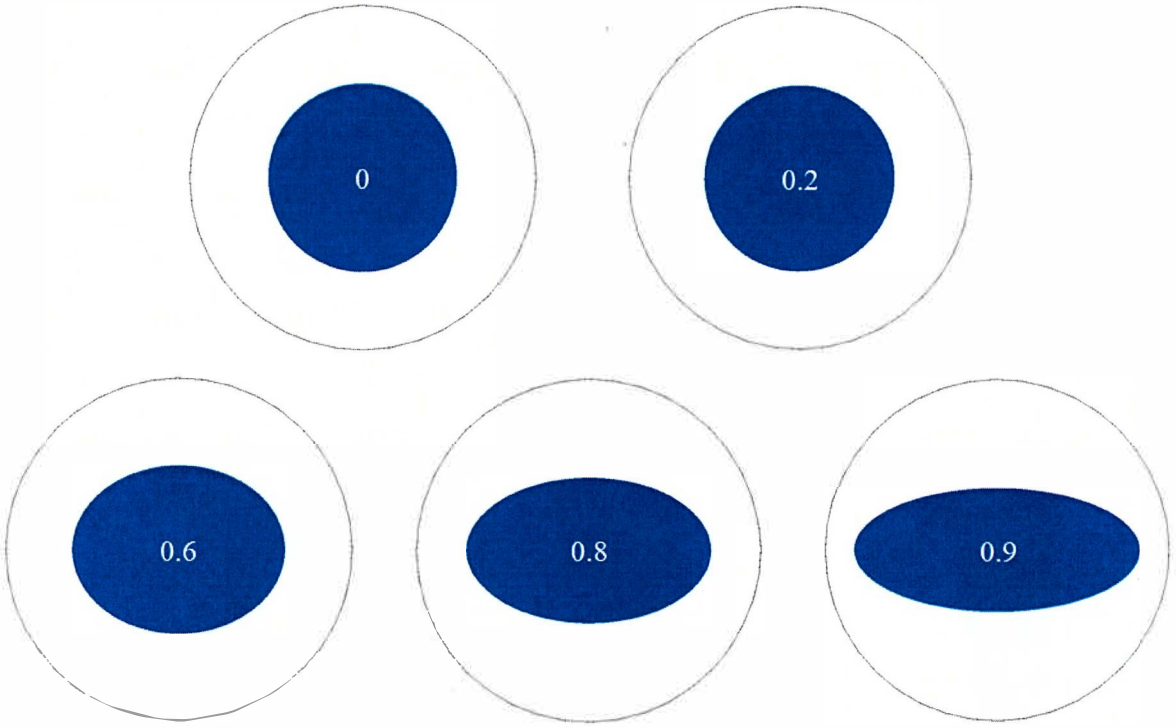

Fig. 4.3: Cross-sectional views of the middle of the stenosis of 70% severity when eccentricity are 0, 0.2, 0.6, 0.8 and 0.9.

4.2 Fluid properties

Blood is taken as fluid where the blood is considered incompressible. The density of the blood is 1050kg/m^3.

Newtonian fluid viscosity is always constant against the shear rate. On the other hand, non-Newtonian fluid viscosity changes depending on the shear rate. The shear rate varies from 1 to 1200 s^{-1} over a cardiac cycle in human arteries [102]. However, Boger [103] showed in his experiment that non-Newtonian fluids should exhibit Newtonian behaviour or their viscosity should remain constant in higher shear rate. The Non-Newtonian behaviour of blood flow is only acceptable, when shear rate is less than100 s^{-1}, stated by Rabby et al. [104]. Thus, blood behaves as non-Newtonian fluid in some parts of the cardiac cycle as well.

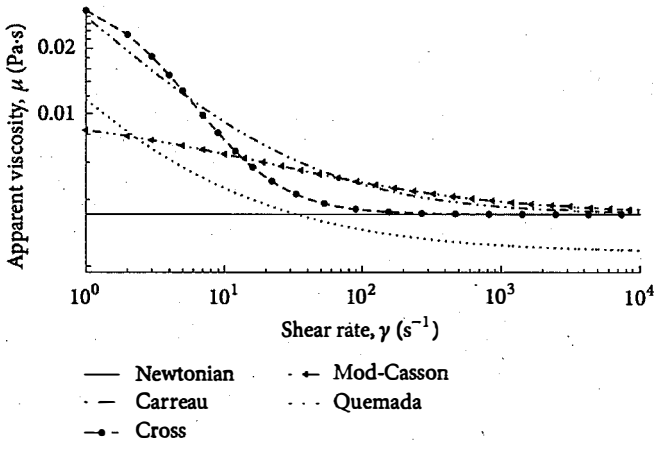

Fig. 4.4. Relations between the shear rate and the apparent blood viscosity for the different models, [105].

The relationship between the shear rates and viscosity for the non-Newtonian blood viscosity models, that is, Carreau, Cross, Modified Casson, and Quemada models along with the Newtonian viscosity model, is presented in Figure 4.4. Blood viscosity is constant in the Newtonian model shown by the solid line. Viscosity in the Carreau and Modified Casson models tends to asymptotic constant viscosity at the shear rate $\gamma > 10^4$ s^{-1}. The Quemada and the Cross models exhibit the non- Newtonian properties of blood at shear rates $\gamma < 10^2$ s^{-1}. Particularly, the Cross model asymptotically matches the constant viscosity at the shear rates $\gamma > 10^2$ s^{-1} whereas the Quemada model shows the asymptotic nature below the constant viscosity.

Thus, Cross model has been taken as the non-Newtonian viscosity model. Malcolm M. Cross [88] proposed a shear rate dependent viscosity model called Cross model. The Cross model is defined by $\mu = \mu_\infty + (\mu_0 - \mu_\infty)\left[1 + \left(\frac{|\dot{\gamma}|}{\gamma_c}\right)^m\right]^{-1}$

Where, $\mu_0 = 0.0364 Pa.s$ is the usual molecular blood viscosity for zero shear rates, $\mu_\infty = 0.00345 Pa.s$ when shear rates is high, shear rates, $\gamma_c = 2.63\ s^{-1}$ is the reference shear rate, $\dot{\gamma}$ is the instantaneous shear rate, and m=1.45 is the constant.

4.3 Governing equations

In the present study, we simulated our numerical modeling on blood flows with low Reynolds numbers ranging approximately from 86 to 966. In this range of Reynolds numbers, the viscous sub-layer is very much thick, so flow should be laminar theoretically. However, we used 85% constriction in a Carotid Artery for simulation, so blood passes through the throat and post stenotic region with high velocity. Naturally the Reynolds number will increase at the throat. Figure (4.5) presents the comparison of Re-Number variation with time at inlet and throat region of 85% stenotic Carotid Artery. The highest Reynolds number is about 3736 at the throat.

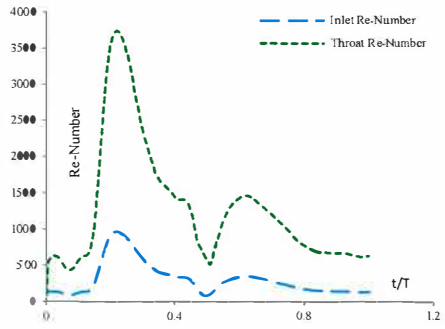

Fig. 4.5. Re-Number variation with time at 85% stenotic Carotid Artery.

Flow velocity at post stenotic region increases but pressure of that region decreases. In this situation, turbulent flow is expected at post stenotic region especially for highly severe stenotic artery. Neither laminar flow modeling nor standard two-equation models are suitable for this kind of blood flow. So, Wilcox

low-Re turbulence model is more acceptable for flow analysis found by Varghese and Frankel [89]. Therefore the Wilcox low-Re k-w turbulence model for our simulation has been chosen. However, in some part of this study laminar flow model has been used as governing equation for minimizing the complexity.

To strengthen the logic of using low Reynolds number k-w turbulence model in the calculation, the numerical results by the low Re-number k-w model were compared with the results by the laminar model in terms of velocity and wall shear stress. Figures 4.6 – 4.9 have shown the comparison of the velocity by the low-Re k-w model with the laminar model at early systole, peak systole, early diastole and diastole respectively for the Healthy Carotid Artery. Moreover, figures 4.10 – 4.13 have presented the comparison of the wall shear stress by the low-Re k-w model with the laminar model at early systole, peak systole, early diastole and diastole respectively for the Healthy Carotid Artery. From the figures it is revealed that the velocity and wall shear stress profiles by the low Re-number k-w model are in good agreement with the results by the laminar model. However, some little discrepancies are found in the results of velocity and wall shear stress distribution at early diastole due to disturbed flow. Therefore, there is no barrier to use low Reynolds number k-w turbulence model for the calculation. The equations are presented in the chapter three.

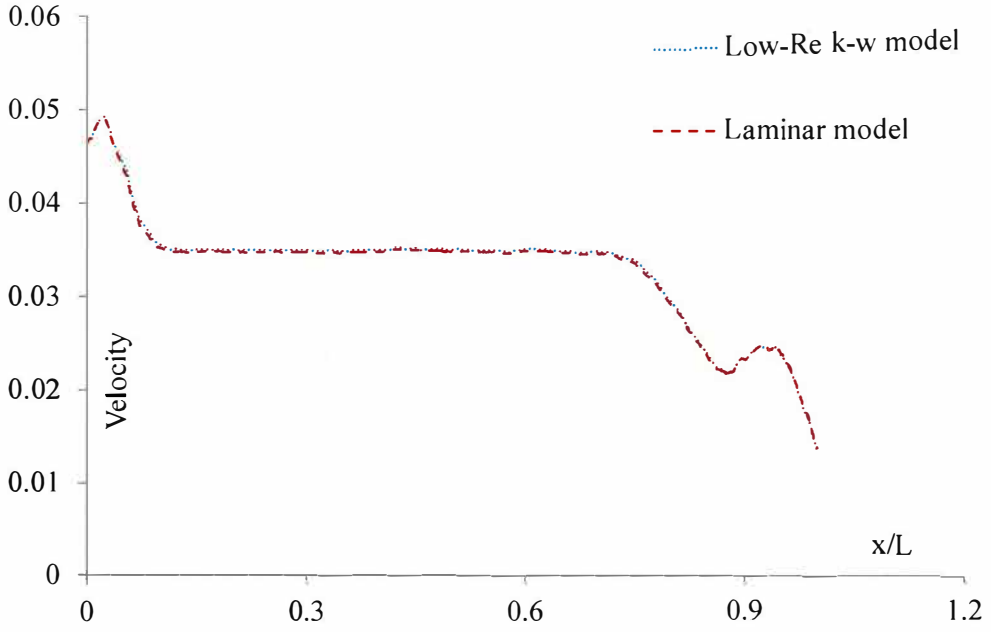

Fig. 4.6: Comparison of the velocity by the low-Re k-w model with the laminar model at early systole for the Healthy Carotid Artery.

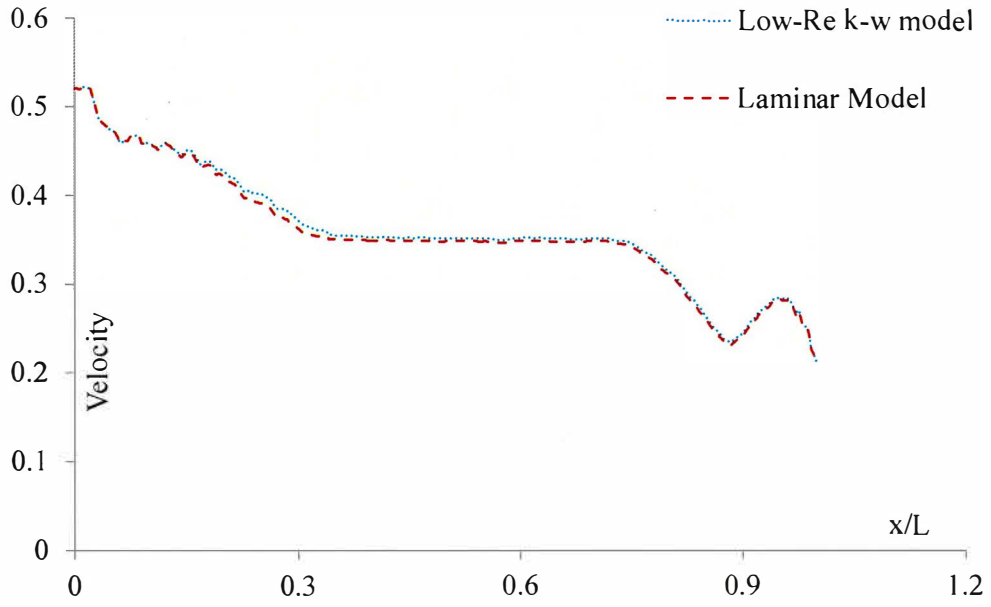

Fig. 4.7: Comparison of the velocity by the low-Re k-w model with the laminar model at peak systole for the Healthy Carotid Artery.

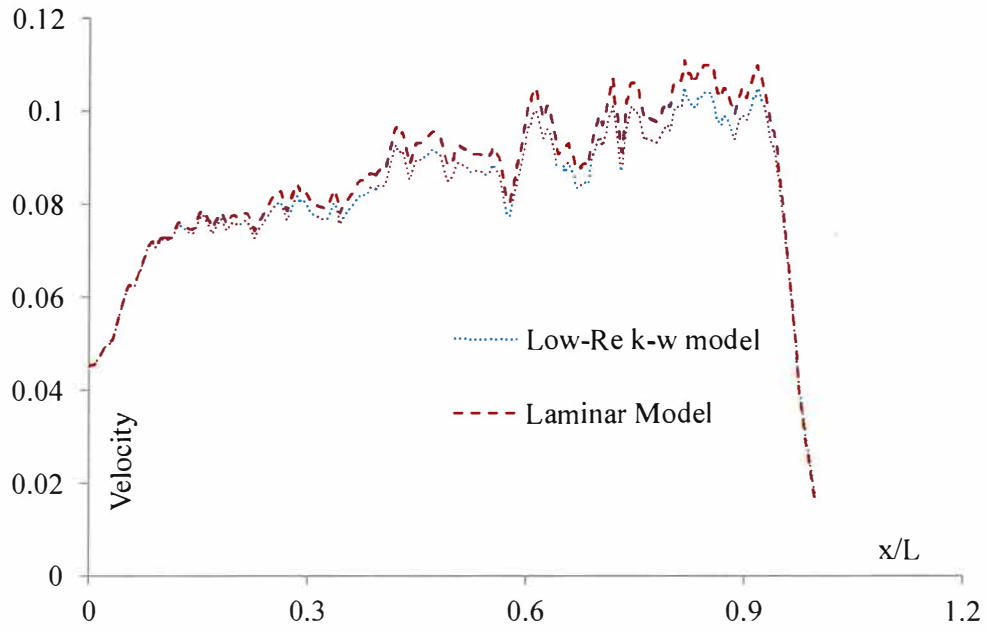

Fig. 4.8: Comparison of the velocity by the low-Re k-w model with the laminar model at early diastole for the Healthy Carotid Artery.

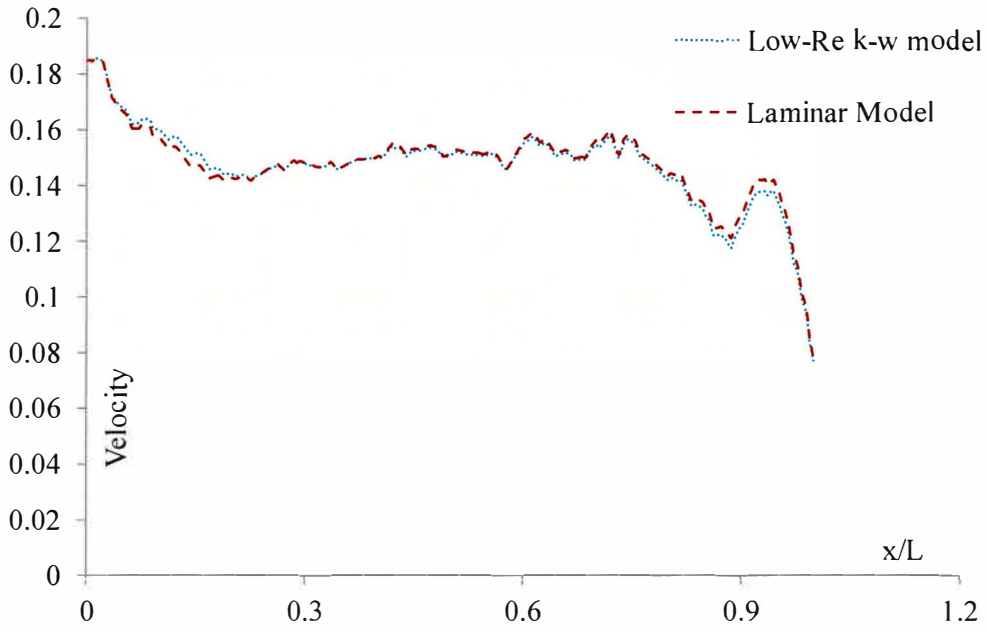

Fig. 4.9: Comparison of the velocity by the low-Re k-w model with the laminar model at diastole for the Healthy Carotid Artery.

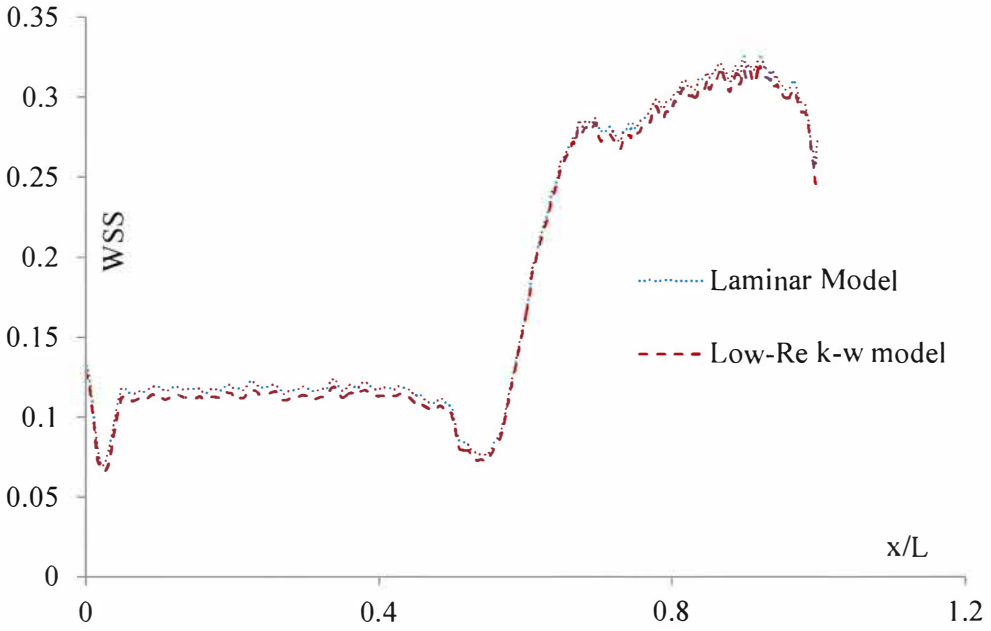

Fig. 4.10: Comparison of the Wall Shear Stress by the low-Re k-w model with the laminar model at early systole for the Healthy Carotid Artery.

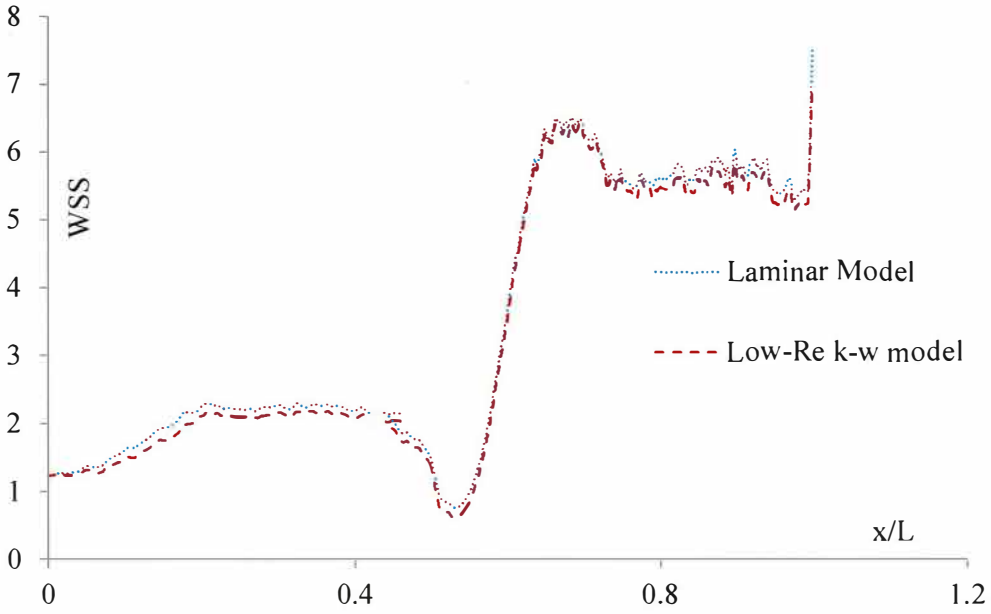

Fig. 4.11: Comparison of the Wall Shear Stress by the low-Re k-w model with the laminar model at peak systole for the Healthy Carotid Artery.

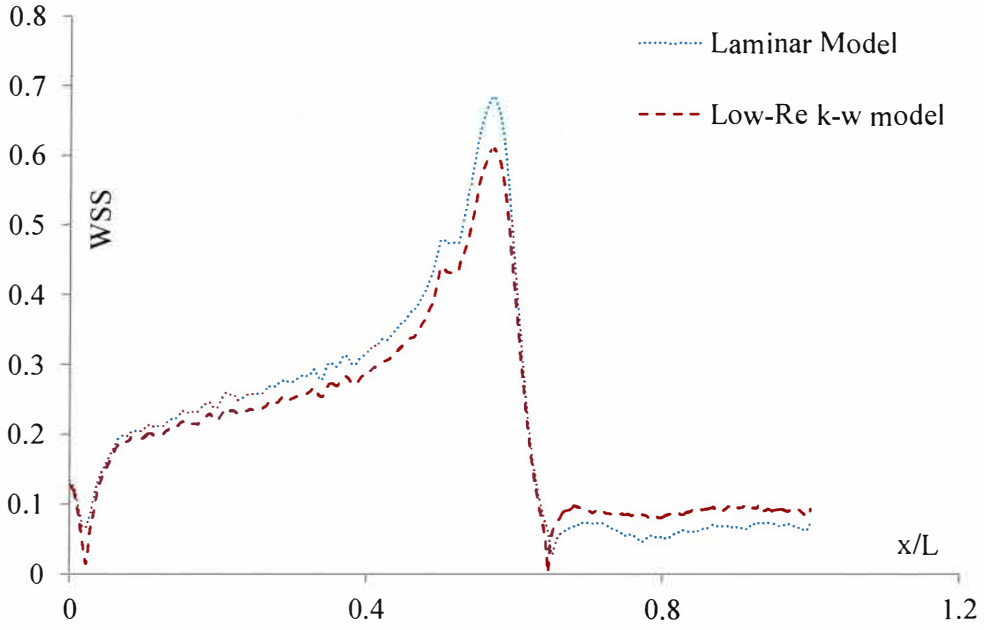

Fig. 4.12: Comparison of the Wall Shear Stress by the low-Re k-w model with the laminar model at early diastole for the Healthy Carotid Artery.

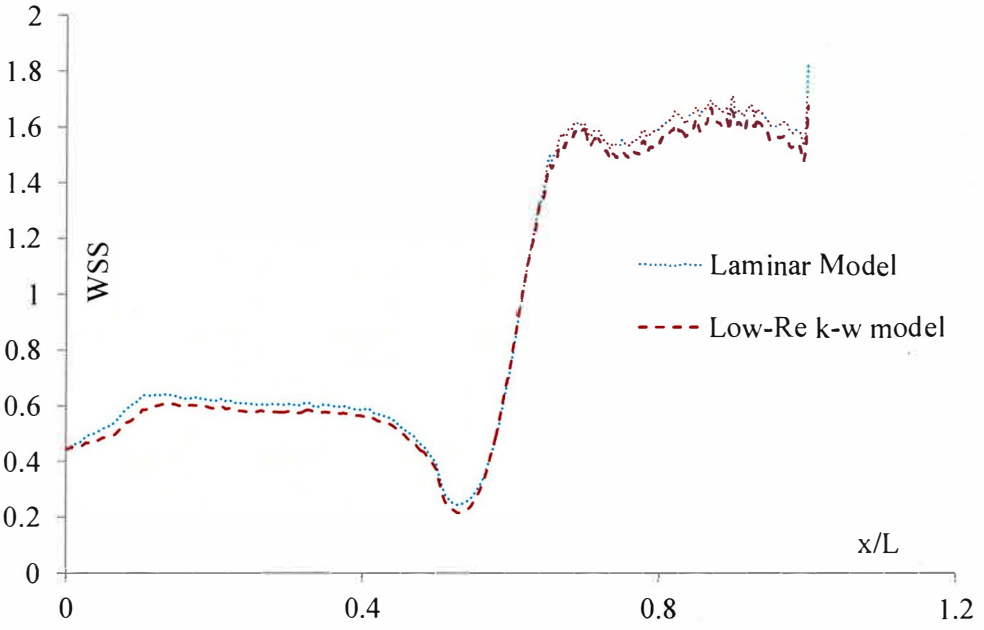

Fig. 4.13: Comparison of the Wall Shear Stress by the low-Re k-w model with the laminar model at diastole for the Healthy Carotid Artery.

4.4 Boundary conditions

Physiological, parabolic and spiral velocity profile has been imposed for the inlet boundary condition. Moreover, time dependent pressure profile has been taken for outlet boundary condition. For this purpose one user defined function has been written in C++ programming language to demonstrate the inlet and outlet boundary conditions. Axial velocity profile –

$$u_x = u\left(1 - \frac{y^2+z^2}{radius^2}\right) \tag{4.1}$$

Tangential velocity profile -

$$u_\theta = cu\left(\frac{(y^2+z^2)^{1/2}}{radius}\right) \tag{4.2}$$

The tangential velocity (u_θ) has been applied in the inlet as the spiral component and constant (c) determines the intensity of the flow spirality. Besides, the values of 'c' have been changed from 0 to 2.5 for different simulations, which have been presented in Table 1 of the Appendix 1. However, the spiral velocity has been shown by the Figure 4.15 (c). Where –

$$u = \sum_{n=0}^{n=16}(A_n\, cos(nft) + B_n\, sin(nft)) \tag{4.3}$$

Pressure outlet profile –

$$p = \sum_{n=0}^{n=16}(C_n \cos(nft) + D_n \sin(nft)) \quad (4.4)$$

Where, A_n, B_n, C_n and D_n are the coefficients getting from Finol and Amon [94], which have been presented in the Table 4.1 and 4.2. Since cardiac pulse cycle is 0.82sec, f is found from the equations (4.3, 4.4). Where –

$$f = \frac{2\pi}{0.82} = 7.66 \text{ rad/sec} \quad (4.5)$$

Table 4.1: Harmonic coefficients for physiological waveform of velocity profiles.

n	A_n	B_n	n	A_n	B_n	n	A_n	B_n
0	0.166667	0	6	0.01735	0.01915	12	-0.00341	0.005463
1	-0.03773	0.0985	7	-0.00648	0.002095	13	-0.00194	0.000341
2	-0.10305	0.012057	8	-0.01023	-0.0078	14	-0.00312	-0.00017
3	0.007745	-0.06763	9	0.008628	-0.00663	15	0.000157	-0.00299
4	0.025917	-0.02732	10	0.002267	0.001817	16	0.001531	0.000226
5	0.037317	0.024517	11	0.005723	0.003352			

Table 4.2: Harmonic coefficients for physiological waveform of pressure profiles.

n	C_n	D_n	n	C_n	D_n	n	C_n	D_n
0	90	0	6	1.4574	1.6086	12	-0.28644	0.458892
1	-3.16932	8.274	7	-0.54432	0.17598	13	-0.16296	0.028644
2	-8.6562	1.012788	8	-0.85932	-0.6552	14	-0.26208	-0.01428
3	0.65058	-5.68092	9	0.724752	-0.55692	15	0.013188	-0.25116
4	2.177028	-2.29488	10	0.190428	0.152628	16	0.128604	0.018984
5	3.134628	2.059428	11	0.480732	0.281568			

Fig. 4.14 (a) and 4.14 (b) show physiological waveform of inlet velocity and pressure outlet profiles respectively. Besides, Fig. 4.15 (a) and 4.15 (b) present the graph and contour of the parabolic inlet velocity profile respectively.

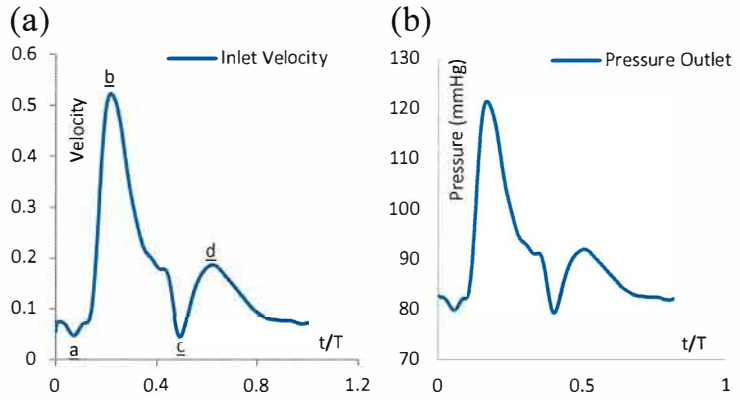

Fig. 4.14. Physiological waveform of (a) velocity and (b) pressure profiles.

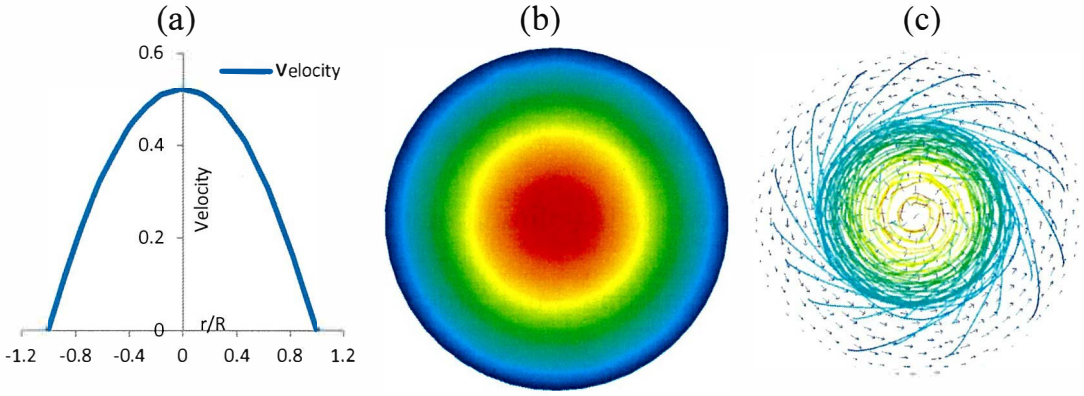

Fig. 4.15. (a) Graph and (b) contour of parabolic inlet velocity profile; and (c) streamlines and vector distribution of the spiral flow at inlet.

The hemodynamic parameters were measured at four different time instants during the cardiac cycle. These four time instants represent critical flow rate phases in the cardiac cycle. In figure 4.14 (a), a, b, c and d represent the positions of early systole (0.0574 sec), peak systole (0.1804 sec), early diastole (0.41 sec) and diastole (0.5125 sec) respectively. However, early systole is the condition when the blood starts its journey of flowing through the arteries. Actually, it is the beginning time of rising arterial pressure. Besides, peak systole happens when the arterial

pressure is highest. On the other hand, when arteries are relaxed and allow for the new blood to flow, it is known as diastole.

4.5 Computational Details

4.5.1 Numerical Scheme: The numerical simulations are performed by well-known software ANSYS Fluent 18.1. A pressure based algorithm is chosen as the solver type. This solver is generally selected for an incompressible fluid. As there is no heat transfer in the blood flow process, energy equation is not solved. Since turbulent is expected for the throat of 85% severity, a low Re $k-\omega$ turbulent mode is used throughout the work. In solution methods, the SIMPLE algorithm is selected for pressure-velocity coupling. First Order Upwind scheme is employed as a numerical scheme for discretization of the momentum equation. Figure 4.16 shows the velocity distribution in 55% stenotic artery for 1^{st}, 2^{nd}, and 3^{rd} order upwind schemes for checking scheme independence. The time step is set to 0.00041 sec with 2000 number of total time steps. Maximum 20 iterations are performed per each time step.

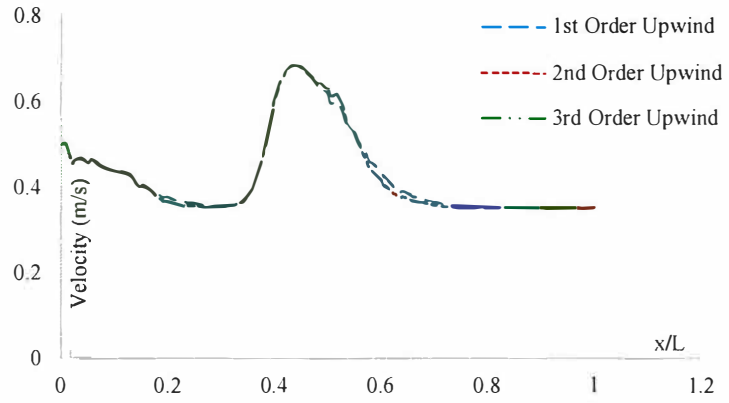

Figure 4.16: Velocity distribution in 55% stenotic artery for different order upwind schemes.

4.5.2 FSI Model: ANSYS provides several methods for performing Fluid-Structural Interaction. One recommended method is two-way coupling employed by utilizing the ANSYS. Thus, two way fluid-structure interaction (FSI) system coupling in ANSYS Fluent has been used for modelling the artery as elastic. Figure 4.17 shows the two way FSI model in ANSYS workbench. Actually, the solution to two-way fluid-structure interaction requires co-simulation between computational fluid dynamics and structural mechanics. In this method, the fluid and solid portions are solved simultaneously by the system coupling in ANSYS workbench. This is performed by creating fluid and solid geometries separately in ANSYS fluent and ANSYS structure respectively using ANSYS DesignModeler of workbench, applying the appropriate meshing and then applying the appropriate boundary conditions. In engineering data of transient structure the Young's

modulus and Poisson's ratio of the artery are taken as 1.08 pa and 0.49 respectively for modeling the artery as elastic. The appropriate boundary on which FSI occurs is flagged using the surface interface command, which allows the transfer of fluid and solid forces, solid displacements and velocities across the boundary. This effectively allows for effective two-way coupling for the FSI process. In addition to the individual physics solver options, it is necessary to also specify the method in which the FSI process is solved. This includes the transient properties of the process and the order in which the solution is solved. In this study, the solution solves the fluid portion first as the fluid forces will be used to determine the solid model deformation rather than the other way around. It is also important to specify the FSI iteration details including the number of iterations for the coupling process and the convergence criterion for the values that determine convergence. By default, these values are the maximum structural displacement, fluid force, and moment magnitudes. These values are checked to ensure that there is only a 0.5% difference by default between successive iterations to achieve a converged status. After specifying these details, the solution process can be run.

The FSI iterative process for this study started by solving the fluid portion first. The fluid pressures that were derived by solving the fluid portion were taken and applied to the interface boundary. The loadings on each node were derived via interpolation along the interface boundary and then this loading determined the

structural response, i.e. displacement and velocity. Once the solid model had been solved, the new nodal locations along the interface boundary determined the morphing of the fluid model meshing. Following the mesh update, the fluid model would interpolate to derive the values for the new mesh. Then, the fluid model was solved again and the process was repeated. This was repeated until the structural displacement and moment magnitudes, which were related to the fluid force, were converged as discussed earlier. Once convergence was reached, the processor exited the FSI loop and proceeded to the next time-step in the solution. This iterative process is illustrated below in Figure 4.18.

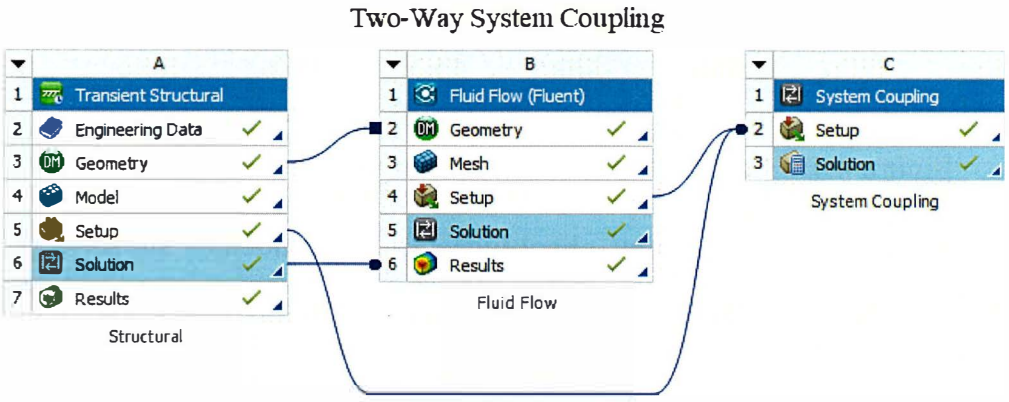

Figure 4.17: Two way fluid-structure interaction system coupling in ANSYS fluent.

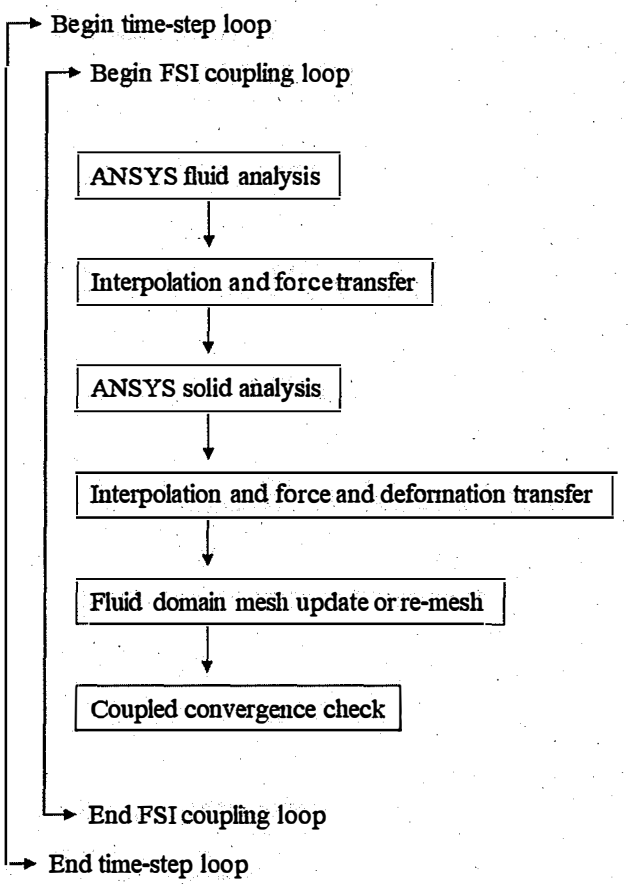

Figure 4.18: Basic setup of a two-way coupling method for FSI

4.5.3 Mesh independency checking: Grid dependency study is the first preference of any numerical simulation. For this purpose an extensive test is carried out with different sizes of mesh such as mesh0 (755211 element), mesh1 (825280 element) and mesh2 (902227 element) respectively. Figure 4.19 shows the pressure distributions for 65% stenosis artery with mentioned mesh sizes. In all cases, the pressure distributions are same. It implies that the solution is grid independence.

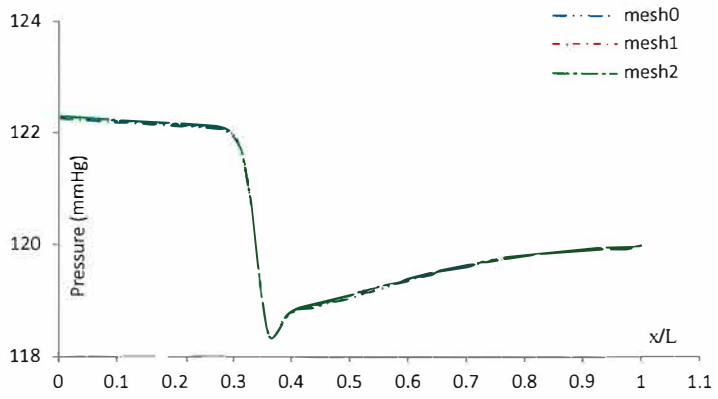

Figure 4.19: Mesh independency checking with pressure distribution in 65% stenotic artery from different mesh sizes.

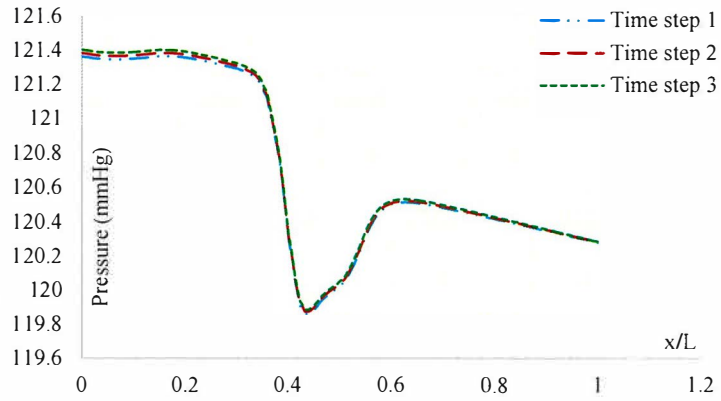

Figure 4.20: Time-Step independency checking with pressure distribution in 55% stenotic artery for different time step sizes.

4.5.4 Time-Step sizes and cardiac cycle independency checking: three time step sizes such as Time-step 1 (0.041 sec), Time-step 2 (0.0041 sec) and Time-step 3 (0.00041 sec) are taken to check independency. Figure 4.20 shows the pressure distributions for 55% stenotic artery with mentioned time step sizes. In both cases,

the pressure distributions are same. It implies that the solution is time step sizes independence.

However, Figure 4.21 shows the velocity distribution at peak systole in 55% stenotic artery for different cardiac cycles for checking the cardiac cycle independence. Peak systole in first, second, third, fourth and fifth cardiac cycles are 0.1804 sec., 1.0004 sec., 1.8204 sec., 2.6404 sec., and 3.4604 sec. respectively. It implies that the solution is cardiac cycle independence.

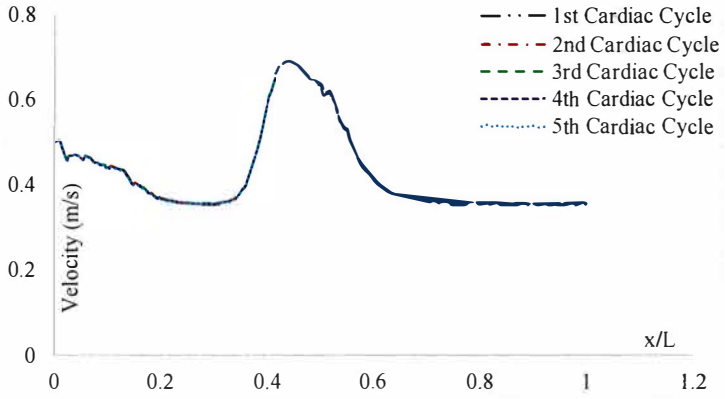

Figure 4.21: Velocity distribution at peak systole in 55% stenotic artery for different cardiac cycles.

4.5.5 Validation: Before starting of present investigation the numerical simulation is needed to be validated. Validation of the present numerical computation is done by plotting the steady velocity profile at 2.5D downstream from the stenosis throat and comparing it with the velocity profile of Varghese and Frankel [89]. For this case, a parabolic velocity profile is assumed as inlet

boundary condition. The mean inlet velocity corresponds to Reynolds number 500 and the flow is assumed to be steady. The results are shown in the Figure 4.22, where a good agreement can be found with Varghese and Frankel [89].

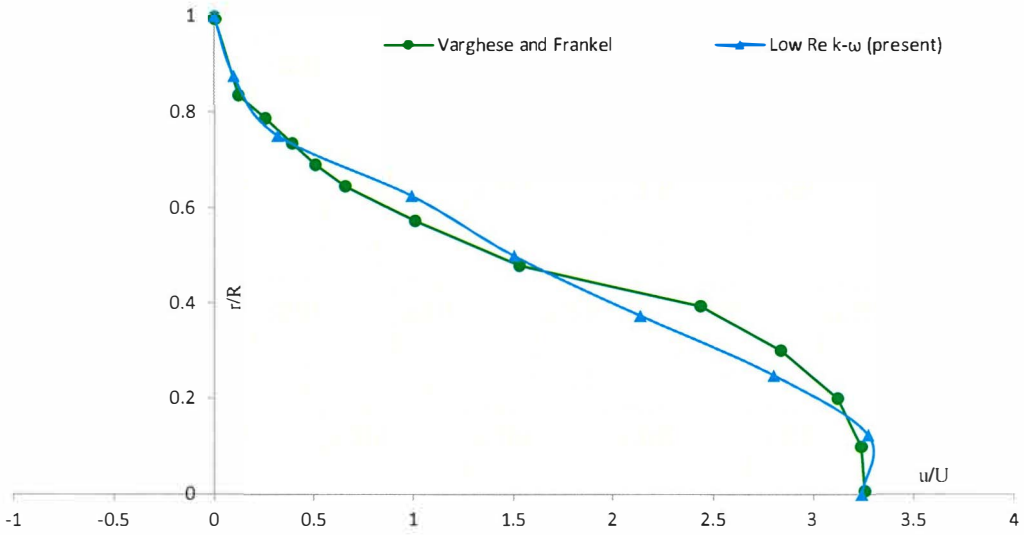

Figure 4.22: Comparison of computed steady velocity profile.

Another validation of the two way system coupling computation is done by plotting the unsteady velocity profiles at three different locations in the post-stenotic region 1D, 2.5D and 4.3D from the center of the stenotic throat and comparing it with the velocity profile of rigid wall and the experimental data obtained by Ohja et al [93]. The flow waveform is actually the same as used by Ohja et al in their experiment. The period of the flow cycle in this computation equals 0.35 s. For this computation blood is taken as Newtonian fluid. The comparative results are shown in the Figures 4.23 – 4.25. It is found greater

differences between the numerical and experimental data to occur during the flow deceleration phase. This simulation gave a maximum difference of 15% and an average of 5% at 1D. It was found that better agreement was achieved in the immediate post-stenotic region. A noted effect within the FSI model is that the flow waveform trough is further widened and the crest further narrowed than in the rigid model. In the acceleration phase, it is seen that the FSI model has a lower gradient than even the rigid model. This is again attributed to the vessel wall movement, which expands further during the acceleration phase to accommodate the increasing pressure, which drives the flow.

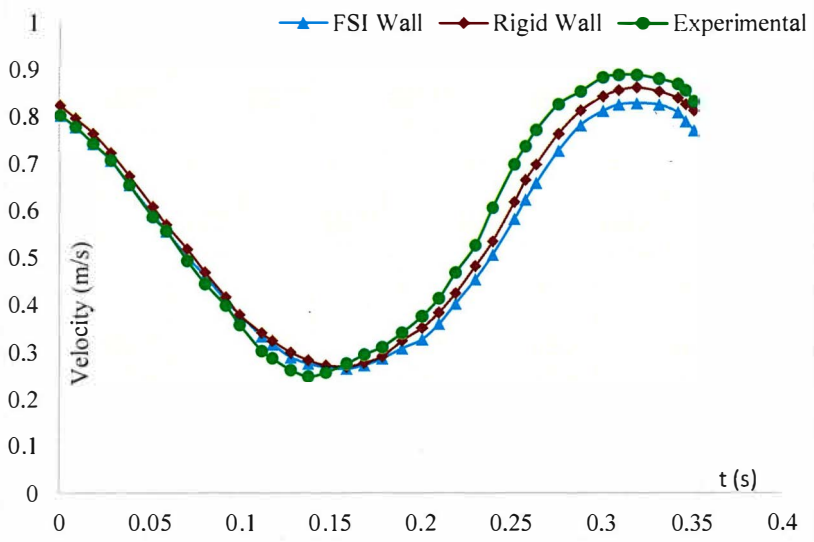

Figure 4.23: Comparison of centerline axial velocity between FSI model, rigid wall model and experimental measurements at post-stenotic distances 1D.

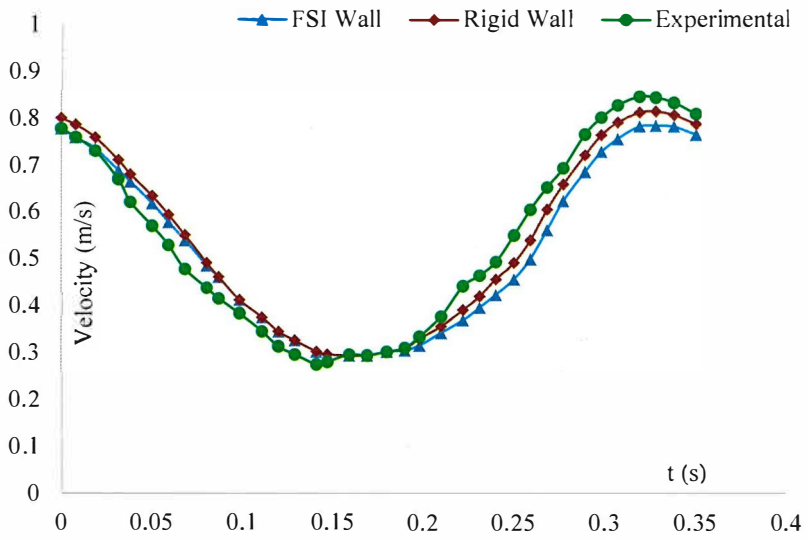

Figure 4.24: Comparison of centerline axial velocity between FSI model, rigid wall model and experimental measurements at post-stenotic distances 2.5D.

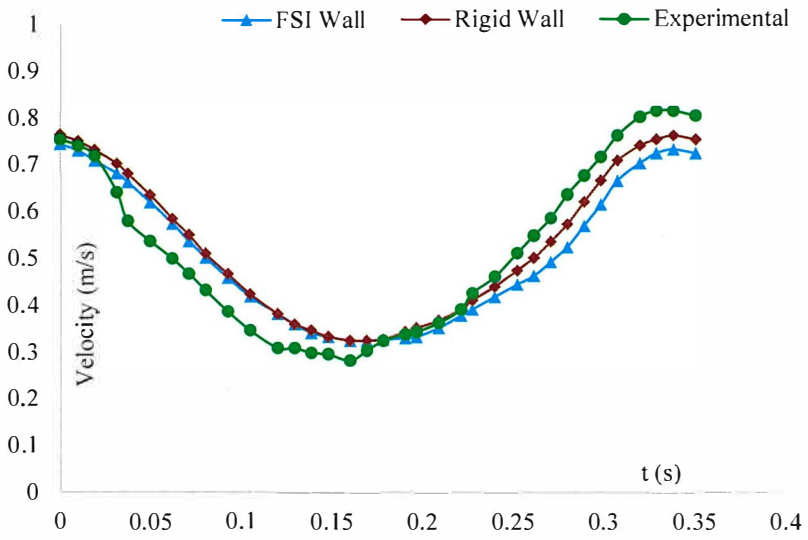

Figure 4.25: Comparison of centerline axial velocity between FSI model, rigid wall model and experimental measurements at post-stenotic distances 4.3D.

4.6 Statistical analysis

ANSYS fluent has been used for calculation to get statistical data of physiological parameters. The main objective of this study is to find out relationship among the parameters with the stenotic shape and flow spirality. The wall shear stress, pressure, and velocity are considered as the dependent variables, whereas the stenotic severity, eccentricity, length and flow spirality are taken as independent variables to analyse the relationship among them. However, stenotic severity, eccentricity, length and flow spirality are taken as non-dimensional variables. Well known statistical software SPSS has been used for the analysis. Multivariable linear regression analyses have been used to determine the relationships among them. However, P value less than 0.05 has been considered as significant level for the study.

Chapter 5

Results and Discussion

Overview

This chapter presents various results of this study by depicting graphs, contour's images and table representations, then results are discussed for better understanding.

5.1 Results and discussion of blood flow through carotid arteries

The computational results are taken to study the influence of stenosis and bifurcation on the flow behavior. Actually, transient or unstable flow separation that creates flow disturbance regions is associated with a predisposition to atherosclerosis at branches, bifurcations and curvatures in the arterial circulation. Therefore, a study has been performed to demonstrate the significant changes of flow behaviour through arterial stenosis as well as to understand the blood dynamics in carotid arteries of different severities by analyzing the velocity, streamline, pressure and wall shear stress distributions.

The interaction between hemodynamic and the endothelium is an important determinant of cardiovascular function. Actually, Wall Shear Stress is very essential factor for understanding the severity level of arterial diseases. Endothelium lining the circulatory system is highly sensitive to hemodynamic

shear stresses that act at the vessel surface in the direction of blood flow. A prolonged high wall shear stress fragments the internal elastic lamina of vessels and gives rise to the initial change involved in the formation of an atherosclerosis or an aneurysm. Actually, it is a flow-induced stress that can be described as the frictional force of viscous blood. Besides, it is the force per unit area created when a tangential force due to blood flow acts on the vessel's surface (endothelium). Thus, it acts directly on the vascular endothelium as a biological stimulator that modulates the cellular function of the endothelium. However, it can be determined by the mean fluid flow rate, its viscosity, and the physical dimensions of blood vessels. For Poiseuille flow, shear stress (τ) is directly proportional to the velocity of blood flow, and inversely proportional to the cube of the arterial radius (R), where Q is flow rate and μ is fluid viscosity. Then, $\tau = 4\mu Q/R^3$. Thus, small changes in R greatly influence τ, and vice versa. In the arterial circulation, WSS has a vital role in determining where most vascular pathology originates. Moreover, it is responsible for the development of endothelial phenotypic changes in which the metabolic balance is disrupted that are associated with the initiation and development of the atherosclerosis. High WSS elongates the endothelial cells and force to align in the direction of the flow. On the other hand, low WSS had negligible effect on the cell but increases intercellular permeability and consequently increases the plaque formation in the region. Thus, endothelial cells

react differently to the high and low WSS. Consequently, WSS is mostly responsible for creating a new stenosis throat. Moreover, the proximity of high and low WSS in a small aneurysm region might enhance the degenerative change of the aneurysm wall.

Figures 5.1, 5.2, and 5.3 show the distributions of Wall Shear Stress in healthy, 65%, and 85% stenotic Carotid arteries respectively at peak systole. No significant variation in WSS has been seen in healthy carotid artery. The highest WSS of the healthy artery is approximately 13 Pa. However, remarkable changes in WSS are noticed at throat and bifurcation regions of the stenotic carotid arteries. Besides, the highest WSS of the 65% and 85% stenotic arteries are about 32 Pa, and 113 respectively. The WSS has increased abnormally at the 85% stenotic Carotid artery. From the figure 5.4, it is clear that bifurcation area of 85% stenotic carotid artery generates the highest WSS, so bifurcation region is the most risky area of the carotid artery.

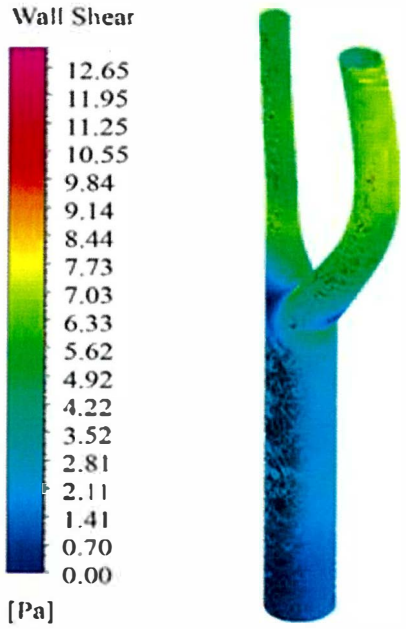

Fig. 5.1: Wall Shear Stress distributions in healthy Carotid artery at peak systole.

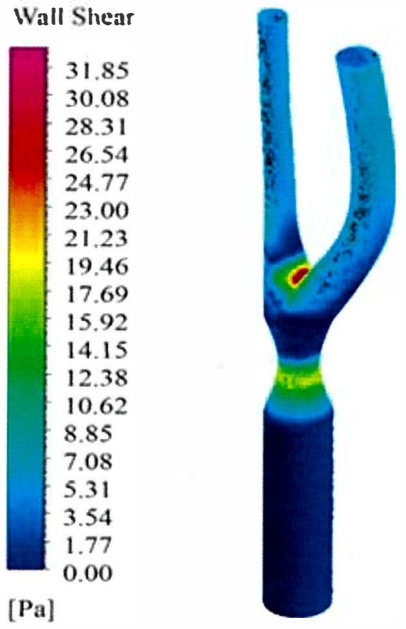

Fig. 5.2: Wall Shear Stress distributions in 65% stenotic Carotid artery at peak systole.

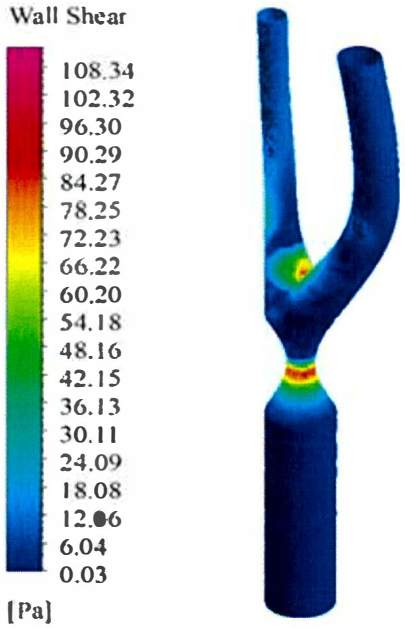

Fig. 5.3: Wall Shear Stress distributions in 85% stenotic Carotid artery at peak systole.

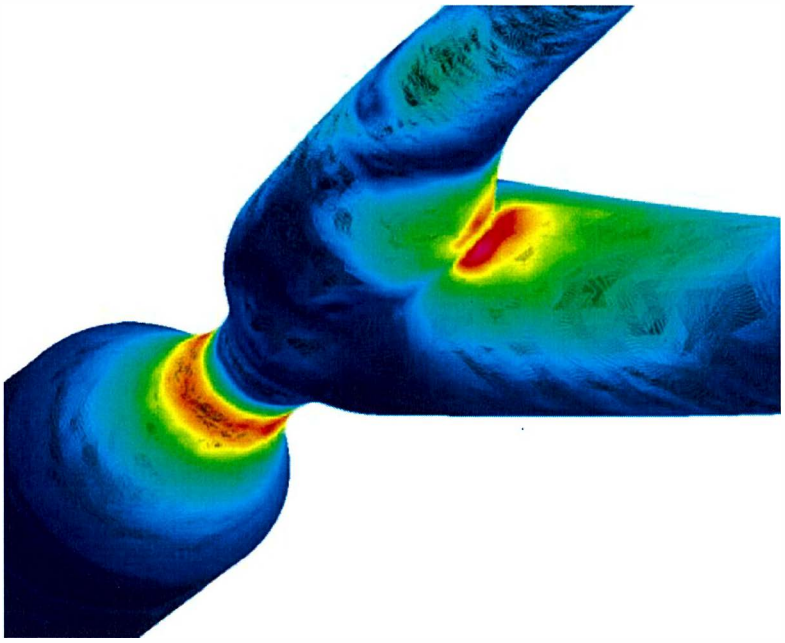

Fig. 5.4: Wall Shear Stress distribution at the throat and bifurcation region of 85% stenotic Carotid artery at peak systole.

Variations of streamlines contours have been investigated for healthy and stenotic carotid arteries to study the flow pattern of blood through the arteries. Streamline distribution for the healthy, 65%, and 85% stenotic arteries at peak-systole are shown in figures 5.5, 5.6, and 5.7 respectively. There is no recirculation region in the healthy artery and streamlines run smoothly throughout the geometries. However, a very small recirculation region is noticed after the throat and near the bifurcation area of 65% stenotic carotid artery, except this most of the streamlines run smoothly throughout the geometry. A disturbed flow has been found in 85% stenotic carotid artery. The recirculation region has started at the throat and continued to be disturbed at the internal and external carotid arteries. The stenotic jets have been appeared in the stenotic carotid arteries due to the constriction of the arteries. From figure 4.5 it has been noticed that Reynolds number rose abnormally at peak systole at throat region of 85% stenotic carotid artery. Thus, it was expectable that the flow might be disturbed at peak systole in the 85% stenotic carotid artery. However, at early diastole the Reynolds number is very low. Thus, the flow should be smooth, but from figures 5.8, 5.9, and 5.10 it has been found that the flows are very disturbed in the healthy, 65%, and 85% stenotic arteries respectively, and the recirculation region have also appeared, even in the healthy artery. How is it possible without any constriction of artery and with very low Reynolds number?

Thus, steady flow has been investigated in the healthy artery remaining all the condition same as like as unsteady flow at early diastole. The result has been shown in the figure 5.11 and it has been noticed that there is no recirculation region and the flow is very smooth. Therefore, it can be said that transient or unstable flow can create flow disturbance regions in the arteries as well.

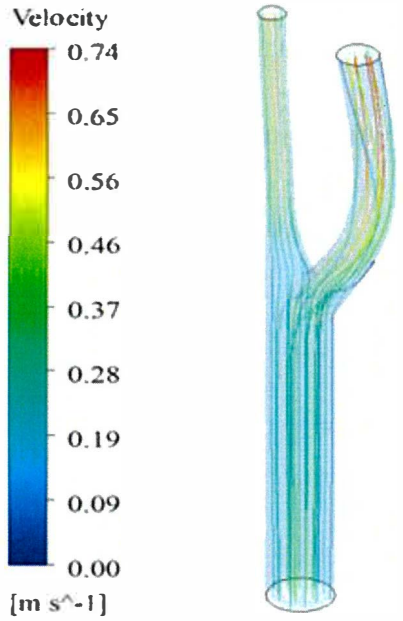

Fig. 5.5: Streamlines distributions in healthy Carotid artery at peak systole.

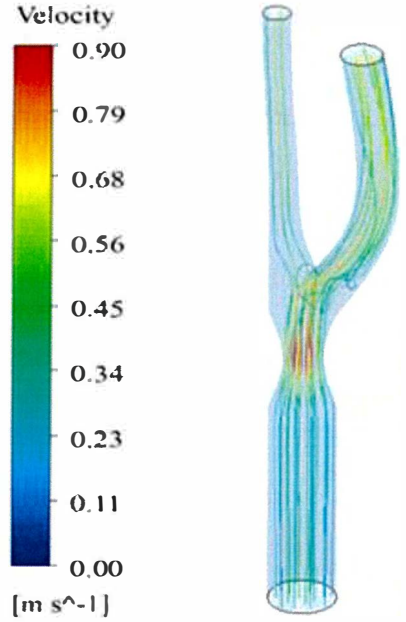

Fig. 5.6: Streamlines distributions in 65% stenotic Carotid artery at peak systole.

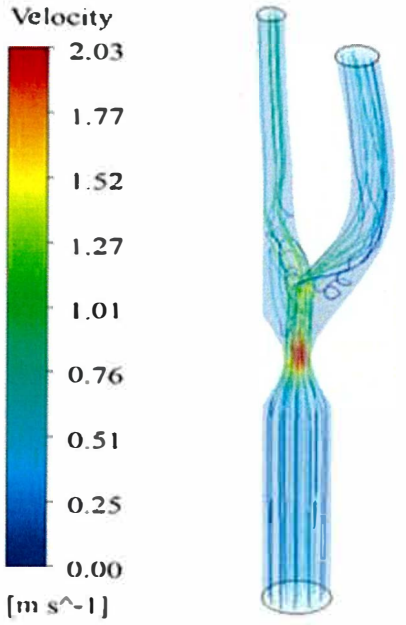

Fig. 5.7: Streamlines distributions in 85% stenotic Carotid artery at peak systole.

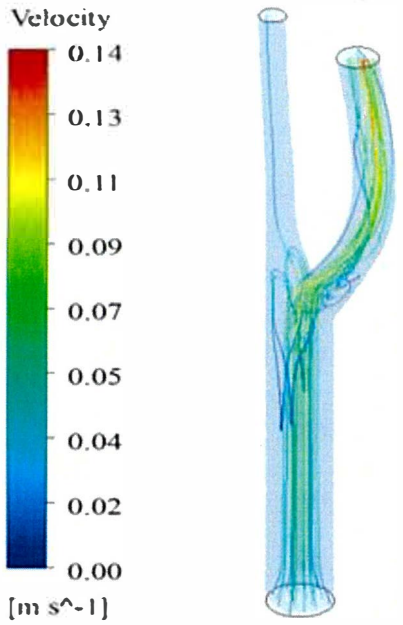

Fig. 5.8: Streamlines distributions in healthy Carotid artery at early diastole.

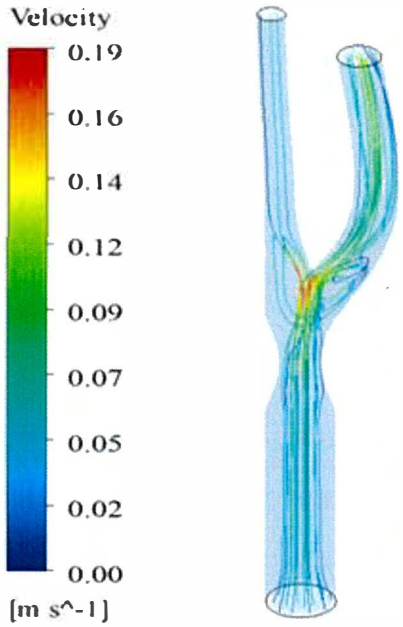

Fig. 5.9: Streamlines distributions in 65% stenotic Carotid artery at early diastole.

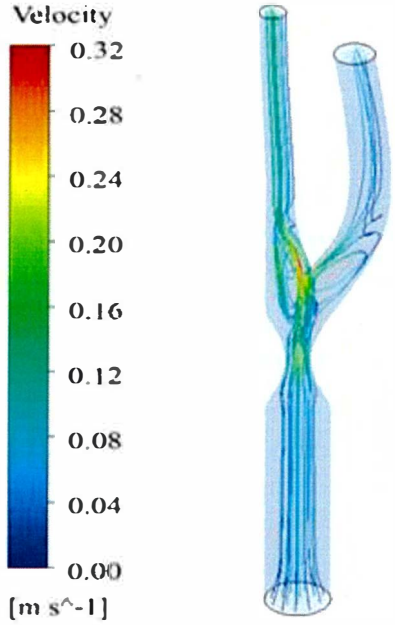

Fig. 5.10: Streamlines distributions in 85% stenotic Carotid artery at early diastole.

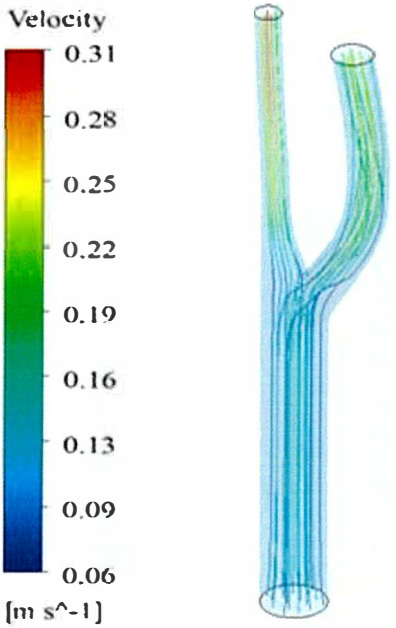

Fig. 5.11: Streamlines distributions for steady flow in healthy Carotid artery.

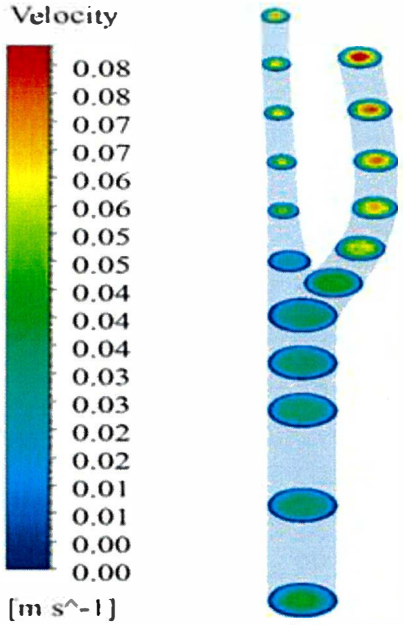

Fig. 5.12: Axial velocity on different axial slices of healthy Carotid Artery at early systole.

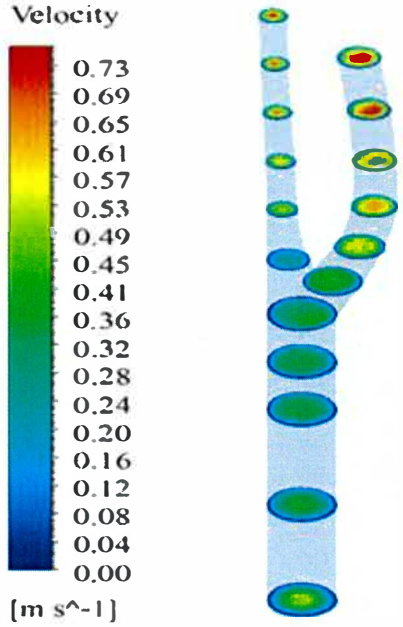

Fig. 5.13: Axial velocity on different axial slices of healthy Carotid Artery at peak systole.

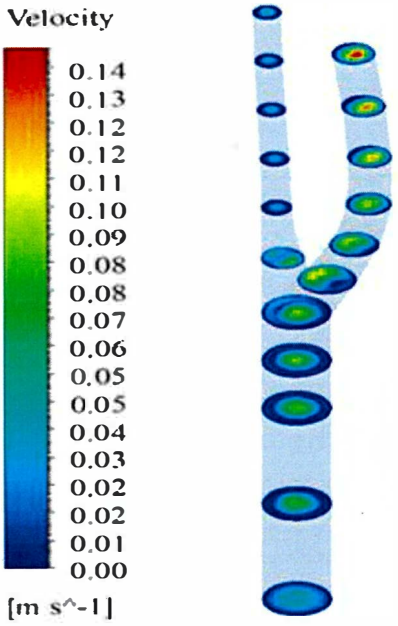

Fig. 5.14: Axial velocity on different axial slices of healthy Carotid Artery at early diastole.

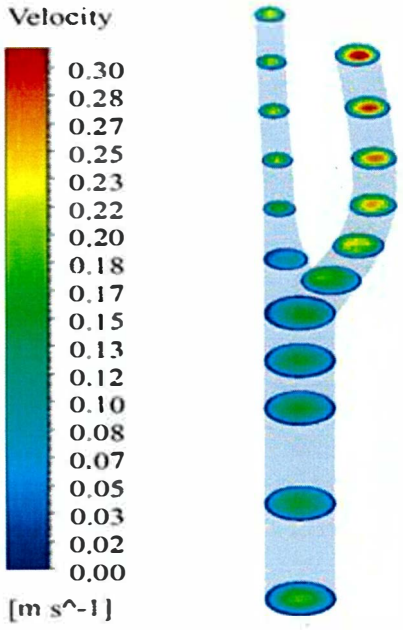

Fig. 5.15: Axial velocity on different axial slices of healthy Carotid Artery at diastole.

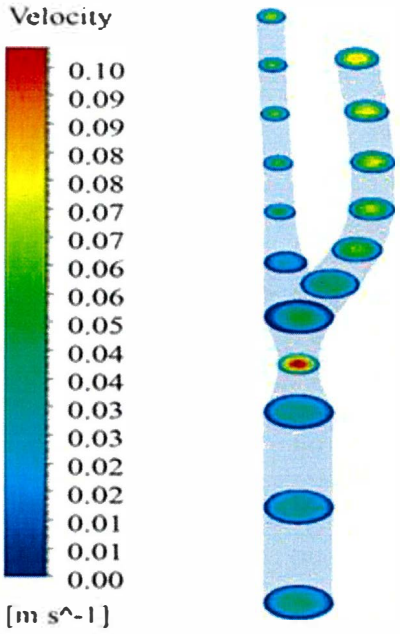

Fig. 5.16: Axial velocity on different axial slices of 65% stenotic Carotid Artery at early systole.

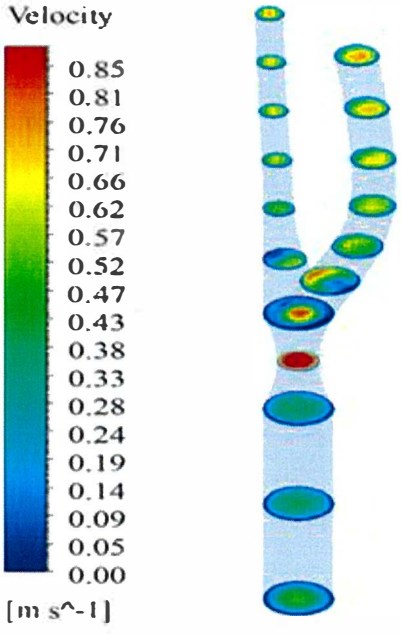

Fig. 5.17: Axial velocity on different axial slices of 65% stenotic Carotid Artery at peak systole.

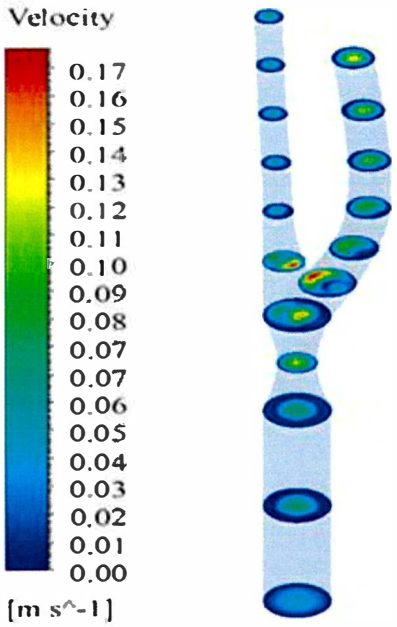

Fig. 5.18: Axial velocity on different axial slices of 65% stenotic Carotid Artery at early diastole.

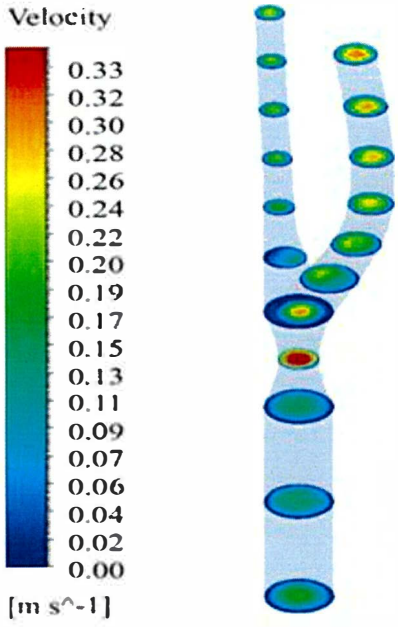

Fig. 5.19: Axial velocity on different axial slices of 65% stenotic Carotid Artery at diastole.

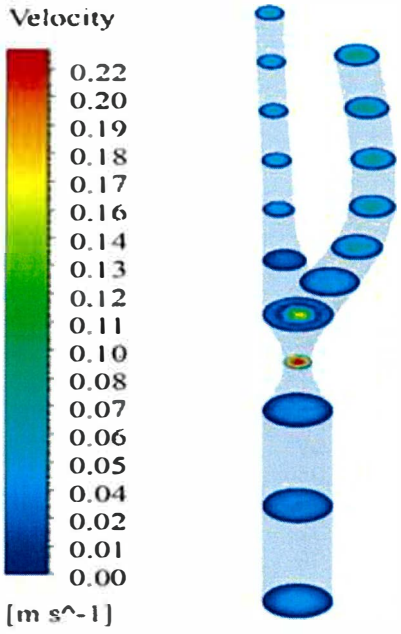

Fig. 5.20: Axial velocity on different axial slices of 85% stenotic Carotid Artery at early systole.

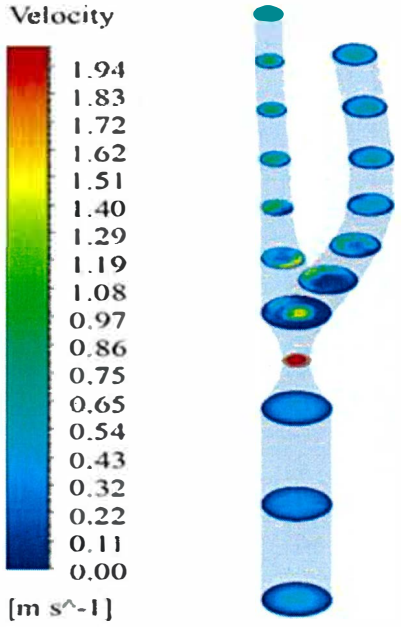

Fig. 5.21: Axial velocity on different axial slices of 85% stenotic Carotid Artery at peak systole.

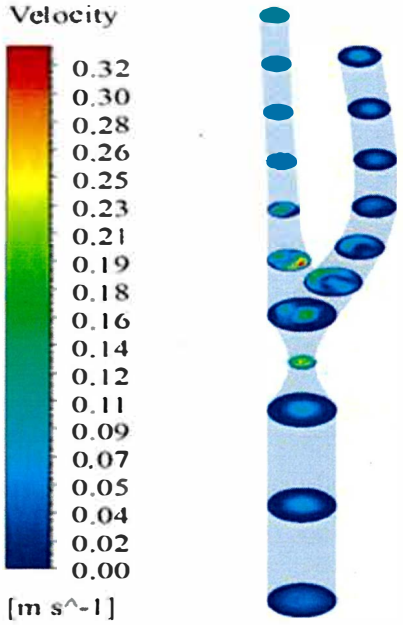

Fig. 5.22: Axial velocity on different axial slices of 85% stenotic Carotid Artery at early diastole.

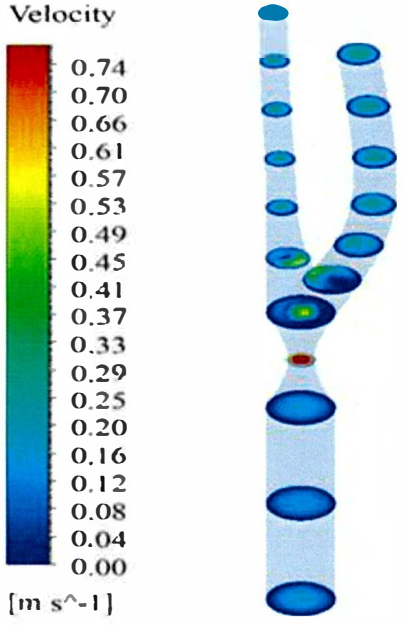

Fig. 5.23: Axial velocity on different axial slices of 85% stenotic Carotid Artery at diastole.

The figures 5.12 – 5.23 present the contour distribution of the axial velocity on different axial slices of carotid arteries at four time instants such as early systole, peak systole, early diastole and diastole. These figures shows the flow disturbances in the carotid arteries. As is observed, the flow has been disturbed in 85% stenotic carotid artery at all of the cardiac cycle. According to the figures, in healthy artery there is no disturbed flow at the whole cardiac cycle except the early diastole. The reason behind this, which has already been described, is unsteady flow condition. Meanwhile, a moderate disturbed flow has been seen in the 65% stenotic carotid artery at the whole cardiac cycle except the early systole. Moreover, a similar pattern but more severe disturbance in the flow is observed in the 85% stenotic carotid artery. In brief, disturbance of flow has risen as the severity of stenosis in the artery has been increased.

From the investigation it is concluded that bifurcation area is the most risky region of carotid artery because highest wall shear stress is observed there. Another observation is that transient or unstable flow can create flow disturbance regions in the arteries. Moreover, the disturbance of flow has risen as the severity of stenosis in the artery has been increased.

5.2 Comparative study of blood flow through arteries of elastic and rigid walls

A study has been done to present the comparisons of results getting from the blood flow through arteries of elastic and rigid walls. In other word, the computational results have been presented to demonstrate the influence of stenosis on the flow behavior as well as to compare the results getting from rigid wall and elastic wall arteries. The flow parameters like pressure, velocity and Wall Shear Stress (WSS) have been observed at specific instants of pulse cycle for the comparison. The discussion has been categorized with the observations of the flow at early systole, peak systole and diastole respectively.

Pressure within the artery is an important characteristic as it can determine the resistance against the flow in the vessel. A large pressure drop promotes forward flow in the artery in the artery. However, the flow will experience resistance and have a tendency to stagnate or even reverse flow if a significant pressure difference is not present in the artery. In transient flows, flow pressure plays a significant role in determining the fluid behavior even in simple geometries. Besides, an abrupt change in pressures produces the regions of extremely low or high pressures, where fluid pressure is used to determine the resulting displacement of the structure.

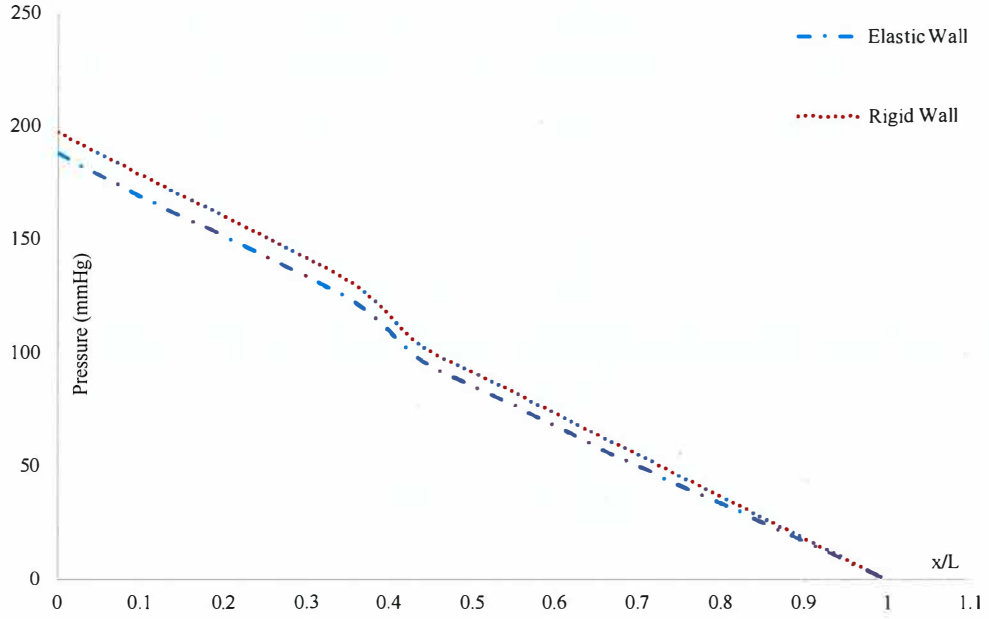

Fig 5.24: The comparison of pressure distributions of elastic wall and rigid wall artery at early systole for 45% stenotic arteries.

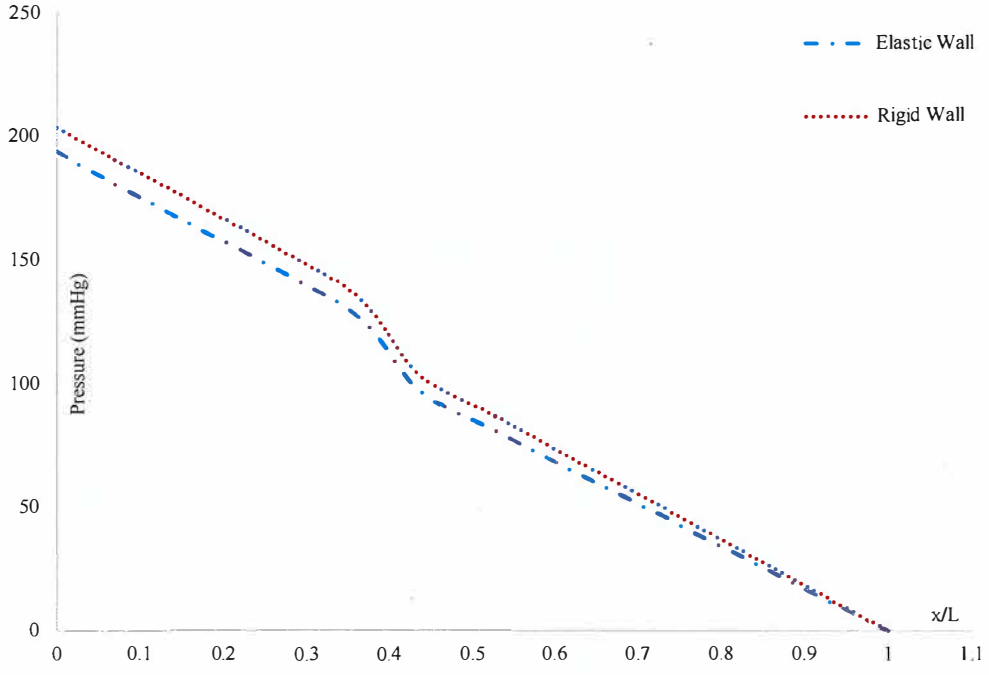

Fig 5.25: The comparison of pressure distributions of elastic wall and rigid wall artery at early systole for 55% stenotic arteries.

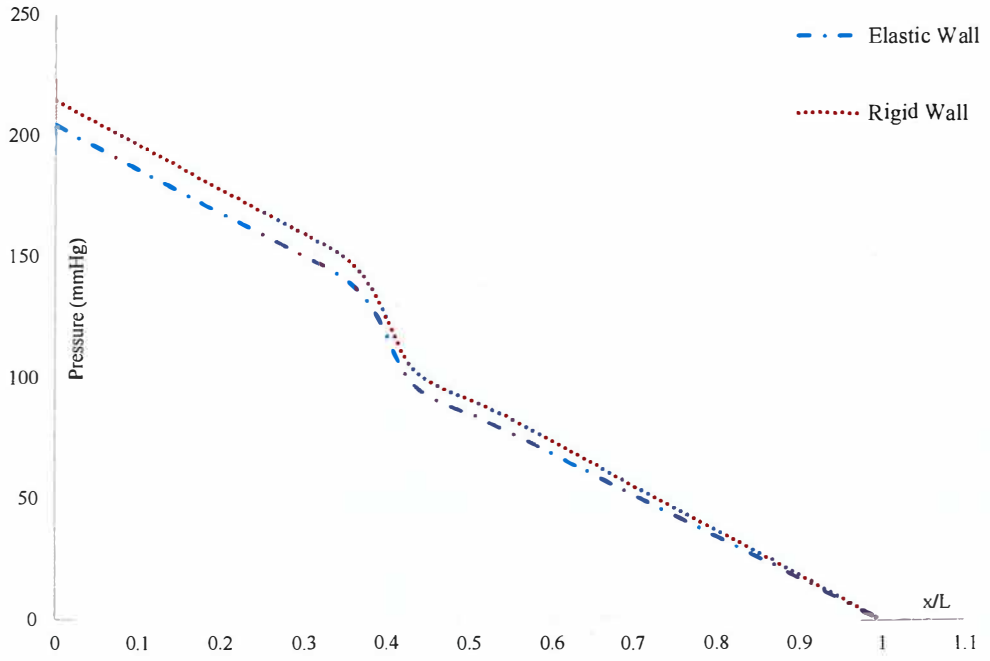

Fig 5.26: The comparison of pressure distributions of elastic wall and rigid wall artery at early systole for 65% stenotic arteries.

The comparison of pressure distributions of elastic wall and rigid wall artery at early systole, peak systole and diastole are shown by the figures 5.24 – 5.35 respectively. However, figure 5.24 – 5.27 show the comparison of pressure distributions of elastic wall and rigid wall artery at early systole for 45%, 55%, 65%, and 75% stenotic arteries respectively. At early systole a significant amount of Pressure difference has been noticed between upstream and downstream of the geometries of 45%, 55%, 65% and 65% severity. Besides, very negligible amount of pressure drop has found at the stenotic throat region at the arteries of all severities. Pressure distribution for elastic body and rigid body artery are almost

same. Thus, the results have been shown in the figures 5.24 – 5.27, where a good agreement can be found with elastic body and rigid body.

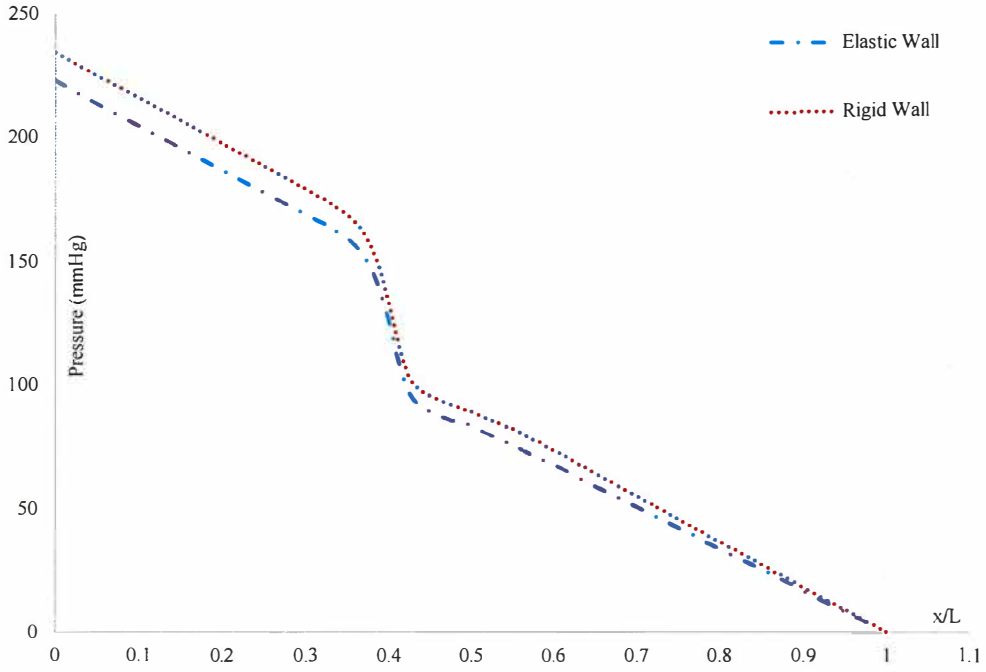

Fig 5.27: The comparison of pressure distributions of elastic wall and rigid wall artery at early systole for 75% stenotic arteries.

In addition, figures 5.28 – 5.31 show the comparison of pressure distributions of elastic wall and rigid wall artery at peak systole for 45%, 55%, 65%, and 75% stenotic arteries. Significant amount of pressure drop has found at the stenotic throat region of all severity of arteries. Pressure distribution at the arteries of all severities, except at 75% severity, for elastic body and rigid body artery are almost same. At 75% severity, pressure distributions for elastic body and

rigid body artery at upstream are different, but same at the stenotic throat and downstream.

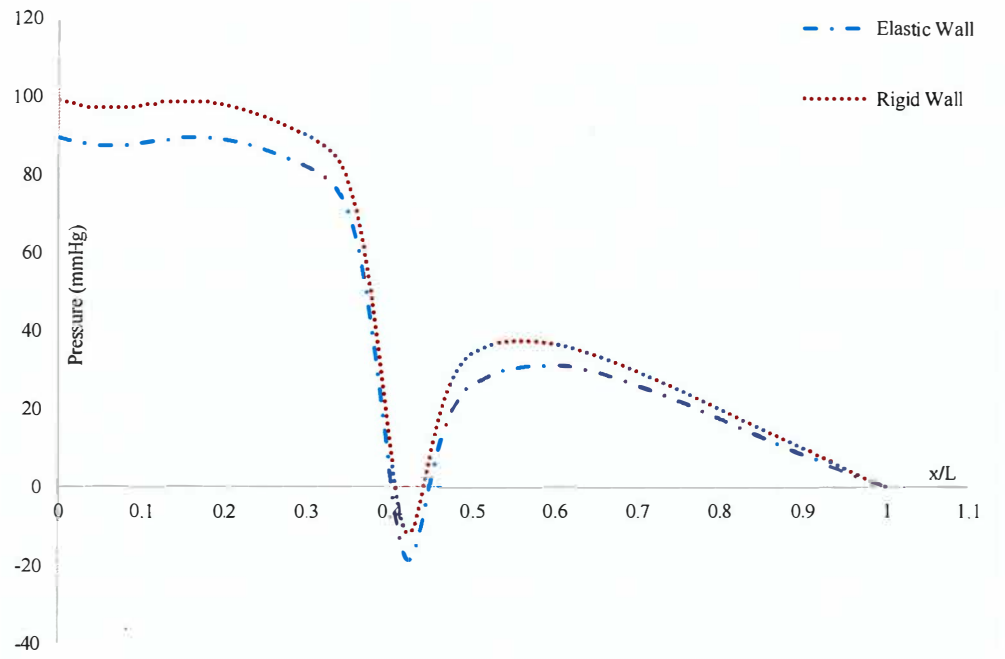

Fig 5.28: The comparison of pressure distributions of elastic wall and rigid wall artery at peak systole for 45% stenotic arteries.

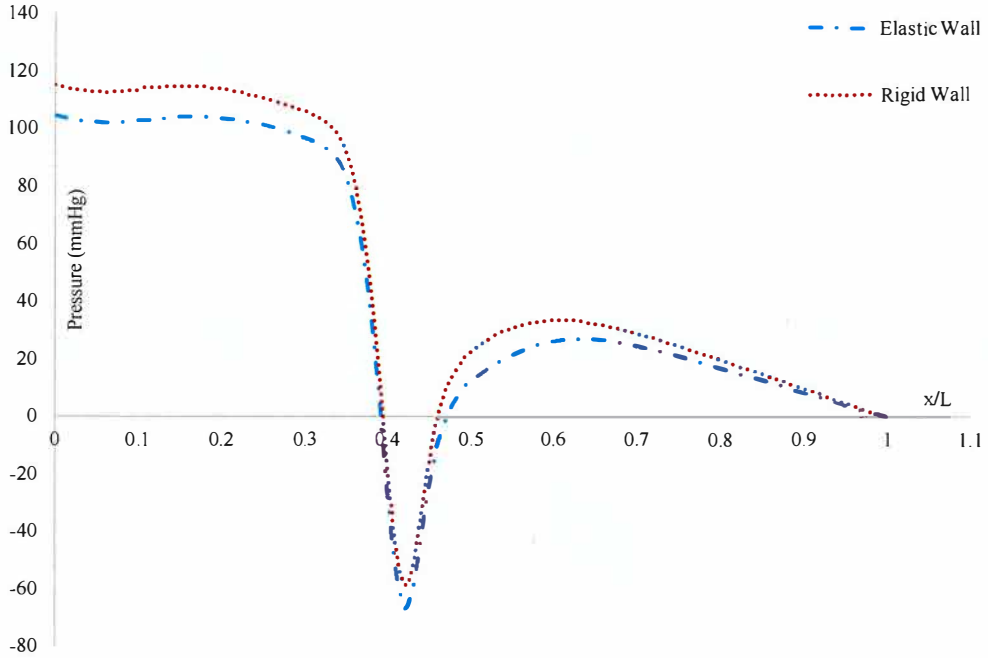

Fig 5.29: The comparison of pressure distributions of elastic wall and rigid wall artery at peak systole for 55% stenotic arteries.

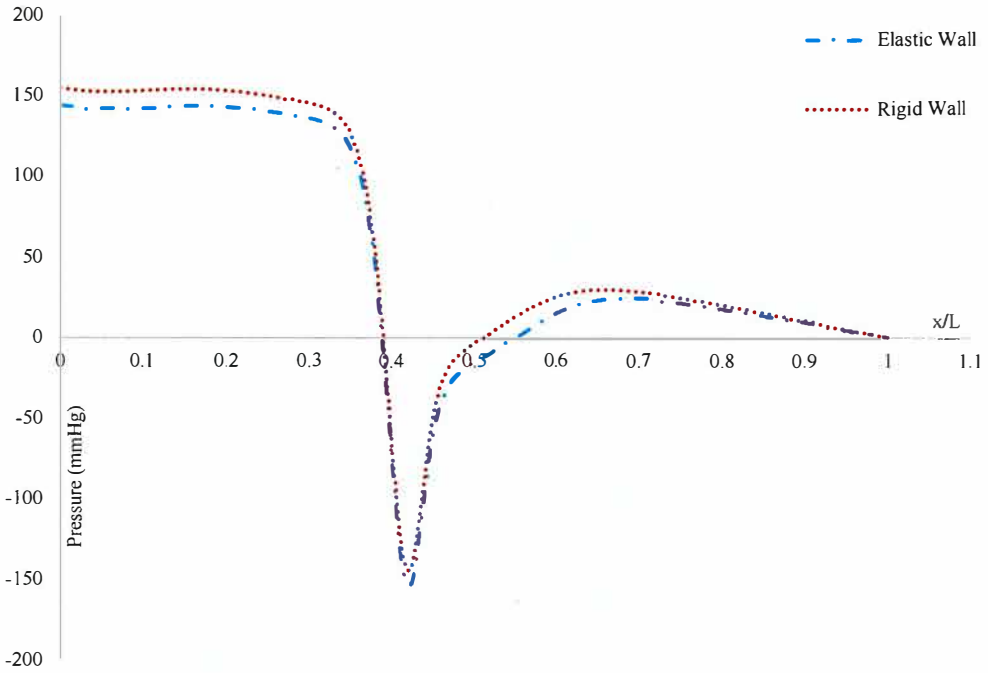

Fig 5.30: The comparison of pressure distributions of elastic wall and rigid wall artery at peak systole for 65% stenotic arteries.

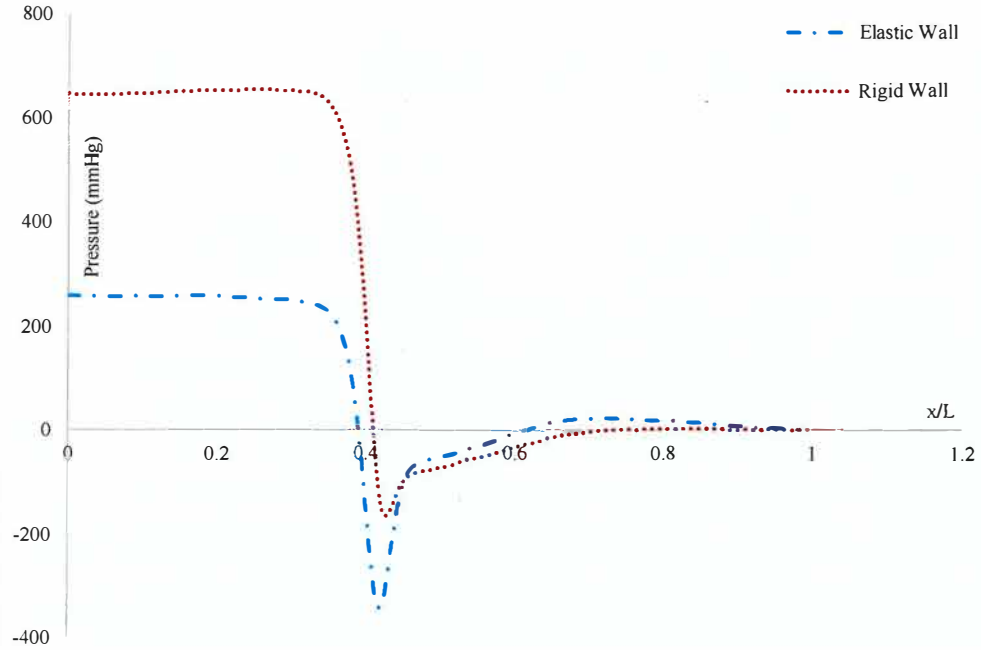

Fig 5.31: The comparison of pressure distributions of elastic wall and rigid wall artery at peak systole for 75% stenotic arteries.

Moreover, figures 5.32 – 5.35 show the comparison of pressure distributions of elastic wall and rigid wall artery at diastole for 45%, 55%, 65%, and 75% stenotic arteries. At diastole a significant amount of Pressure difference has been noticed between upstream and downstream of the geometries, but pressure of the downstream is higher than that of the upstream. Thus, the flow will experience resistance and stagnation or reverse flow may be found in the artery.

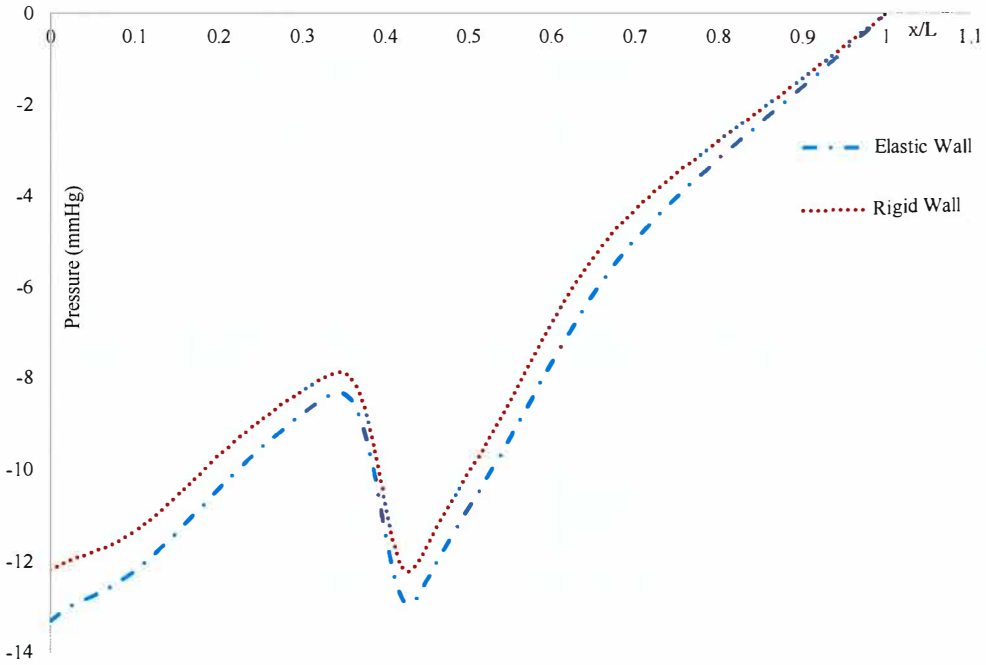

Fig 5.32: The comparison of pressure distributions of elastic wall and rigid wall artery at diastole for 45% stenotic arteries.

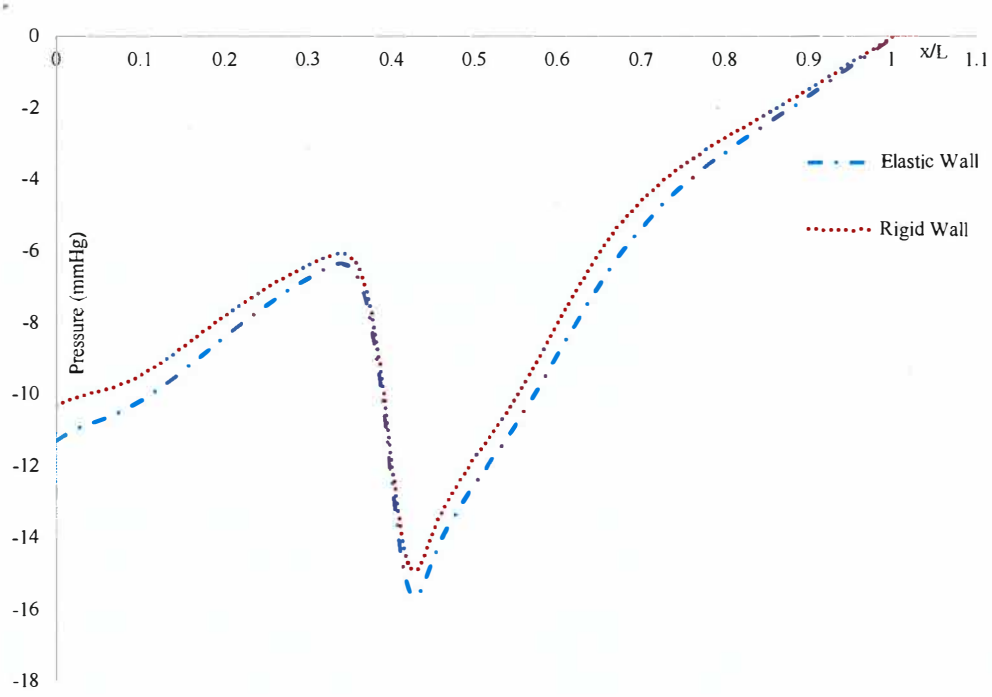

Fig 5.33: The comparison of pressure distributions of elastic wall and rigid wall artery at diastole for 55% stenotic arteries.

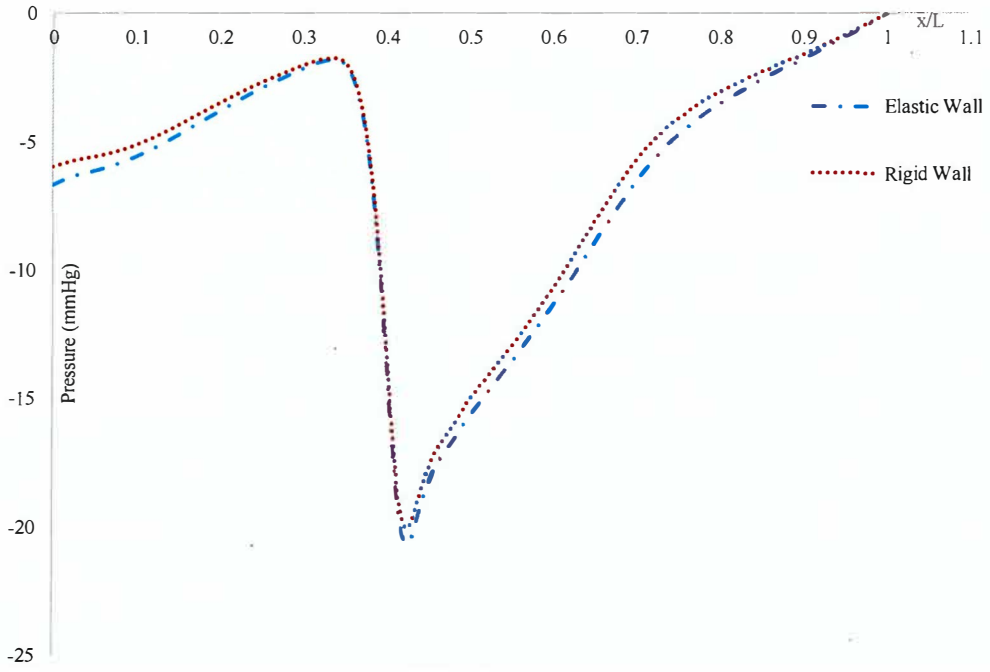

Fig 5.34: The comparison of pressure distributions of elastic wall and rigid wall artery at diastole for 65% stenotic arteries.

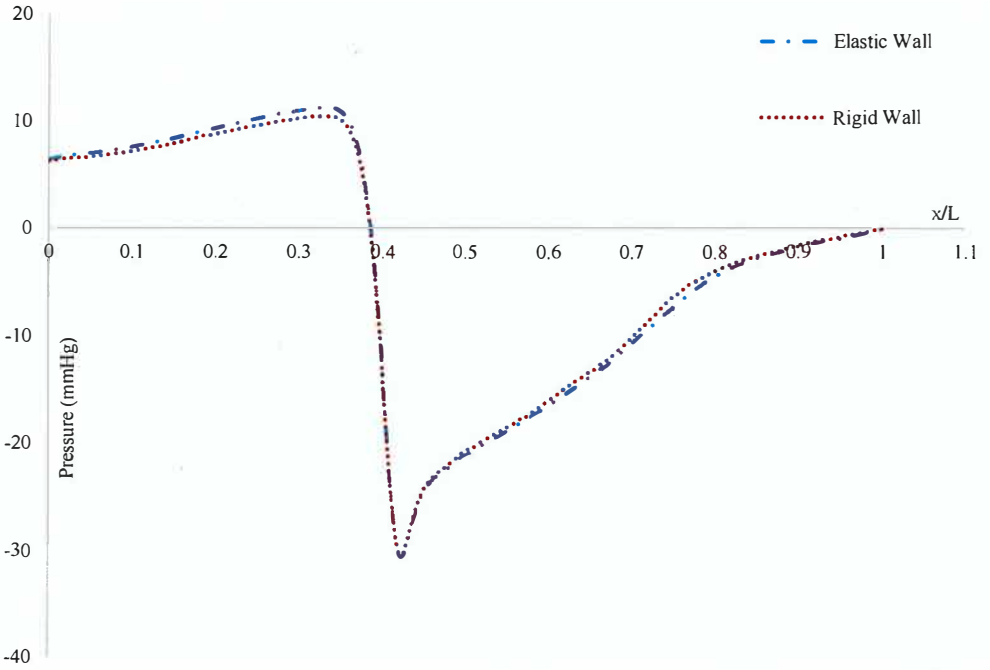

Fig 5.35: The comparison of pressure distributions of elastic wall and rigid wall artery at diastole for 75% stenotic arteries.

Flow velocity is volume flow rate, which determines the amount of blood passing through the artery to other organs. Geometry of artery can affect the flow path which causes receiving fewer life sustaining nutrients. However, it can also increase the deposition of harmful materials. Thus, it is important to investigate blood flow velocities to understand its behavior within arteries. The comparison of velocity distributions of elastic wall and rigid wall artery at early systole, peak systole and diastole are shown by the figures 5.36 – 5.43 respectively. However, figures 5.36 – 5.39 show the comparison of velocity distributions of elastic wall and rigid wall artery at peak systole for 45%, 55%, 65%, and 75% stenotic arteries respectively. At peak systole, results of velocity of elastic wall and rigid wall artery are almost same at the upstream, throat and downstream region. Long stenotic jet is found at the throat region of the arteries of all severities at the peak systole. Blood flow rate is also high through at the peak systole. Moreover, figures 5.40 – 5.43 show the comparison of velocity distributions of elastic wall and rigid wall artery at diastole for 45%, 55%, 65%, and 75% stenotic arteries respectively. At diastole, results of velocity of elastic wall and rigid wall artery are also same at the upstream, throat and downstream region. However, very little stenotic jet is found at the throat region of the arteries of all severities at the diastole. Blood flow rate is also very low through at the diastole as like as at the early systole.

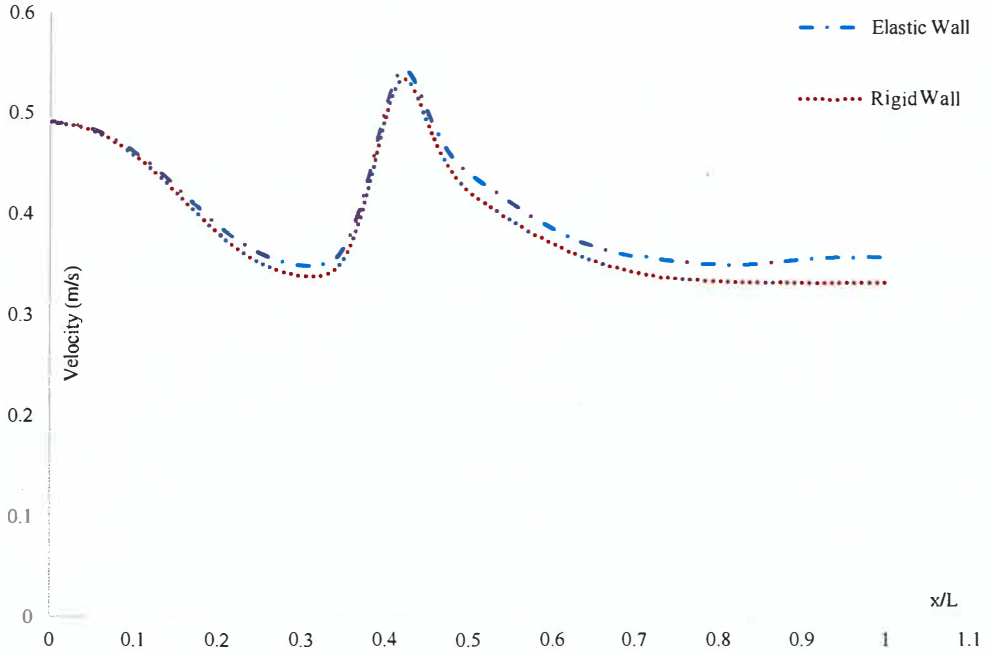

Fig 5.36: The comparison of velocity distributions of elastic wall and rigid wall artery at peak systole for 45% stenotic arteries.

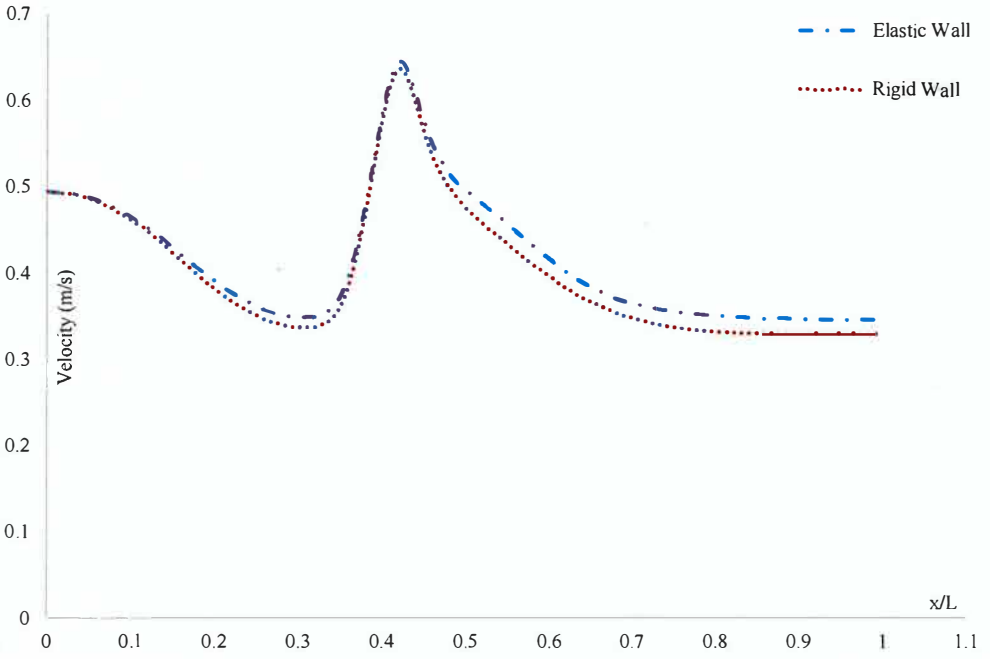

Fig 5.37: The comparison of velocity distributions of elastic wall and rigid wall artery at peak systole for 55% stenotic arteries.

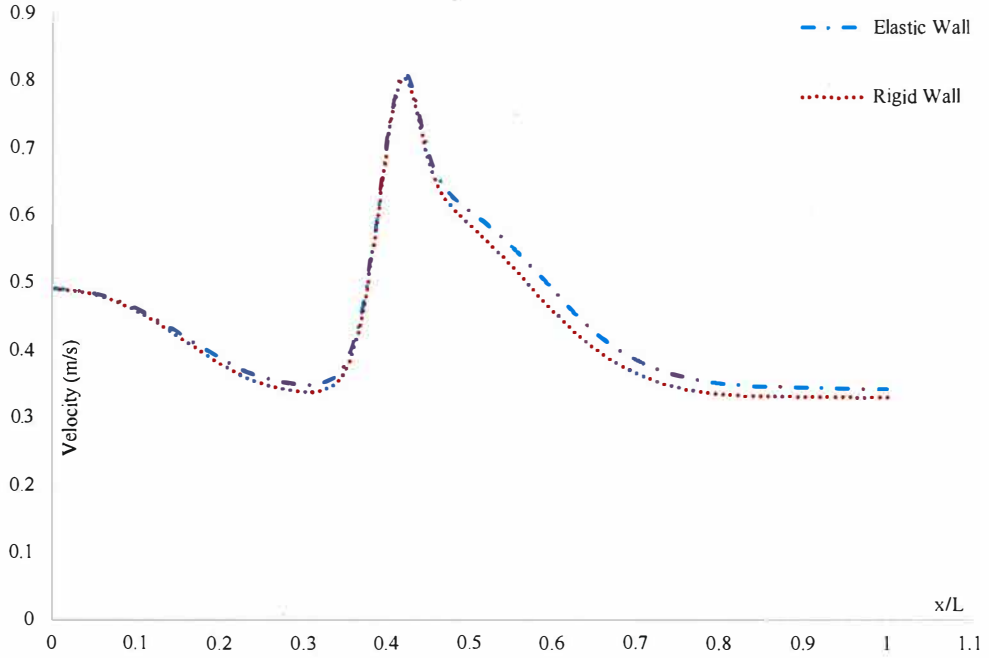

Fig 5.38: The comparison of velocity distributions of elastic wall and rigid wall artery at peak systole for 65% stenotic arteries.

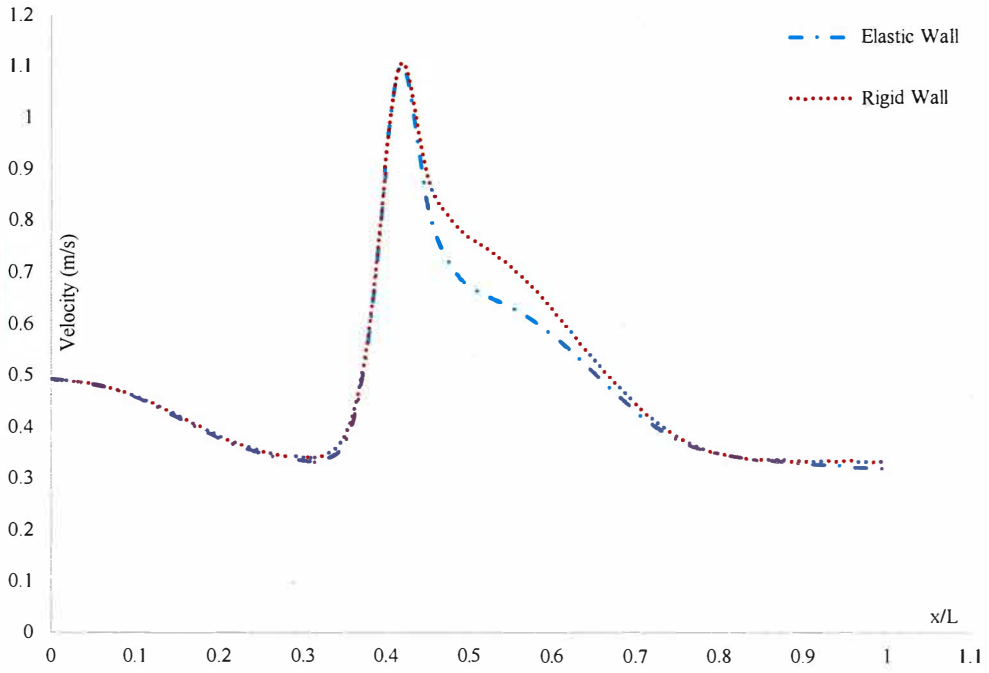

Fig 5.39: The comparison of velocity distributions of elastic wall and rigid wall artery at peak systole for 75% stenotic arteries.

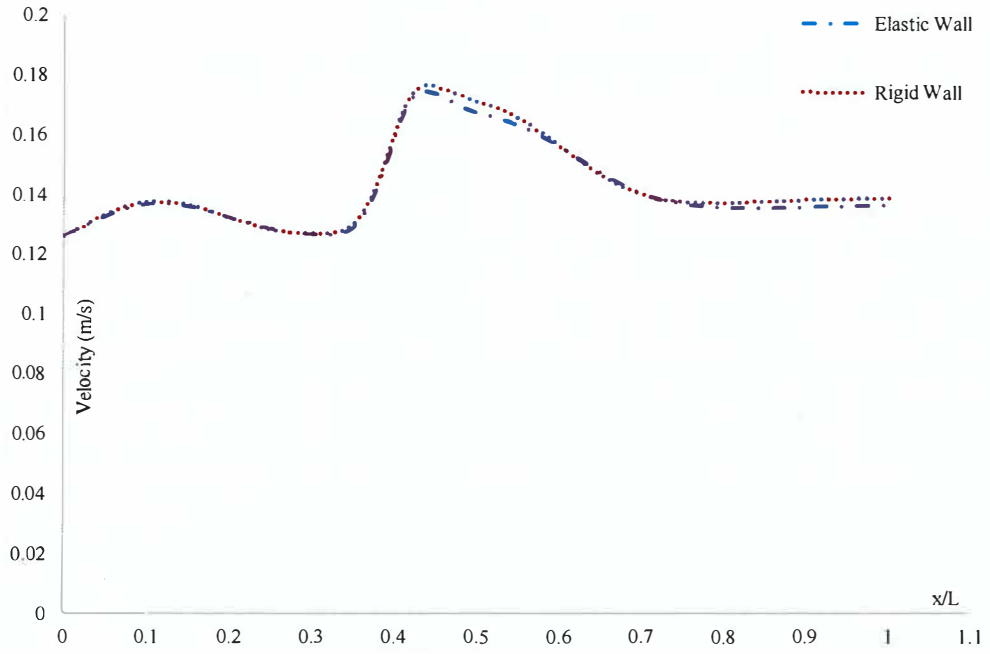

Fig 5.40: The comparison of velocity distributions of elastic wall and rigid wall artery at diastole for 45% stenotic arteries.

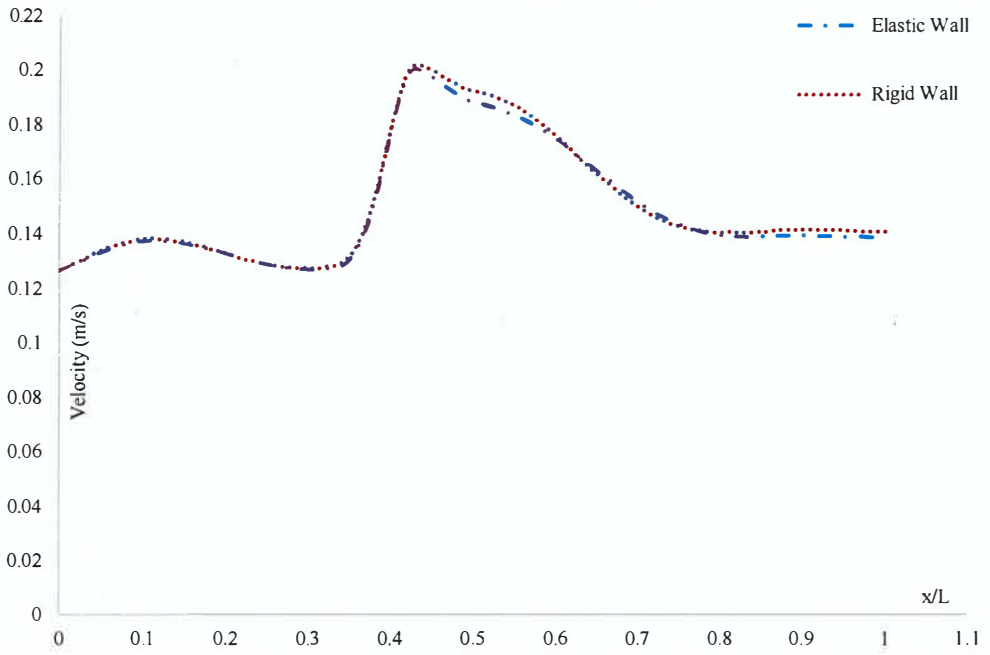

Fig 5.41: The comparison of velocity distributions of elastic wall and rigid wall artery at diastole for 55% stenotic arteries.

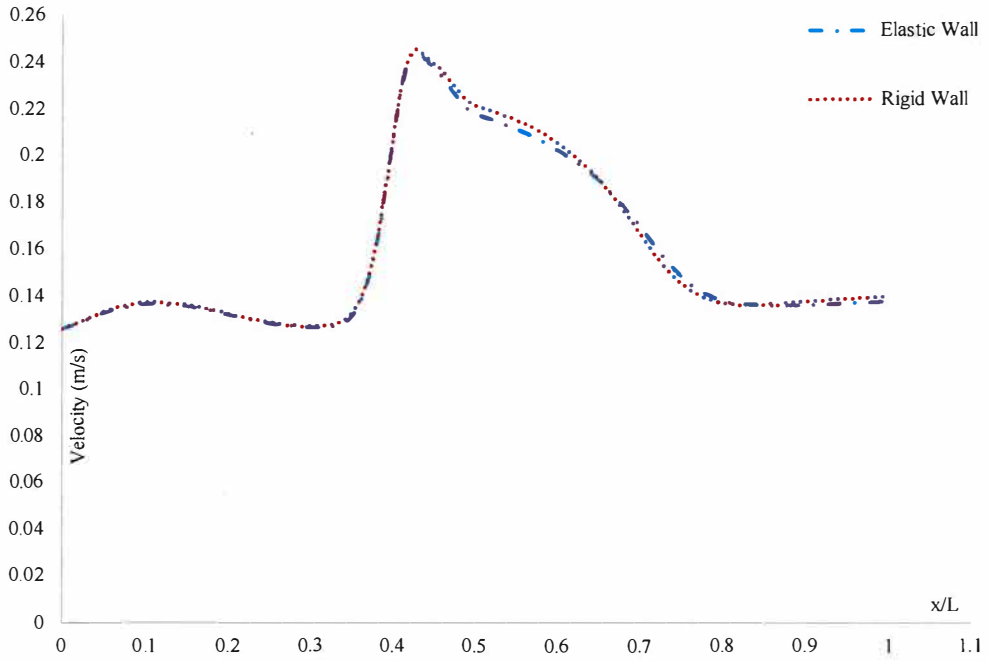

Fig 5.42: The comparison of velocity distributions of elastic wall and rigid wall artery at diastole for 65% stenotic arteries.

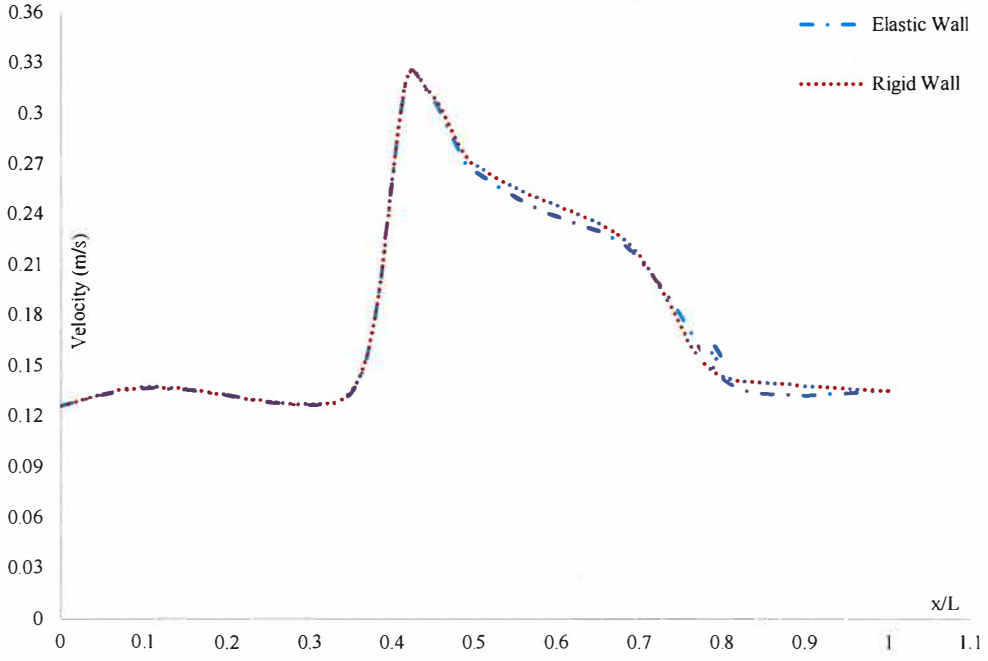

Fig 5.43: The comparison of velocity distributions of elastic wall and rigid wall artery at diastole for 75% stenotic arteries.

Results of velocity of elastic wall and rigid wall artery are almost same at the upstream, throat and downstream region at peak systole. Moreover, results of velocity of elastic wall and rigid wall artery are also same at the upstream, throat and downstream region at the diastole. However, very little stenotic jet is found at the throat regions of the arteries of all severities at the diastole, but long stenotic jet is found at the same regions at the peak systole. Blood flow rate is also very low through at the diastole.

However, wall shear stress (WSS) is one of the main hemodynamic forces to influence vascular endothelial cells, which plays a vital role in the development and progression of atherosclerotic plaques and arterial aneurysms. Arterial endothelium is highly sensitive to hemodynamic shear stresses that act at the vessel surface in the direction of blood flow. Besides, it works directly on the endothelium as a biological stimulator by controlling the cellular function. However, high wall shear stress in normal arteries is believed to have protective roles to form stenosis, but it enhances platelet activation and subsequent aggregation and even plaque rupture in stenotic arteries. High prolonged high wall shear stress elongates the endothelial cells and force to align in the direction of the flow. Consequently, it fragments the internal elastic layer of the arteries and initially starts to form atherosclerosis or an aneurysm. In addition to high WSS, regions of relatively low WSS in normal arteries are also believed to have a higher

propensity to form the stenosis. It is because of low WSS had a negligible effect on the cell but increases intercellular permeability and consequently increases the plaque formation in the arteries. Thus, endothelial cells react differently to the high and low WSS as well as stenosis can be formed for both in high and low wall shear stress in the arteries. However, wall shear stresses on vessel walls have been difficult to acquire experimentally but have a strong link with the formation of arterial stenosis. This quantity requires precise and numerous measurements about the vessel wall, which is difficult, even for the technology presently available. It is, therefore, preferable to derive this numerically from simulations. Wall shear stress behavior also plays a role in vessel wall behavior in cases where the structural response is considered and could be responsible for wall rupture.

The comparison of wall shear stress distributions of the elastic wall and rigid wall artery at early systole, peak systole, and diastole are shown by figures 5.44 – 5.55 respectively. However, figure 5.44 – 5.47 show the comparison of wall shear stress distributions of the elastic wall and rigid wall artery at early systole for 45%, 55%, 65%, and 75% stenotic arteries respectively. At early systole, the results of wall shear stress of elastic wall and rigid wall are little different only at the downstream region of 45% and 55% stenotic arteries, but the results of wall shear stress of elastic wall and rigid wall are almost same at all region of 65% and 75% stenotic arteries. The WSS of a rigid body artery is a little greater than of elastic

body artery at the throat region of 65% stenotic artery. Alternatively, The WSS of the elastic body artery is a little greater than of a rigid body artery at the throat region of a 75% stenotic artery.

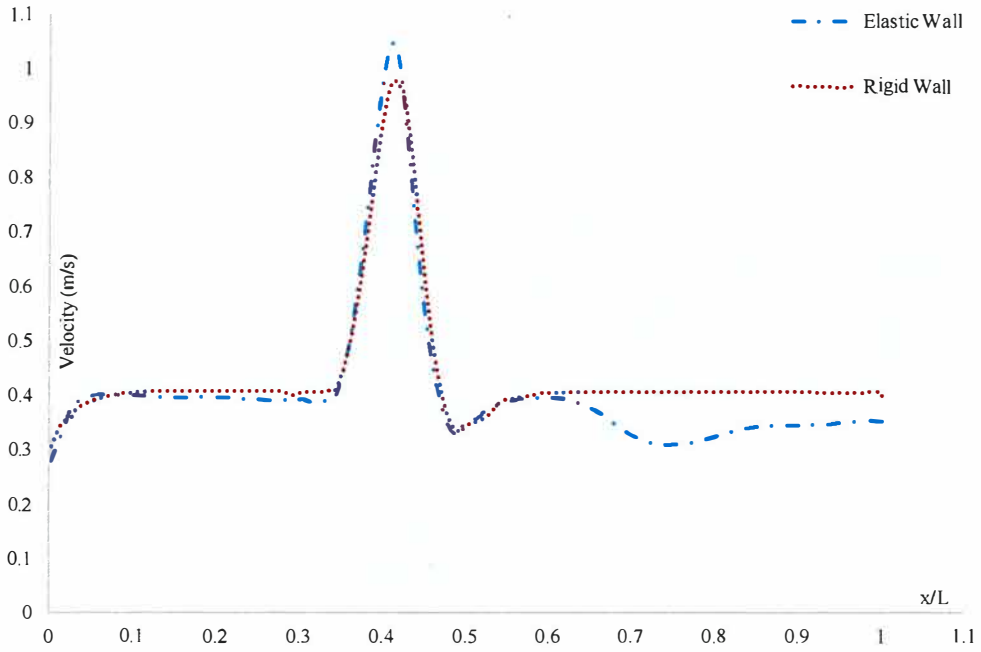

Fig 5.44: The comparison of WSS distributions of elastic wall and rigid wall artery at early systole for 45% stenotic arteries.

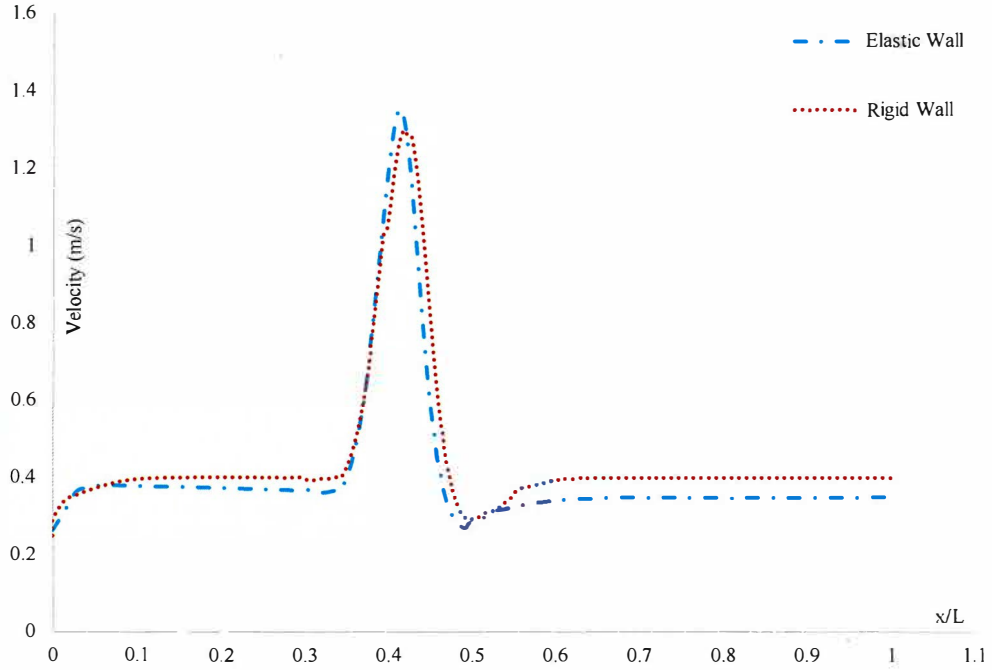

Fig 5.45: The comparison of WSS distributions of elastic wall and rigid wall artery at early systole for 55% stenotic arteries.

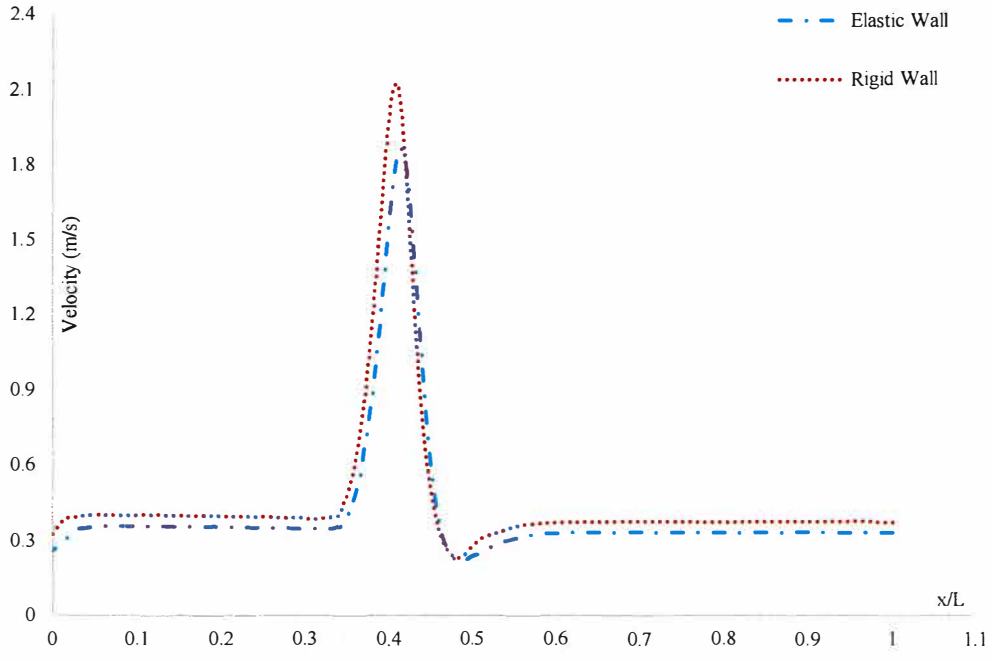

Fig 5.46: The comparison of WSS distributions of elastic wall and rigid wall artery at early systole for 65% stenotic arteries.

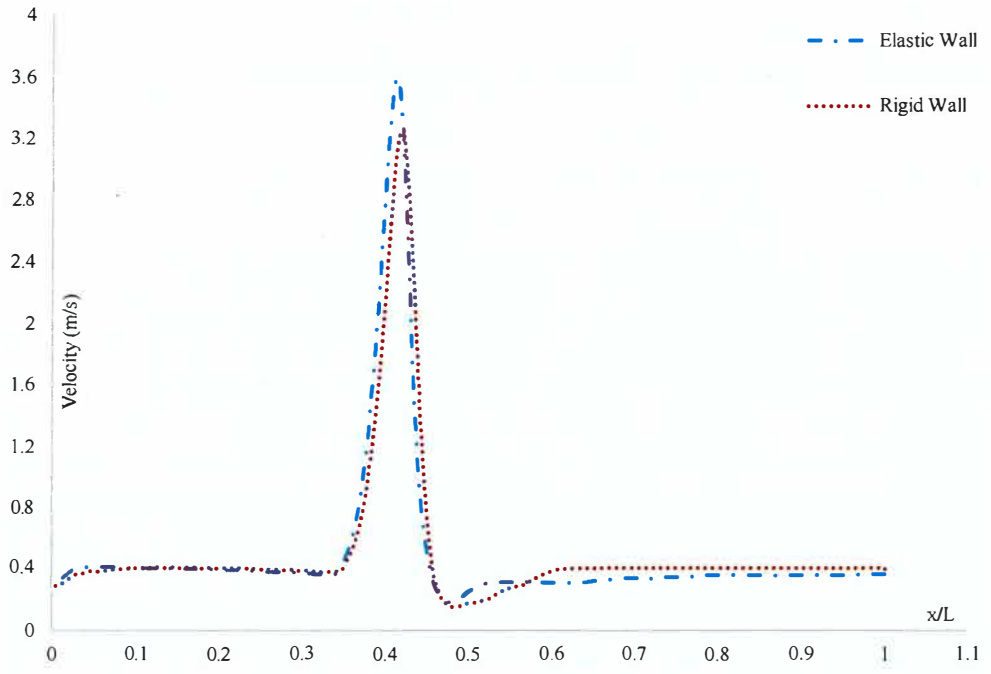

Fig 5.47: The comparison of WSS distributions of elastic wall and rigid wall artery at early systole for 75% stenotic arteries.

Moreover, figures 5.48 – 5.51 show the comparison of wall shear stress distributions of the elastic wall and rigid wall artery at peak systole for 45%, 55%, 65%, and 75% stenotic arteries respectively. At peak systole the results of wall shear stress of elastic wall and rigid wall are little different at the throat region of 45% and 75% stenotic arteries, the rest of the region are almost the same. The results of the elastic wall and rigid wall are in good agreement for 55% and 65% stenotic arteries. The WSS of the elastic body artery is a little greater than of a rigid body artery at the throat region of 45% and 55% stenotic artery. Alternatively, The WSS of a rigid body artery is a little greater than of elastic body artery at the throat region of the 75% stenotic artery.

Besides, figures 5.52 – 5.55 show the comparison of wall shear stress distributions of the elastic wall and rigid wall artery at diastole for 45%, 55%, 65%, and 75% stenotic arteries. At diastole, the results of wall shear stress of elastic wall and rigid wall are in very good agreement in all regions of 45%, 55%, 65%, and 75% stenotic arteries.

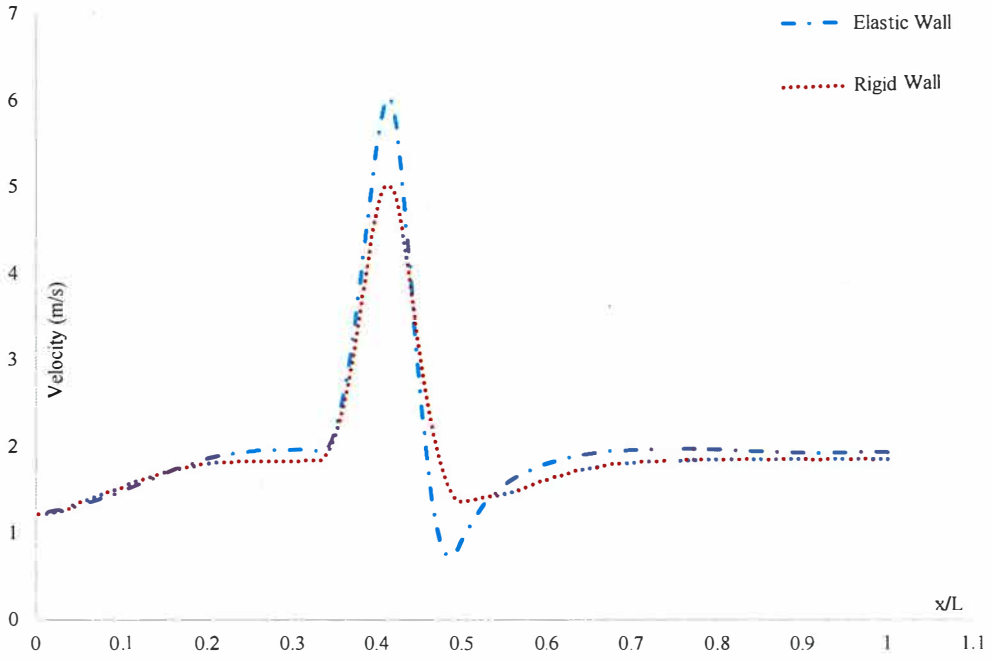

Fig 5.48: The comparison of WSS distributions of elastic wall and rigid wall artery at peak systole for 45% stenotic arteries.

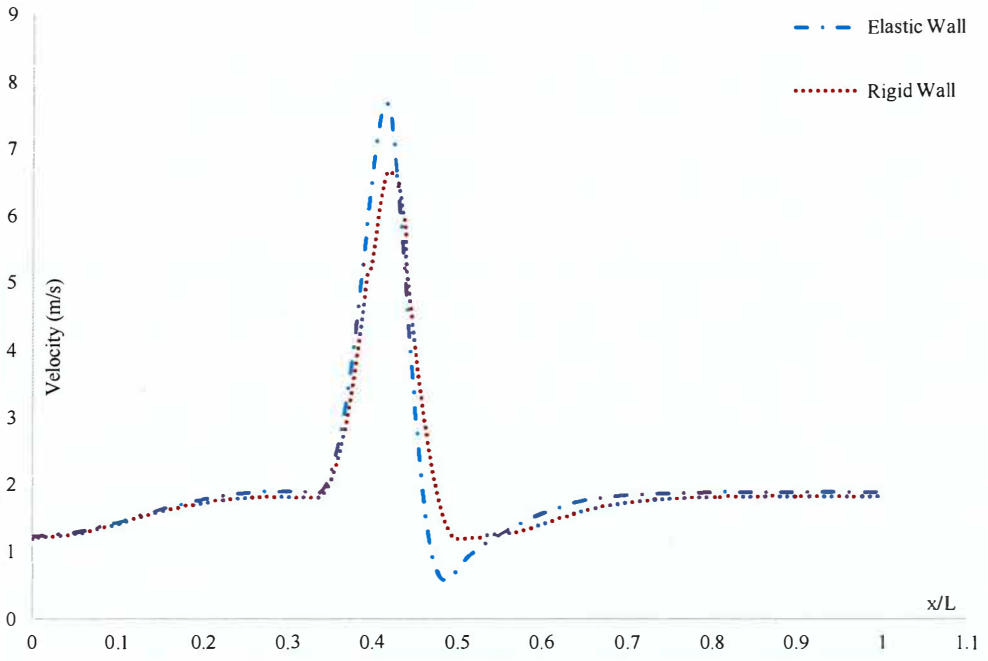

Fig 5.49: The comparison of WSS distributions of elastic wall and rigid wall artery at peak systole for 55% stenotic arteries.

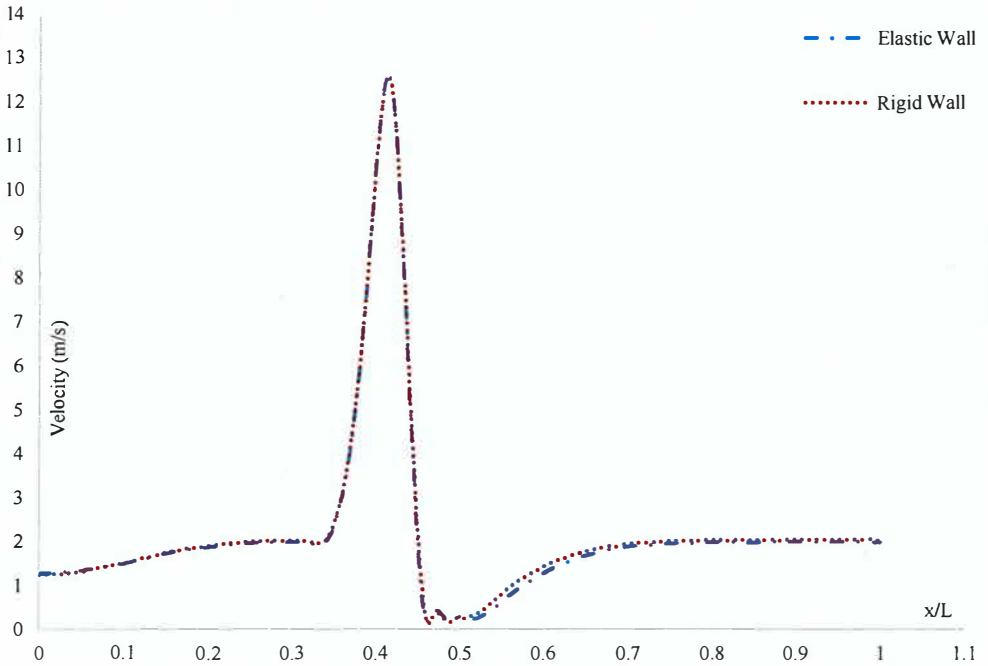

Fig 5.50: The comparison of WSS distributions of elastic wall and rigid wall artery at peak systole for 65% stenotic arteries.

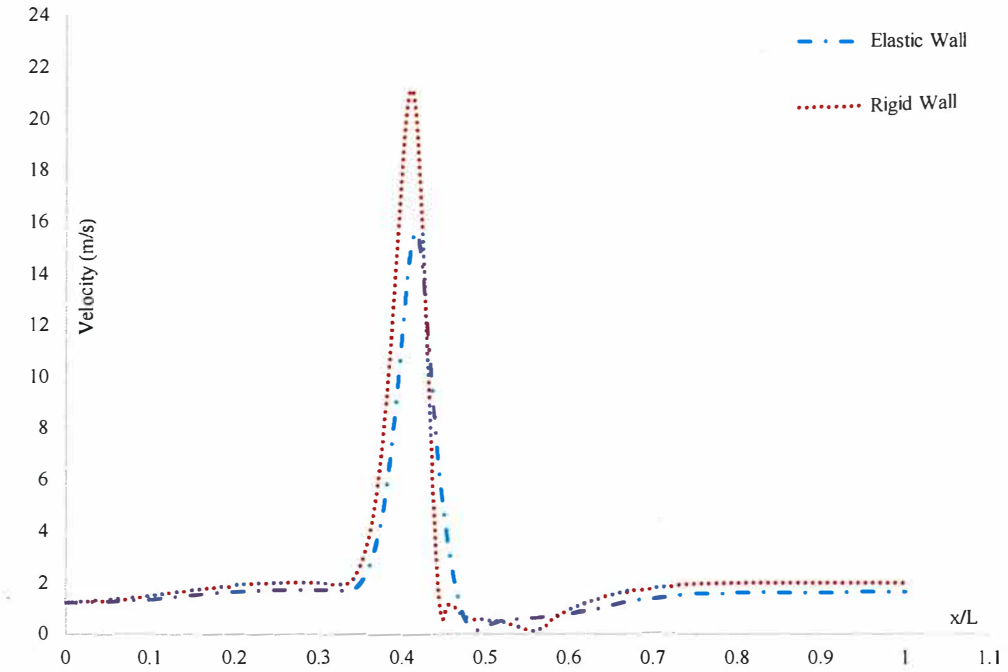

Fig 5.51: The comparison of WSS distributions of elastic wall and rigid wall artery at peak systole for 75% stenotic arteries.

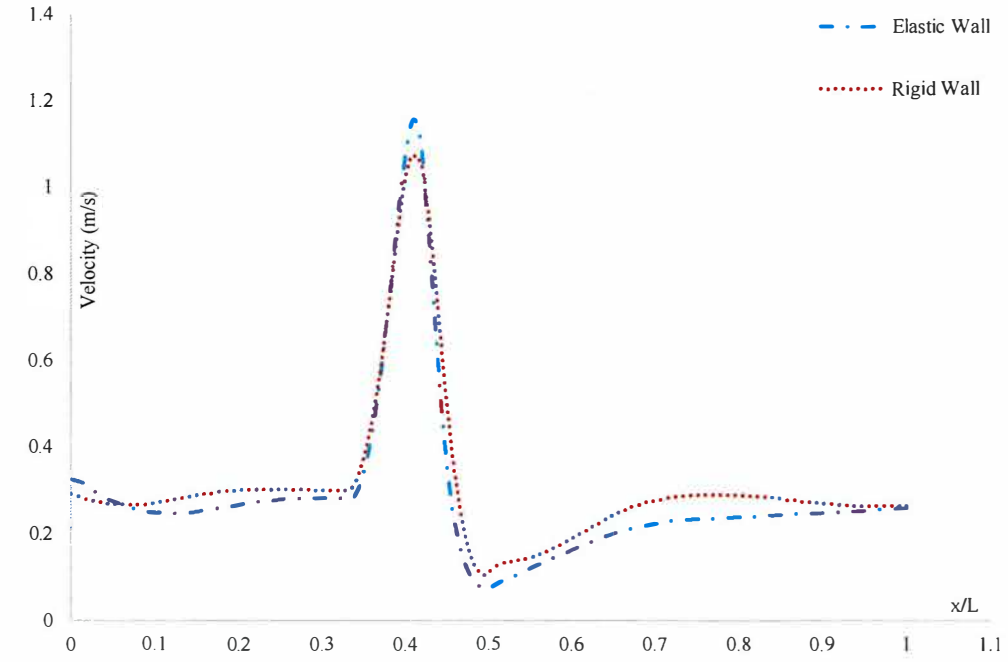

Fig 5.52: The comparison of WSS distributions of elastic wall and rigid wall artery at diastole for 45% stenotic arteries.

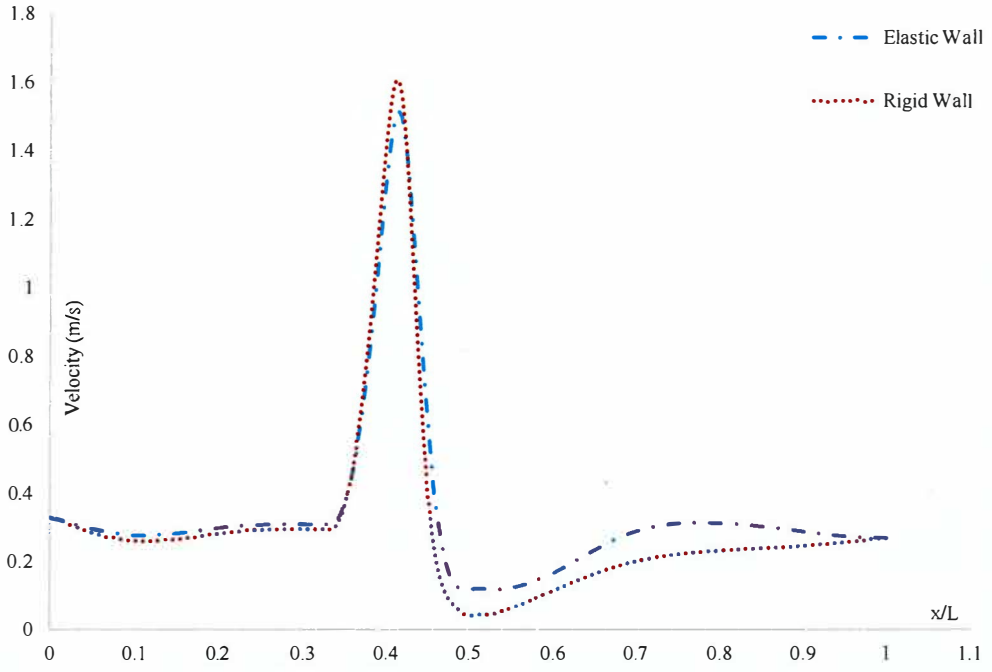

Fig 5.53: The comparison of WSS distributions of elastic wall and rigid wall artery at diastole for 55% stenotic arteries.

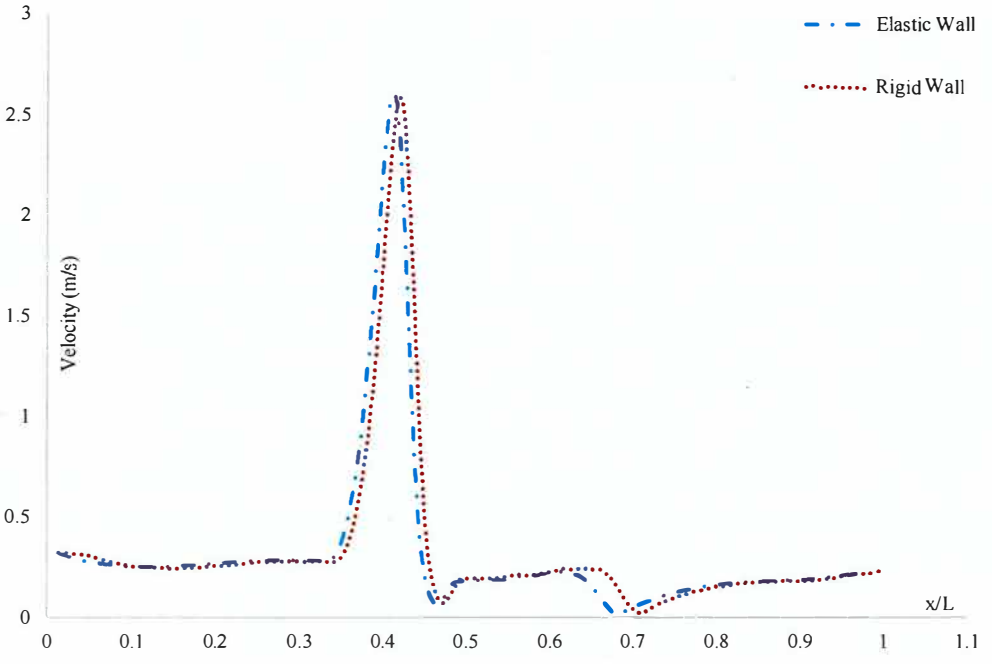

Fig 5.54: The comparison of WSS distributions of elastic wall and rigid wall artery at diastole for 65% stenotic arteries.

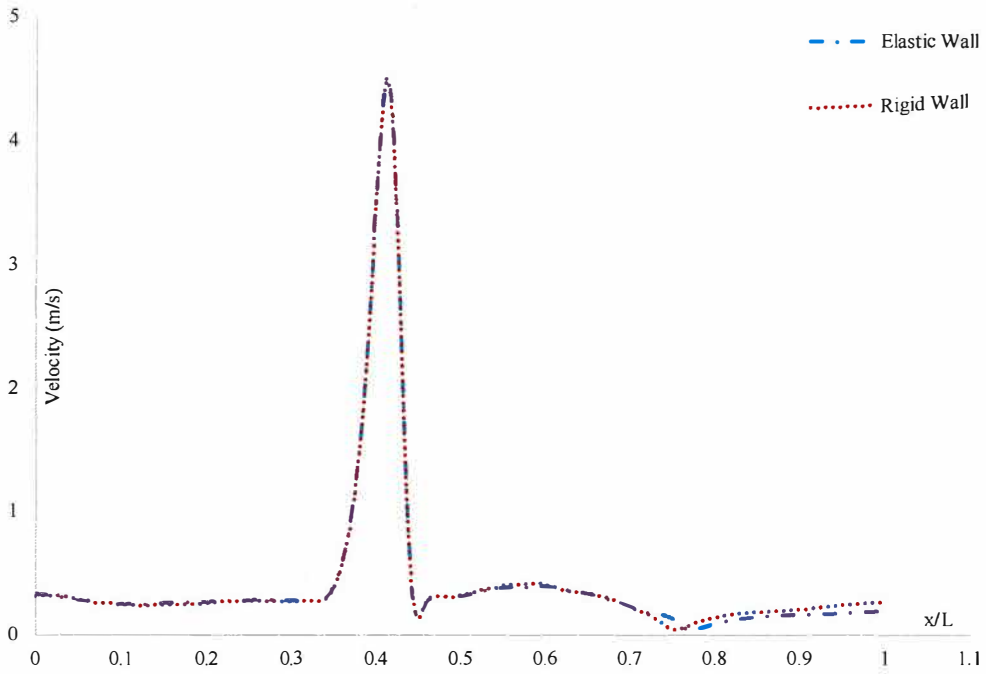

Fig 5.55: The comparison of WSS distributions of elastic wall and rigid wall artery at diastole for 75% stenotic arteries.

The results of wall shear stress of elastic wall and rigid wall are little different only at the downstream region of 45% and 55% stenotic arteries, but the results of wall shear stress of elastic wall and rigid wall are in good agreement throughout the geometry of 65% and 75% stenotic severities at early systole. However, the WSS of a rigid body artery is a little greater than of elastic body artery at the throat region of the 65% stenotic artery, but the same result is an alternative for the 75% stenotic artery. Besides, the results of wall shear stress of elastic wall and rigid wall are little different at the throat region of 45% and 75% stenotic arteries, rest of the region are almost same, but the same results are in good agreement for 55% and 65% stenotic arteries at peak systole. The WSS of

elastic body artery is little greater than of rigid body artery at the throat region of 45% and 55% stenotic artery, but the same result is an alternative for the 75% stenotic artery. However, the results of wall shear stress of elastic wall and rigid wall are in very good agreement at all regions of 45%, 55%, 65%, and 75% stenotic arteries at diastole. As there is no big difference in the results of the comparative study, so arterial wall has been considered as rigid wall for simulation of statistical analysis for minimizing the computational time.

5.3 Statistical analysis

Statistical analysis is the main part of this thesis. The purpose is to analyze the effects of stenosis for different stenotic eccentricity, severities, and length. The focus is to investigate the influences of stenotic severities, eccentricity, and length on the hemodynamic parameters such as velocities, pressure and wall shear stress. For this investigation, 120 simulations have been performed for getting the statistical data from the numerical results. All geometries for the simulations are taken as rigid wall artery. Detail discussion can be found in chapter four.

Statistical analysis has been presented by table representation to investigate the impact of stenotic shape and flow spirality on hemodynamic parameters like wall shear stress, pressure, and velocity. Thus, eight regression cases have been presented in this study. WSS_{max}, WSS_{min}, WSS_{ave}, $Pressure_{max}$, $Pressure_{drop}$,

$Velocity_{max}$, $Velocity_{min}$, and $Velocity_{ave}$ are the dependent variable for the consecutive cases respectively, whereas independent variables are same in all eight cases. However, the independent variables are stenotic severity, eccentricity, length and flow spirality. Stenotic severity, Eccentricity, length, and Spirality (c) are changing from 25% to 85%, 0 to 0.09, 1D to 3D, and 0 to 2.5 respectively, where (c) can be found from the equation (4.5). All independent variables are non-dimensional. The residual sum of squares and significant level of the cases have been presented in Table 5.1. Residual sum squares in first case is 0.734 which means 73.4% of the variation of WSS_{max} can be explained by the stenotic severity, eccentricity, length and flow spirality. Similarly, it can be said that WSS_{min}, WSS_{ave}, $Pressure_{max}$, $Pressure_{drop}$, $Velocity_{max}$ and $Velocity_{ave}$ are dependent on stenotic severity, eccentricity, length and flow spirality by 55.6%, 63.6%, 61.4%, 66%, 82.1% and 78.7% respectively. However, $Velocity_{min}$, can't be explained by the stenotic severity, eccentricity, length and flow spirality because the p-value of $Velocity_{min}$ is greater than 0.05. On the other hand, p-value of all other cases is zero which is less than 0.05, so null hypothesis must be rejected and it can be said that the cases are statistically significant. Actually, the p-value for each term tests the null hypothesis that the coefficient is equal to zero (no effect). A low p-value which is less than 0.05 indicates that the null hypothesis can be rejected. In other words, a predictor that has a low p-value is likely to be a meaningful because

changes in the predictor's value are related to changes in the response variable. Conversely, a larger (insignificant) p-value suggests that changes in the predictor are not associated with changes in the response. In the Table 5.2 – 5.9 it is found that p-value of the flow spirality is greater than 0.05 in first, third, fourth, fifth, sixth, and eighth cases, which indicates that changes in the flow spirality are not associated with changes in the WSS_{max}, WSS_{ave}, $Pressure_{max}$, $Pressure_{drop}$, $Velocity_{max}$ and $Velocity_{ave}$. Similarly, stenotic eccentricity in second, fourth, fifth, sixth and eighth cases and stenotic length in second, third, and fifth cases are also statistically insignificant.

Table 5.1: Residual sum of squares and significant level or P-value of the cases

Case	Dependent Variable	Residual sum of squares	Significant Level p-value
1	WSS_{max}	0.734	0.00<0.05
2	WSS_{min}	0 .556	0.00<0.05
3	WSS_{ave}	0.636	0.00<0.05
4	$Pressure_{max}$	0.614	0.00<0.05
5	$Pressure_{drop}$	0.660	0.00<0.05
6	$Velocity_{max}$	0.821	0.00<0.05
7	$Velocity_{min}$	0.037	**0.359>0.05**
8	$Velocity_{ave}$	0.787	0.00<0.05

Besides, regression coefficients represent the mean change in the response variable for one unit of change in the predictor variable while holding other predictors constant. From the Table 5.2, first case presented that the coefficients of severity, eccentricity and length are 122.5, 10.426 and -6.363 respectively, whereas spirality is negligible because of the higher p-value. Thus, the stenotic severity and eccentricity have positive relationship, but the stenotic length has inverse relationship with WSS_{max} distribution and flow spirality has no influence on the WSS_{max}. That means, if the stenotic severity and eccentricity increase, the WSS_{max} distribution will also increase, whereas if the stenotic length increases, the WSS_{max} distribution will decrease. However, the stenotic severity is the most influencing factor for WSS_{max} in the first case, so when the stenotic severity is raised by 1% keeping others predictors unchanged, the WSS_{max} will expect to increase by 122.5 Pa. Besides, if stenotic eccentricity increases by 0.1 keeping others predictors constant, the WSS_{max} will be expected to increase by 10.426 Pa. On the other hand, stenotic length has inverse relationship with the WSS_{max} of the first case. Thus, the WSS_{max} will expect to decrease by 6.363 Pa when the length increases by 0.1 D and other predictors are constant.

In case 2 of the Table 5.3, it is observed that the P-value of Stenotic severity, eccentricity, and length and flow spirality are 0, 0.842, 0.482 and 0 respectively. Thus, the stenotic eccentricity and length have no influence on the WSS_{min} due to

higher P-value. However, the regression coefficient of the stenotic severity and flow spirality are -0.032 and 0.128 respectively. Thus, the stenotic severity and flow spirality have the influence on the WSS_{min} distribution. Besides, the WSS_{min} has opposite response for the variation of the severity, but flow spirality is positively related to WSS_{min}. According to the regression coefficient it can be said that the WSS_{min} will expect to decrease by 0.032 Pa when the severity increases by 1% and other predictors are constant. On the other hand, the WSS_{min} will expect to increase by 0.128 Pa when the flow spirality increases by one unit but other predictors are constant.

Table 5.2: Coefficients and P-value of the predictors in the case 1.

Case	Dependent Variable	Independent Variables	Coefficients (Pa)	Significant Level p-value
1	WSS_{max}	Constant	-33.641	0.00 < 0.05
		Severity	122.5	0.000<0.05
		Eccentricity	10.426	0.037<0.05
		Length	-6.363	0.001<0.05
		Spirality	5.440	**0.712>0.05**

Table 5.3: Coefficients and P-value of the predictors in the case 2.

Case	Dependent Variable	Independent Variables	Coefficients (Pa)	Significant Level p-value
2	WSS_{min}	Constant	0.023	0.00<0.05
		Severity	-0.032	0.00<0.05
		Eccentricity	0.001	**0. 84>0.05**
		Length	-0.001	**0. 48>0.05**
		Spirality	0.128	0.00 <0.05

Table 5.4: Coefficients and P-value of the predictors in the case 3.

Case	Dependent Variable	Independent Variables	Coefficients (Pa)	Significant Level p-value
3	WSS_{ave}	Constant	-1.402	0.00<0.05
		Severity	4.7	0.00<0.05
		Eccentricity	0.797	0.00<0.05
		Length	0.165	**0.07>0.05**
		Spirality	0.697	**0.35>0.05**

In case 3 of the Table 5.4, it is observed that the P-value of Stenotic severity, eccentricity, and length and flow spirality are 0, 0, 0.07 and 0.35 respectively.

Thus, the stenotic length and flow spirality have no influence on the WSS_{ave} due to higher P-value. Thus, the Stenotic severity and eccentricity have an influence on the WSS_{ave} distribution and the regression coefficient of them have revealed that they have positive relationship with the WSS_{ave}. According to the regression coefficient it can be said that if the stenotic severity and eccentricity will be increased by one unit, the WSS_{ave} will expect to increase by 4.7 Pa and 0.797 Pa respectively.

Table 5.5: Coefficients and P-value of the predictors in the case 4.

Case	Dependent Variable	Independent Variables	Coefficients (mmHg)	Significant Level p-value
4	$Pressure_{max}$	Constant	115.557	0.00<0.05
		Severity	10.7	0.00<0.05
		Eccentricity	0.595	**0.29>0.05**
		Length	0.355	0.04<0.05
		Spirality	0.992	**0.55>0.05**

In case 4 of the Table 5.5, it is observed that the P-value of Stenotic severity, eccentricity, and length and flow spirality are 0, 0.29, 0.04 and 0.55 respectively. Thus, the stenotic eccentricity and flow spirality have no influence on the $Pressure_{max}$ due to higher P-value. Thus, the stenotic severity and length have an

influence on the $Pressure_{max}$ distribution and the regression coefficient of them have revealed that they have positive relationship with the $Pressure_{max}$. According to the regression coefficient it can be said that if the stenotic severity and length will be increased by one unit, the $Pressure_{max}$ will expect to increase by 10.7 mmHg and 0.355 mmHg respectively.

Table 5.6: Coefficients and P-value of the predictors in the case 5.

Case	Dependent Variable	Independent Variables	Coefficients (mmHg)	Significant Level p-value
5	$Pressure_{drop}$	Constant	-7.29	0.00<0.05
		Severity	16.10	0.00<0.05
		Eccentricity	0.82	**0.28>0.05**
		Length	0.51	**0.07>0.05**
		Spirality	1.24	**0.59>0.05**

In case 5 of the Table 5.6, it is observed that the P-value of Stenotic severity, eccentricity, and length and flow spirality are 0, 0.28, 0.07 and 0.59 respectively. Thus, the stenotic eccentricity, length and flow spirality have no influence on the $Pressure_{ave}$ due to higher P-value. Thus, only the stenotic severity has an influence on the $Pressure_{ave}$ distribution and the regression coefficient of severity has revealed that it has positive relationship with the $Pressure_{ave}$. According to the

regression coefficient it can be said that if the stenotic severity will be increased by one unit, the $Pressure_{ave}$ will expect to increase by 16.10 mmHg.

Table 5.7: Coefficients and P-value of the predictors in the case 6.

Case	Dependent Variable	Independent Variables	Coefficients (m/s)	Significant Level p-value
6	$Velocity_{max}$	Constant	-0.415	0.00<0.05
		Severity	2.03	0.00<0.05
		Eccentricity	0.07	**0.23>0.05**
		Length	0.05	0.04<0.05
		Spirality	0.08	**0.67>0.05**

In case 6 of the Table 5.7, it is observed that the P-value of Stenotic severity, eccentricity, and length and flow spirality are 0, 0.23, 0.04 and 0.67 respectively. Thus, the stenotic eccentricity and flow spirality have no influence on the $Velocity_{max}$ due to higher P-value. Thus, the stenotic severity and length have the influence on the $Velocity_{max}$ distribution and the regression coefficient of severity and length has revealed that they have positive relationship with the $Velocity_{max}$. According to the regression coefficient it can be said that if the stenotic severity will be increased by one unit, the $Velocity_{max}$ will expect to increase by 2.03 m/s.

Moreover, the $Velocity_{max}$ will expect to increase by 0.05 m/s when the length increases by 0.1 D and other predictors are constant.

Table 5.8: Coefficients and P-value of the predictors in the case 7.

Case	Dependent Variable	Independent Variables	Coefficients (m/s)	Significant Level p-value
7	$Velocity_{min}$	Constant	0.052	0.00<0.05
		Severity	-0.01	**0.09>0.05**
		Eccentricity	**0.00**	**0.42>0.05**
		Length	**0.00**	**0.28>0.05**
		Spirality	**0.00**	**0.62>0.05**

In case 7 of the Table 5.8, it is observed that the P-value of Stenotic severity, eccentricity, and length and flow spirality are 0.09, 0.42, 0.28 and 0.62 respectively. Thus, the stenotic severity, eccentricity, length and flow spirality have no influence on the $Velocity_{min}$ due to higher P-value. Thus, $Velocity_{min}$ can't be explained by the stenotic severity, eccentricity, length and flow spirality.

In case 8 of the Table 5.9, it is observed that the P-value of Stenotic severity, eccentricity, and length and flow spirality are 0.00, 0.28, 0.03 and 0.68 respectively. Thus, the stenotic eccentricity and flow spirality have no influence on

the $Velocity_{ave}$ due to higher P-value. However, the regression coefficient of the stenotic severity and length are 0.36 and 0.01 respectively. Thus, $Velocity_{ave}$ can be explained by the stenotic severity and length by 0.36 m/s and 0.01 m/s respectively when other predictors are constant.

Table 5.9: Coefficients and P-value of the predictors in the case 8.

Case	Dependent Variable	Independent Variables	Coefficients (m/s)	Significant Level p-value
8	$Velocity_{ave}$	Constant	0.07	0.00<0.05
		Severity	0.36	0.00<0.05
		Eccentricity	0.01	**0.28>0.05**
		Length	0.01	0.03<0.05
		Spirality	0.02	**0.68>0.05**

According to Table 5.2 – 5.9, the fitted lines for WSS_{max}, WSS_{min}, WSS_{ave}, $Pressure_{max}$, $Pressure_{drop}$, $Velocity_{max}$ and $Velocity_{ave}$ are presented by the following equations.

$$WSSmax(Pa) = -33.641(Pa) + 122.5(Pa) * severity + 10.426(Pa) * eccentricity - 6.363(Pa) * length + e \quad (5.1)$$

$$WSSmin(Pa) = 0.023(Pa) - 0.032(Pa) * Severity + 0.128(Pa) * Spirality + e \quad (5.2)$$

$$WSSave(Pa) = -1.402(Pa) + 4.7(Pa) * severity + 0.797(Pa) * eccentricity + e \quad (5.3)$$

$$Pressuremax = 115.557 + 10.7 * severity + 0.355 * length + e \quad (5.4)$$

$$Pressuredrop(mmHg) = -7.29(mmHg) + 16.10(mmHg) * severity + e \quad (5.5)$$

$$Velocitymax(m/s) = -0.415(m/s) + 2.03(m/s) * severity + 0.05(m/s) * length + e \quad (5.6)$$

$$Velocityave(m/s) = 0.07(m/s) + 0.36(m/s) * severity + 0.01(m/s) * length + e \quad (5.7)$$

The impacts of the stenotic Severity, Eccentricity, Length and flow Spirality on the physiological parameters are presented in table 5.10 – 5.13. Table 5.10 shows the impacts of stenotic Severity on the physiological parameters. From the table 5.10, it can be described that, if the stenotic severity is raised by 1% keeping others predictors unchanged, the WSS_{max}, WSS_{ave}, $Pressure_{max}$, $Pressure_{drop}$, $Velocity_{max}$, and $Velocity_{ave}$, will expect to increase by 122.5 Pa, 4.7 Pa, 10.7 mmHg, 16.10 mmHg, 2.03 m/s, and 0.36 m/s respectively whereas, WSS_{min} will

expect to decrease by 0.032 Pa. Besides, the stenotic severity has the impacts on all physiological parameters except the minimum velocity. Therefore, stenotic severity is a very influential factor in the physiological parameters.

Table 5.10: The impacts of stenotic severity on the physiological parameters.

Independent Variable	Dependent Variable	Coefficients
Stenotic severity	WSS_{max}	122.5 (Pa)
	WSS_{min}	-0.032 (Pa)
	WSS_{ave}	4.7 (Pa)
	$Pressure_{max}$	10.7 (mmHg)
	$Pressure_{drop}$	16.10 (mmHg)
	$Velocity_{max}$	2.03 (m/s)
	$Velocity_{ave}$	0.36 (m/s)

Table 5.11: The impacts of stenotic eccentricity on the physiological parameters.

Independent Variable	Dependent Variable	Coefficients
Stenotic Eccentricity	WSS_{max}	10.426 (Pa)
	WSS_{ave}	0.797 (Pa)

Table 5.11 shows the impacts of stenotic eccentricity on the physiological parameters. From table 5.11 it can be described that, if the stenotic eccentricity

increases by 0.1 keeping other predictors unchanged, the WSS_{max} and WSS_{ave} will expect to increase by 10.426 Pa and 0.797 Pa respectively. Besides, the stenotic eccentricity has the impacts only on the maximum and average wall shear stresses. Therefore, stenotic eccentricity is not a very influential factor in the physiological parameters.

Table 5.12: The impacts of stenotic length on the physiological parameters.

Independent Variable	Dependent Variable	Coefficients
Stenotic Length	WSS_{max}	-6.363(Pa)
	$Pressure_{max}$	0.355 (mmHg)
	$Velocity_{max}$	0.05 (m/s)
	$Velocity_{ave}$	0.01 (m/s)

Table 5.13: The impacts of flow spirality on the physiological parameters.

Independent Variable	Dependent Variable	Coefficients
Flow Spirality	WSS_{min}	0.128 (Pa)

Table 5.12 shows the impacts of stenotic length on the physiological parameters. From the table 5.12 it can be described that, if the stenotic length increases by 0.1D keeping others predictors unchanged, the $Pressure_{max}$,

$Velocity_{max}$, and $Velocity_{ave}$, will expect to increase by 0.355 mmHg, 0.05 m/s, and 0.01 m/s respectively whereas, WSS_{max} will expect to decrease by 6.363 Pa. The stenotic length is the second most influential factor in the physiological parameters as it has the impacts on the maximum wall shear stresses, pressure, and velocity as well as average velocity. On the other hand, from table 5.13 it is found that flow spirality is not at all an influencing factor for flow parameters as it has only an impact on the WSS_{min}.

From the above results and discussion, it is clear that the stenotic severity and length are very important influential factors for the shape of the arterial stenosis because of having the impacts on physiological parameters. On the other hand, stenotic eccentricity is not a very important influential factor for the shape of the arterial stenosis.

Chapter 6

Conclusions

Overview: This chapter has presented the conclusion of this studies.

There are several conclusions one can make from this study that can be applied to cases of atherosclerosis. These allow for a further insight on the health complications that can arise from this disease as well as the possible worsening of the condition. Actually, local hemodynamic factors influence the evolution of atherosclerotic disease and may contribute to explaining the differences in distribution and progression of different atherosclerotic plaques. The presence of a low wall shear stress favors progression of the plaque, while a physiologic shear stress has a protective effect in the vascular endothelium. Thus, the main concerns in this case are the wall shear stress and flow pressure, as both have been linked to having an effect on the stenosis. However, the flow velocity profiles are highly dependent on the condition of the blood and artery itself, and do not affect the stenosis significantly. The flow recirculation, however, is responsible for depositions of harmful materials and in this case there tends to be a notable region of recirculation despite the low degree of severity of the stenosis. The size of this recirculation zone varies throughout the flow, however, and during the acceleration phase there is very little evidence of flow recirculation. However, in this study

blood flow through carotid arteries has been investigated to find out flow behaviors insight the arteries with bifurcation and different level of severities. Then, an investigation has been done to specify the difference of flow outcomes from rigid body wall and elastic wall condition. Finally, a statistical analysis has been done to figure out the impact of the stenotic shapes and flow spirality on hemodynamic parametres such as wall shear stress, pressure and velocity.

Thus, numerical simulation has been done on physiological blood flow through carotid arteries with different severities of stenosis. From the investigation it is concluded that the low-Re k-w turbulence model can provide satisfactory information regarding blood flow in arterial stenoses, which is difficult to obtain accurately by experimental methods. Furthermore, bifurcation area is the most risky region of carotid artery because highest wall shear stress is observed there. Another observation is that transient or unstable flow can create flow disturbance regions in the arteries. Moreover, the disturbance of flow has risen as the severity of stenosis in the artery has been increased.

Besides, it can be conclude that a significant amount of Pressure difference has been noticed between upstream and downstream of the geometries at early systole, but very negligible amount of pressure drop has found at the stenotic throat region at the arteries of all severities. A significant amount of pressure drop has

found at the stenotic throat region of all severity of arteries at peak systole. Pressure of the downstream is higher than that of the upstream at diastole. However, pressure distributions for elastic body and rigid body artery at upstream of 75% severity are different, but same at the stenotic throat and downstream. Other than that, pressure distribution for elastic body and rigid body artery are almost same at all time instant.

In addition, blood flow rate is very low at the arteries of all severities at early systole. Results of velocity of elastic wall and rigid wall artery are little different at the upstream and downstream region, but are same at the throat region. However, results of velocity of elastic wall and rigid wall artery are almost same at the upstream, throat and downstream region at peak systole. Moreover, results of velocity of elastic wall and rigid wall artery are also same at the upstream, throat and downstream region at the diastole. However, very little stenotic jet is found at the throat regions of the arteries of all severities at the diastole, but long stenotic jet is found at the same regions at the peak systole. Blood flow rate is also very low through at the diastole as like as at the early systole.

Moreover, the results of wall shear stress of elastic wall and rigid wall are little different only at the downstream region of 45% and 55% stenotic arteries, but the results of wall shear stress of elastic wall and rigid wall are in good agreement throughout the geometry of 65% and 75% stenotic severities at early systole.

However, the WSS of a rigid body artery is a little greater than of elastic body artery at the throat region of the 65% stenotic artery, but the same result is an alternative for the 75% stenotic artery. Besides, the results of wall shear stress of elastic wall and rigid wall are little different at the throat region of 45% and 75% stenotic arteries, rest of the region are almost same, but the same results are in good agreement for 55% and 65% stenotic arteries at peak systole. The WSS of elastic body artery is little greater than of rigid body artery at the throat region of 45% and 55% stenotic artery, but the same result is an alternative for the 75% stenotic artery. However, the results of wall shear stress of elastic wall and rigid wall are in very good agreement at all regions of 45%, 55%, 65%, and 75% stenotic arteries at diastole.

From the statistical analysis it can be concluded that the cases for WSS_{max}, WSS_{min}, WSS_{ave}, $Pressure_{max}$, $Pressure_{drop}$, $Velocity_{max}$ and $Velocity_{ave}$ are statistically significant as p-value are less than 0.05. Besides, 73.4%, 55.6%, 63.6%, 61.4%, 66%, 82.1% and 78.7% of the variation of the WSS_{max}, WSS_{min}, WSS_{ave}, $Pressure_{max}$, $Pressure_{drop}$, $Velocity_{max}$ and $Velocity_{ave}$ respectively can be explained by the stenotic severity, eccentricity, and length and flow spirality. However, $Velocity_{min}$, can't be explained by the stenotic severity, eccentricity, length and flow spirality because the p-value of $Velocity_{min}$ is greater than 0.05. The severity is the most influencing factor for WSS_{max}, but flow spirality has no

influence on the WSS_{max}. Thus, the WSS_{max} has been influenced by the stenotic severity, eccentricity and length, whereas the WSS_{min} has been influenced by the stenotic severity and flow spirality. The stenotic length has an influence on the WSS_{max}, $Pressure_{max}$, $Velocity_{max}$ and $Velocity_{ave}$ whereas the stenotic severity has an influence on all of the dependent variables. The $Pressure_{max}$, $Velocity_{max}$ and $Velocity_{ave}$ have been influenced by the stenotic severity and length, so, stenotic eccentricity and flow spirality have no influence on them. The $Pressure_{drop}$ has been influenced only by the stenotic severity. However, the stenotic shape and flow spirality haven't any influence on the $Velocity_{min}$.

In short, the stenotic severity and length are very important influential factors for the shape of the arterial stenosis because of having the impacts on physiological parameters. On the other hand, stenotic eccentricity is not a very important influential factor for the shape of the arterial stenosis. Moreover, flow spirality is not at all an influencing factor for flow parameters as it has only an impact on the WSS_{min}.

Chapter 7

Recommendations for further studies

Overview

This chapter reviews some important results and discusses the results to recommend for the further studies for biomedical engineers.

7.1 Introduction

There is promising scope of this research is to extend the study to investigate the Magneto Hydro Dynamic (MHD) flow through arterial stenosis in a human body. The effect of magnetic field on blood flow is a very significant topic for bio-medical engineers as the ferrofluids are widely used nowadays in the industry and medicines. The ferrofluids are used as magnetic separation tool, anti-cancer drug carrier, micro-valve application, etc. One important application of these fluids is in chemotherapy application. Besides, the magnetic field can control the heat and blood flow characteristics through the arteries. It has an effect on the resistance to blood flow through arteries. Thus, in this paper, the effect of magnetic field on blood flow through arteries has been discussed. The most recent findings from various research articles are described herein in a systematic way. Moreover, some important results from the articles are presented here. It is observed that the blood

flow resistance in a vessel is mainly regulated by the vessel's radius and length of the blood vessel. Moreover, as the magnetic strength and size of the magnetic particles increase, the accumulation of nano-particles increases, as well. It is also found that the effect of doubling the magnetic field from 4 to 8 tesla increases the pressure drop by nearly 15%, but it shows marginal influence on the wall shear stress. It's believed that experimental study as well as numerical simulations can significantly contribute to further advancements of various applications of bio-magnetic fluid dynamics problems. Thus various studies on bio-magnetic fluid dynamics problems have been reviewed and some important results have been presented in this chapter.

7.2. Reviewed results and discussion

It is desirable that the biomedical engineers will get valuable information from this article regarding the importance of conducting research on blood flow under the influence of the magnetic field. In addition, the effect of magnetic field on blood flow through arteries has been discussed. Actually, the most recent findings from various research articles are described herein in a systematic way. Moreover, some important results from the articles are presented here.

Bali and Awasthi [67] investigated the effect of a magnetic field on the resistance to blood flow through stenotic artery where they graphically presented

results of velocity resistance to the blood flow for different magnetic field. Where, the blood flow resistance is the resistance that must be overcome to push blood through the circulatory system and create flow. Blood flow decreases when there is increased resistance to flow. Increased length of the blood vessel and decreased radius of the blood vessel are the factors that decrease blood flow and increase resistance to flow. Thus, the blood flow resistance in a vessel is mainly regulated by the vessel radius and length of the blood vessel.

Figures 7.1–7.3 describe the variation of resistance to flow (λ) with stenosis height ($<<1$) for different hematocrit values of red cell of the blood (M), and Hartmann number (H = 0, 0.2, 0.6, 1). However, hematocrit level is the ratio of the volume of red cells to the volume of whole blood. Causes of low hematocrit include bleeding such as ulcers, trauma, colon cancer, or internal bleeding. On the other hand, a higher than normal hematocrit can indicate as dehydration that causes to produce too many red blood cells. In addition, Hartmann number is the ratio of electromagnetic force to the viscous force introduced by Hartmann. Blood flow resistance increases with the increase of stenosis height and hematocrit values of red cell, which is depending on hematocrit value of blood. Flow resistance lines for different Hartmann number have been started to increase with the stenosis height from one point when hematocrit value is 4. Moreover, flow resistance decreases with the increases in the value of Hartmann number (H).

Figures 7.4–7.6 depicts the variation of axial velocity (u) with radial axis (r) for different value of Hartmann number and hematocrit value of red cell. The velocity decreases with the increase of radial axis (r) and the magnetic field. Besides, velocity lines are combined in one point at the radial axis value of 10 for all the hematocrit values of red cell. Thus, it is observed that the application of a uniform magnetic field has a definite effect on the velocity of blood flow. However, the axial velocity increases with the increase of the hematocrit value, observed in the figures 7.4 - 7.6.

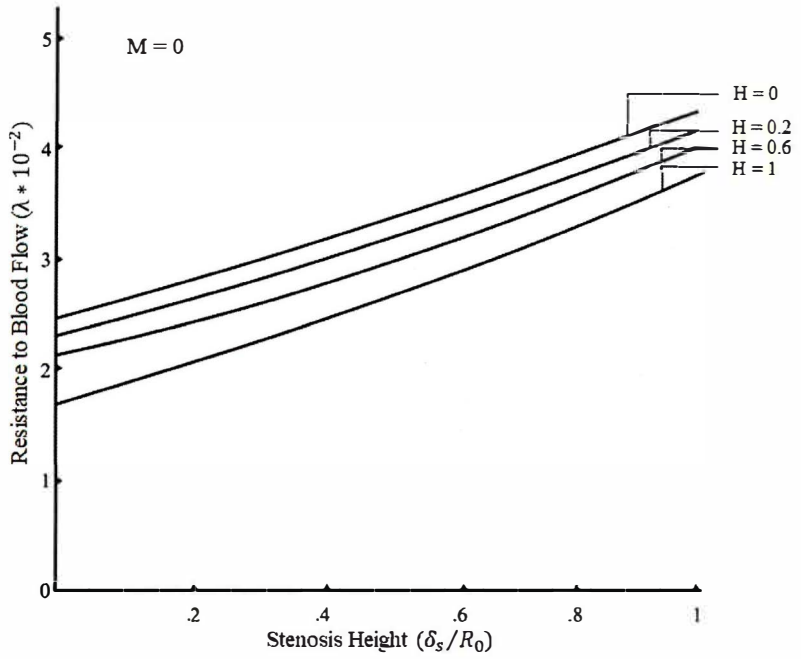

Fig. 7.1. Variation of resistance to blood flow with stenosis height and for M = 0, [67].

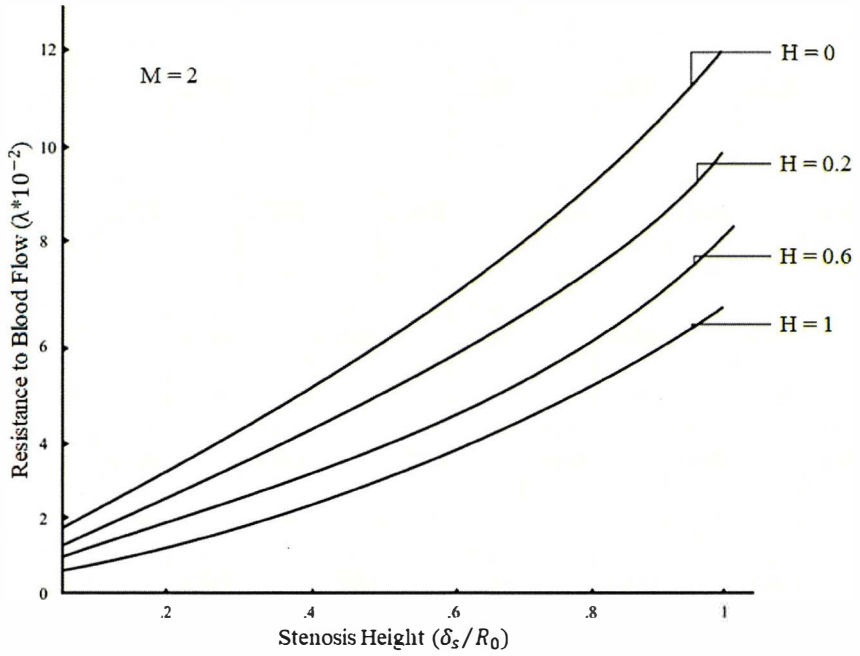

Fig. 7.2. Variation of resistance to blood flow with stenosis height and for M = 2, [67].

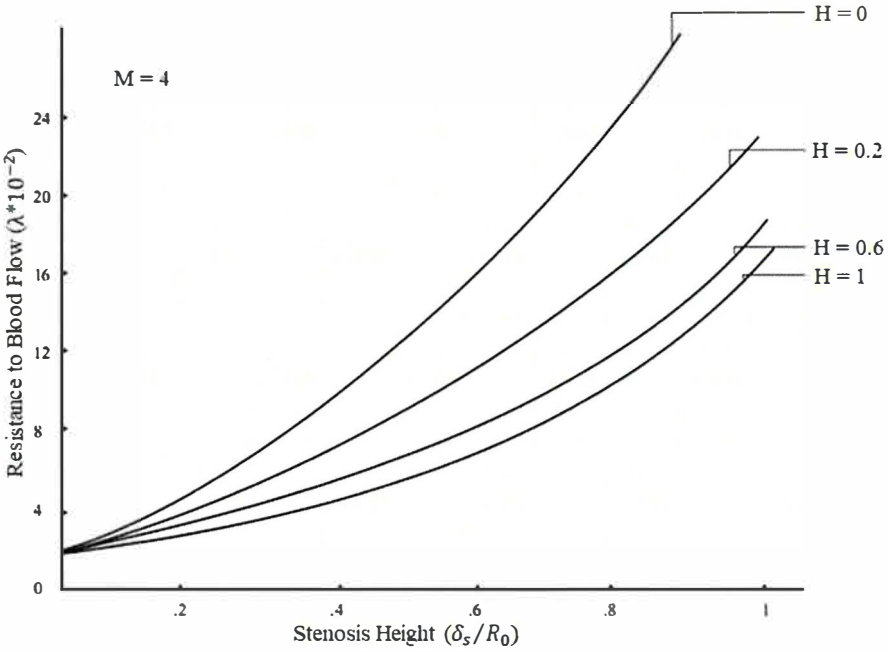

Fig. 7.3. Variation of resistance to blood flow with stenosis height and for M = 4, [67].

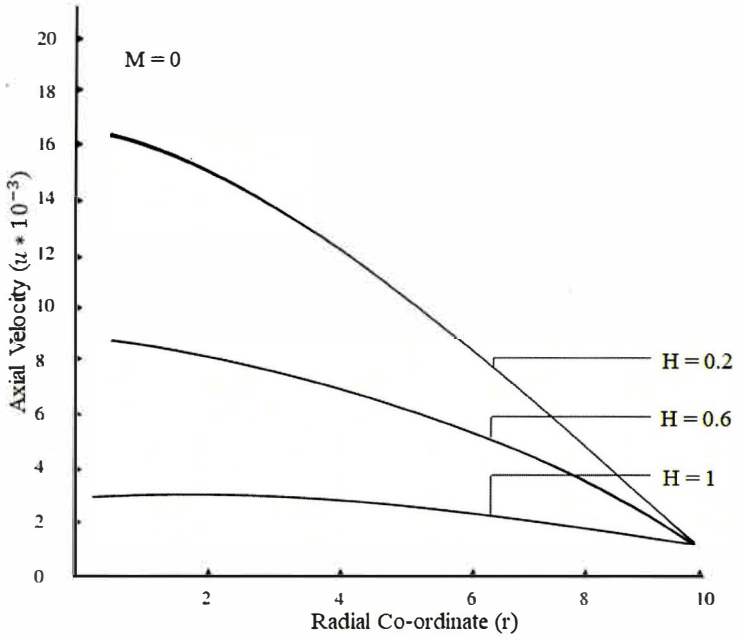

Fig. 7.4. Variation of axial velocity (m/s) with radial co-ordinate and for M = 0, [67].

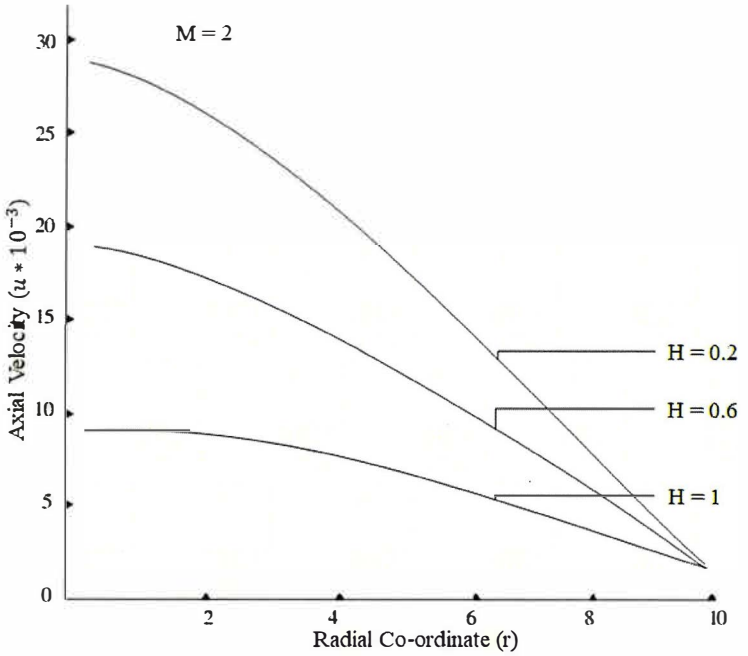

Fig. 7.5. Variation of axial velocity (m/s) with radial co-ordinate and for M = 2, [67].

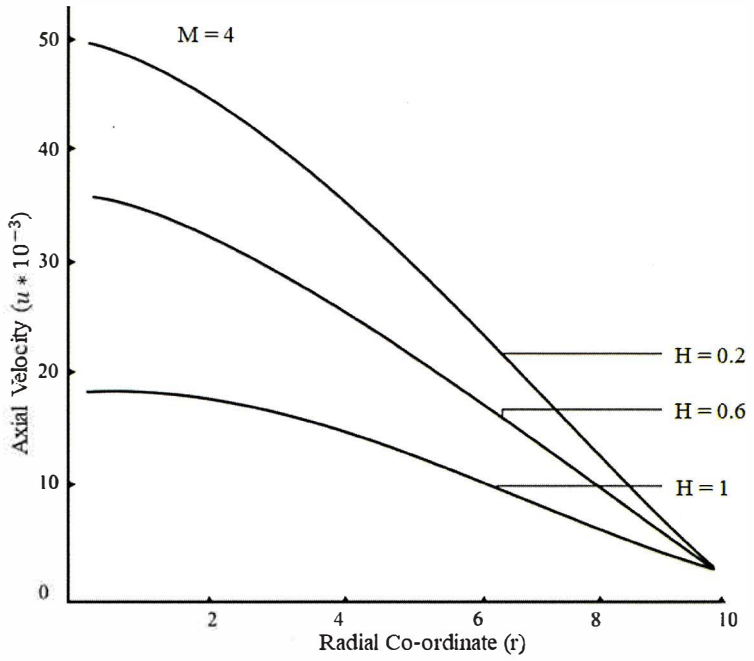

Fig. 7.6. Variation of axial velocity (m/s) with radial co-ordinate and for M = 4, [67].

Habibi and Ghasemi [90] conducted a numerical study of magnetic nano-particles concentration in blood under influence of high gradient magnetic field. The purpose of their study was to investigate the effect of a magnetic field on the volume concentration of magnetic nano-particles of a non-Newtonian bio-fluid (blood) as a drug carrier. They found that the accumulation of magnetic nano-particles near the magnetic source until it looks like a solid object. Besides, the accumulation of nano-particles is due to the magnetic force that overcomes the fluid drag force. As the magnetic strength and size of the magnetic particles increase, the accumulation of nano-particles increases, as well. They presented figure 7.7 that depicts the stream lines at the centre of the channel. There exists a

recirculation inside the particles near the magnet, because the reduction in the velocity and fluid movement over an obstacle. The viscosity contour of the bio-fluid at the channel midpoint where inlet velocity is equal to 0.001 m/s is depicted in figure 7.8. As shown near the solid obstacle and near the wall, where the shear strain is highest, the viscosity decreases while in the middle of the channel it increases. The diameter of particles is changed from 2000 to 200 nm while other conditions remained unchanged for investigating the effect of particles size on the flow field and magnetic nano-particles absorption. Figure 7.9 shows the concentration distribution of the bio-fluid near the magnet source. As shown, absorption of the 200 nm magnetic nano-particles decreases dramatically in comparison with that of 2000 nm particles, because the reduction in magnetic forces in the particles. It is known that magnetic forces are function of the particles volume. The magnetic forces for 200 nm particles are too weak to overcome the hydrodynamic forces, because of the low particles concentration and high inertial forces.

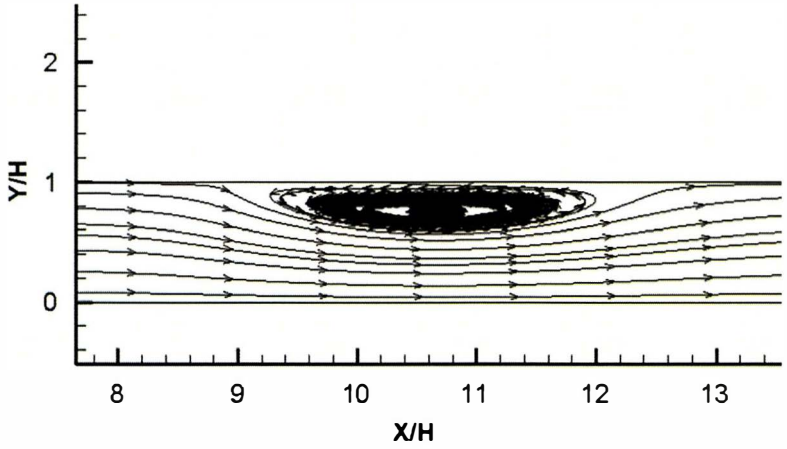

Fig. 7.7. Stream lines in the central portion of channel, [90].

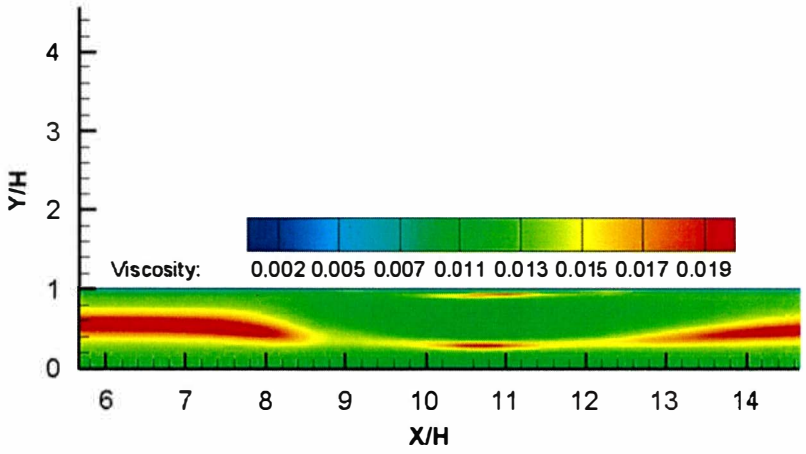

Fig. 7.8. Viscosity (m/s) contour in the central portion of channel, [90].

Figure 7.10 shows the velocity field in central portion of the channel. It is clear that blood flow is less affected by the magnetic forces and therefore it flows freely. One of the most effective methods to increase the nano-particles in the vessel is by decreasing the distance between magnetic source and the blood flow. Thus, for a

200 nm size particle the distance between magnet centre and upper wall is decreased by 2 mm.

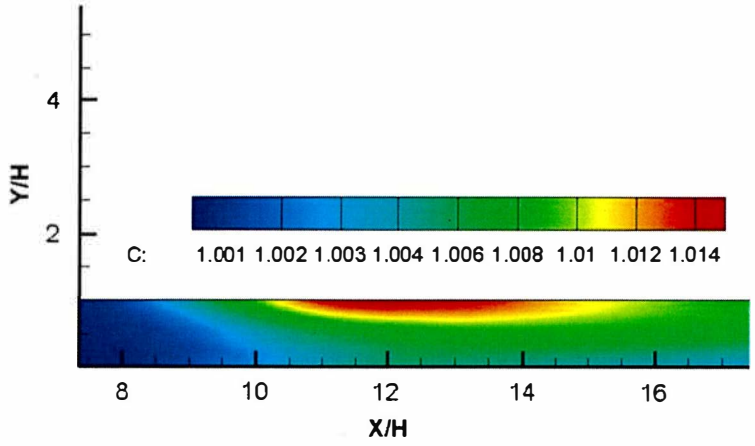

Fig. 7.9. Concentration distribution in the central portion of channel, [90].

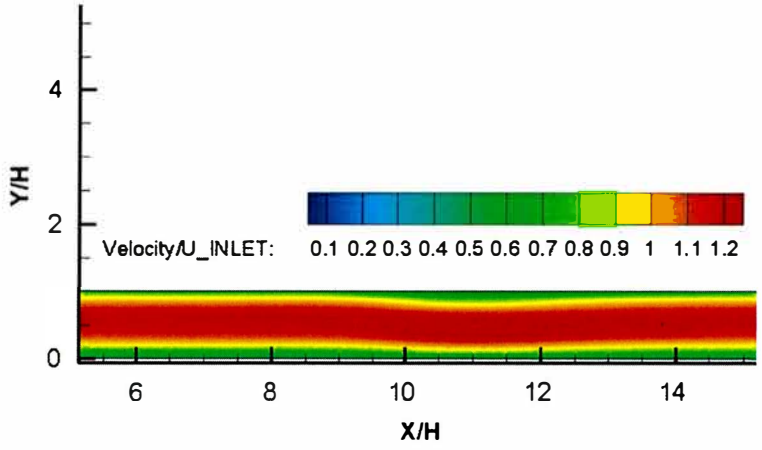

Fig. 7.10. Velocity (m/s) contour in the central portion of channel, [90].

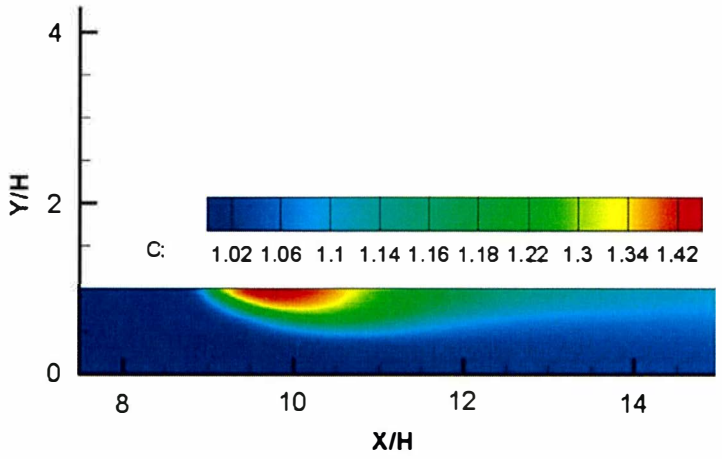

Fig. 7.11. Concentration distribution in the central portion of channel, [90].

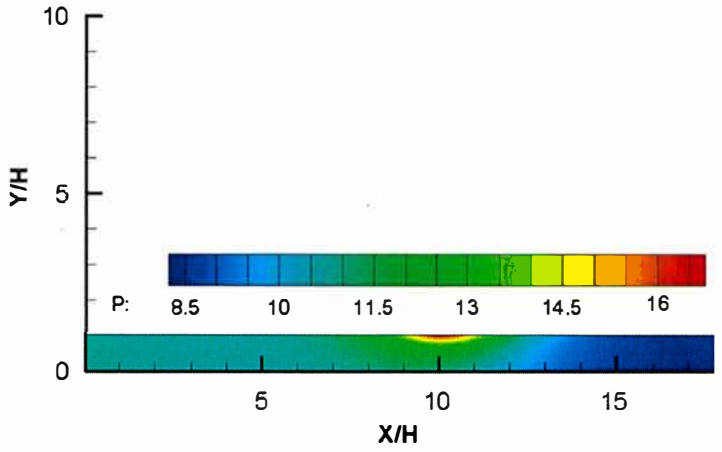

Fig. 7.12. Blood pressure (kPa) contour in the central portion of channel, [90].

Figure 7.11 shows the concentration distribution of 200 nm particles with inlet velocity and magnetic susceptibility equal to 0.001 m/s and 0.004 respectively. It is clear from figure 7.11 that magnetic nano-particles concentration increases by 40% when the position of the magnet gets closer to the upper wall. Figure 7.12 shows the 200 nm magnetic nano-particles blood pressure field, where

the pressure increases near the magnetic source when the particles create a restriction in front of the blood flow. Figure 7.13 shows the upper wall shear stress of various magnetic field strengths. High velocity gradient near the magnet is produced by blood flow and high particle concentration, so the shear stress increases especially near the magnetic source as magnetic field strength increases.

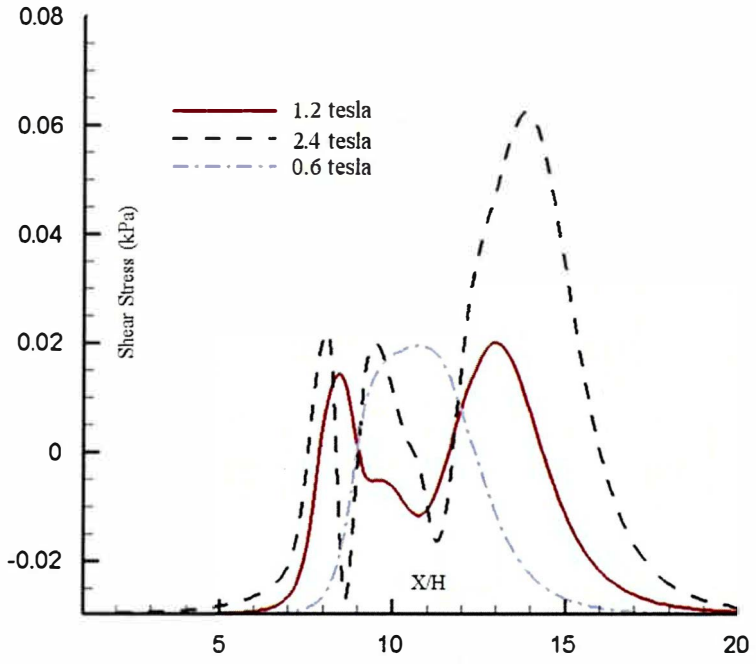

Fig. 7.13. Shear stress (kPa) for various magnetic field strengths, [90].

Alshare and Tashtoush [91] conducted simulations of magneto hemodynamics in stenosed arteries in diabetic or anemic models where they found that using Newtonian viscosity model of blood in contrast to Carreau model underestimates the pressure drop and wall shear stress by nearly 34% and 40%

respectively. It is also found from the figure 7.14 that the effect of doubling the magnetic field from 4 to 8 tesla increases the pressure drop by nearly 15%, but it shows marginal influence on the wall shear stress.

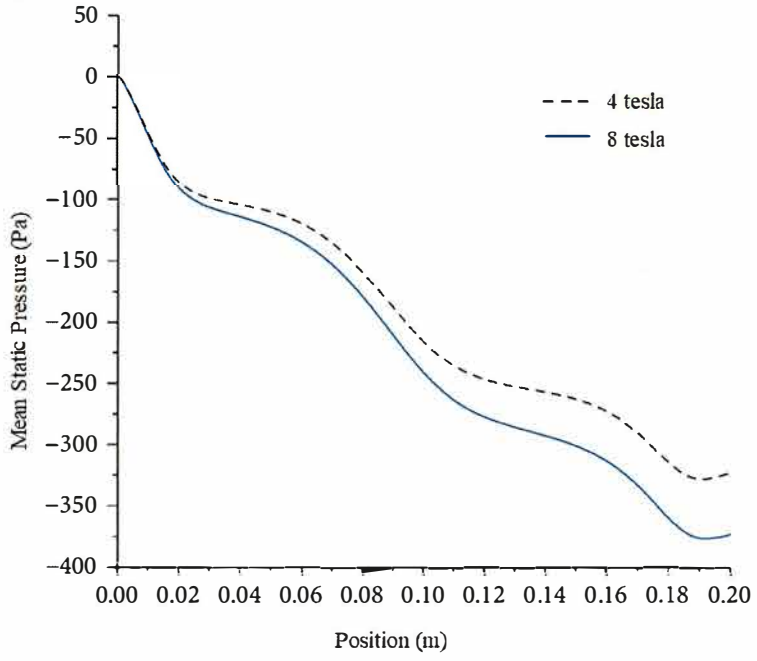

Fig. 7.14: Effect of magnetic field on mean pressure drop for the magnetic field 4 and 8 tesla, [91].

7.3 Conclusion

Bio-magnetic fluid flow is the emerging research field that is attracting the researchers to develop the medical technology using magnetic field. Therefore, some significant research articles on bio-magnetic fluid (blood) flow are reviewed and their results are discussed easily so that the biomedical engineers will get valuable information from this review article regarding the importance of

conducting research on blood flow under the influence of the magnetic field. It is expected that the researcher will take this review study as one of their valuable materials for initiating the research on bio-magnetic fluid flow. However, it is recommended that the blood flow resistance must be overcome to push blood through the circulatory system and create flow, as the blood flow decreases with the increased resistance to flow. Besides, it is found that increased length of the blood vessel and decreased radius of the blood vessel are the factors that decrease blood flow and increase resistance to flow. Thus, the blood flow resistance in a vessel is mainly regulated by the vessel radius and length of the blood vessel. Moreover, it is found that the accumulation of magnetic nano-particles near the magnetic source until it looks like a solid object. Besides, the accumulation of nano-particles is due to the magnetic force that overcomes the fluid drag force. As the magnetic strength and size of the magnetic particles increase, the accumulation of nano-particles increases, as well. It is also found that the effect of doubling the magnetic field from 4 to 8 tesla increases the pressure drop by nearly 15%, but it shows marginal influence on the wall shear stress.

Bio-medical engineers can investigate further numerical as well as experimental study on blood flow through stenotic vessels under magnetic field to understand characteristics of flow behavior by analyzing flow parameters, because nowadays the magnetic field effects are significantly increasing around the patient. Besides,

using magnetic nano-particles in various drugs are also increasing day by day. Thus, bio-medical engineers are suggested to investigate the effects of those nano-particles in the blood under magnetic field environments.

References

[1] S. Khader, and B. Shenoy; Effect of increased severity in patient specific stenosis, *World Journal of Modelling and Simulation*, Vol. 7 (2011) No. 2, pp. 113-122.

[2] M.X. Li, J.J. Beech-Brandt, L.R. John, P.R. Hoskins, and W.J. Easson, Numerical analysis of pulsatile blood flow and vessel wall mechanics in different degrees of stenosis, *J. Biomech*, 40 (2007) 3715-3724

[3] C. Chua, and G. Shread, Changes in flow and wall stresses through arterial constriction offset from the centre of the vessel, *The Anziam Journal*, 2009, 50: C744–C759.

[4] V. Young, A. Patterson M. Graves, Z-Y LI, V. Tavani, T. Tang, and J. H. Gillard, The mechanical triggers of rupture: shear vs pressure gradient, *The British J. of Radiology*, 82 (2009) S39-S45

[5] J. Pinto, K.L. Bessa, D.F. Legendre, and R.H. Mouth, Physiologycal pulsatile waveform through axisymmetric stenosed arteries: Numerical Simulation, *ABCM Symposium in Bioengineering*, 1 (2006).

[6] S. Lee, and S. Lee, Direct numerical simulation of transitional flow in a stenose carotid bifurcation, *Journal of Biomechanics*, 41, 2551–2561, 2008.

[7] S.A. Ahmed, and D.P. Giddens, Pulsatile Poststenotic Flow Studies with Laser Doppler Anemometry, *J. Biomech.*, 17 (1984) 695-705.

[8] G. Lorenzini, and E. Casalena, CFD analysis of pulsatile blood flow in an atherosclerotic human artery with eccentric plaques, *Journal of Biomechanics*, 41, 1862–1870, 2008.

[9] Pedley, T. J., The Fluid Mechanics of Large Blood Vessels, *Cambridge University Press*, 1980.

[10] Berger, S. A., Jou, L. D., Flow in stenotic vessels, *Annual Reviews of Fluid Mechanics*, 32, 347-382, 2000.

[11] Chien, S., Hemorheology in clinical medicine, *Recent advances in Cardiovascular Diseases 2 (Suppl.)*, 21, 1981.

[12] Mandal, P. K., An unsteady analysis of non-Newtonian blood flow through tapered arteries with a stenosis, *International Journal of Non-Linear Mechanics*, 40, 151-164, 2005.

[13] Thurston, G. B., Viscoelasticity of human blood, *Journal of Biophysics*, 12, 1205-1212, 1972

[14] Thurston, G. B., Frequency and shear rate dependence of viscoelasticity of human blood, *Biorheology*, 10, 375-381, 1973

[15] Cho, Y. I. And Kensey K. R., Effects of the non-Newtonian viscosity of blood in flows in a diseased arterial vessel, Part 1: Steady flows, *Biorheology*, 28, 241-262, 1991

[16] Walawender, W. P., Chen T. Y. and Cala, D. F., An approximate Casson fluid model for tube flow of blood, *Biorheology*, 12, 111-119, 1975

[17] Cokelet, G. R. The rheology of the human blood. Chapter 4 in *Biomechanics: Its Functions and Objectives*, edited by Fun, Y. C., Perrone, N. and Anliker, M. Prentice- Hall, Englewood Cliffs, NJ: 63-103, 1972

[18] Powell, R. E., and Eyring, H., Mechanism for Relaxation Theory of Viscosity, *Nature*, 154, 427-428, 1944

[19] Johnston, B.M., Johnston, P. R., Corney, S. and Kilpatrick, D., Non-Newtonian blood flow in human right coronary arteries: steady state simulations, *Journal of Biomechanics*, 37, 709-720, 2004

[20] Johnston, B. M., Johnston P. R., Corney, S. and Kilpatrick, D., Non-Newtonian blood flow in human right coronary arteries: Transient simulations, *Journal of Biomechanics*, 39, 6, 1116-1128, 2006

[21] Perktold, K., Peter, R. and Resch, M., Pulsatile non-Newtonian blood flow simulation through a bifurcation with an aneurysm, *Biorheology*, 26, 1011-1030, 1989

[22] Gijsen, F.J.H., Allanic, E., Vosse, F.N. and Janssen, J.D., The Influences of the non-Newtonian Properties of Blood on the Flow in Large Arteries: Unsteady Flow in a 90 Curved Tube, *Journal of Biomechanics*, 32, 705-713, 1999.

[23] Formaggia, L., Lamponi, D. and Quarteroni, A., One-Dimensional Models for Blood Flow in Arteries, *Journal of Engineering Mathematics*, 47, 251-276, 2003.

[24] Lee, K.W. and Xu, X.Y., Modelling of Flow and Wall Behaviour in a Mildly Stenosed Tube, *Medical Engineering & Physics*, 24, 575-586, 2002.

[25] Chakravarty, S., Mandal, P.K., A Nonlinear Two-Dimensional Model of Blood Flow in an Overlapping Arterial Stenosis Subjected to Body Acceleration, *Mathematical and Computer Modelling*, 24, 43-58, 1996.

[26] Giddens DP, Mabon RF, Cassanova RA., Measurements of disordered flows distal to subtotal vascular stenoses in the thoracic aortas of dogs, *Circ. Res.*, 39, 112-119, 1976.

[27] Saad AA, Giddens DP., Velocity measurements in steady flow through axisymmetric stenoses at moderate Reynolds numbers, *J. Biomech.*, 16, 505-516, 1983.

[28] Strandness DE JR., Didisheim P, Clowes AW, Watson JT., Vascular Disease – Current Research and Clinical Applications, Orlando, USA: Grune and Stratton, 1987.Eds.

[29] Clark C., The propagation of turbulence produced by a stenosis, *J. Biomech.*, 13, 591-604, 1980.

[30] Cassanova RA, Giddens DP., Disorder distal to modelled stenoses in steady and pulsatile flow. *J. Biomech.*, 11, 441-453, 1978.

[31] Smith, F. T., The separation flow through a severely constricted symmetric tube, *Journal of Fluid Mechanics*, 90, 725-754, 1979.

[32] Deshpande, M. D., Geidens, D. P. and Mabon F. R., Steady laminar flow through modelled vascular stenosis, *Journal of Biomechanics*, 09, 165-174, 1976.

[33] Young, D. F., Tsai, F. Y., Flow characteristics in models of arterial stenosis: I steady flow, *Journal of Biomechanics*, 06, 395-410, 1973.

[34] Tatukder, N., Karayannacos, P.E., Nerem, R. M., Vasko, J.S., An experimental study of the fluid dynamics of multiple noncritical stenoses, *J. Biomech. Eng.*, 99, 2, 74-82, 1977.

[35] Kumar, A.,. Awasthi, U., A mathematical model for blood flow in a multiple stenosis artery, *Int. J. Math. Analysis*, 4, 50, 2465-2472, 2010.

[36] Falk, E., Shah, P.K., Fuster, V., Coronary plaque disruption, *Circulation*, 92, 3, 657 -71, 1995.

[37] Javadzadegan, A., et al., Correlation between Reynolds number and eccentricity effect in stenosed artery models, *Technol Health Care*, 21, 4, 357-67, 2013.

[38] Javadzadegan, A., et al., Flow recirculation zone length and shear rate are differentially affected by stenosis severity in human coronary arteries, *Am J Physiol Heart Circ Physiol*, 304, 4, H559-66, 2013.

[39] Houston, J.G., et al., Spiral laminar flow in the abdominal aorta: a predictor of renal impairment deterioration in patients with renal artery stenosis?, *Nephrol Dial Transplant*, 19, 7, 1786-91, 2004.

[40] Frazin L.J., Vonesh M.J., Chandran K.B., Shipkowitz T., Yaacoub A.S., McPherson D.D., Confirmation and initial documentation of thoracic and abdominal aortic helical flow. An ultrasound study. *ASAIO J.*, 42, 951-6, 1996.

[41] Stonebridge, P.A. and Brophy C.M., Spiral laminar flow in arteries? *The Lancet*, 338(8779), 1360-1361, 1991; DOI: 10.1016/0140-6736(91)92238-w

[42] Stonebridge, P.A., et al., Spiral laminar flow in vivo, *Clin Sci (Lond)*, 91, 1, 17-21, 1996.

[43] A. Javadzadegan, F. Babak, M. Behnia, M. Behnia, Fluidstructure interaction investigation of spiral flow in a model of abdominal aortic aneurysm, *European Journal of Mechanics, B/Fluids*, 46, 109-117, 2014.

[44] A. Javadzadegan, A. Simmons, T. Barber, Spiral blood flow in aorta-renal bifurcation models. Comput Methods Biomech Biomed Engin, 19, 9, 964-76, 2016.

[45] Chen, Z., et al., Swirling flow can suppress flow disturbances in endovascular stents: a numerical study, *ASAIO J.*, 55, 6, 543-9, 2009.

[46] Grigioni, M., et al., A mathematical description of blood spiral flow in vessels: application to a numerical study of flow in arterial bending, *J. Biomech,* 38, 7, 1375-86, 2005.

[47] Linge, F., Hye, M.A., Paul, M.C., Pulsatile spiral blood flow through arterial stenosis, *Comput Methods Biomech Biomed Engin*, 17, 15, 1727-37, 2014.

[48] Paul, M.C., Larman, A., Investigation of spiral blood flow in a model of arterial stenosis, *Med EngPhys*, 31, 9, 1195-203, 2009.

[49] Ha, H., Lee, S.J., Effect of swirling inlet condition on the flow field in a stenosed arterial vessel model, *Med Eng Phys*, 36, 1, 119-28, 2014.

[50] Fulker, D., et al., Flow visualisation study of spiral flow in the aorta-renal bifurcation, *Comput Methods Biomech Biomed Engin*, 20, 13, 1438-1441, 2017.

[51] Morbiducci, U., et al., Mechanistic insight into the physiological relevance of helical blood flow in the human aorta: an in vivo study, *Biomech Model Mechanobiol*, 10, 3, 339-55, 2011.

[52] Barbara J. Ballermann, Alan Dardik, Eudora Eng, Ailian Liu., Shear stress and endothelium, *Kidney International*, vol. 54, Suppl. 67, S-100-S-108, 1998.

[53] Gibbons G. H. and Dzau V. J., The emerging concept of vascular remodelling, *N. Engl J. Med.*, 330, 1431-1438, 1994.

[54] Malek MA, Alper SL, Izumo S., Hemodynamic shear stress and its role in atherosclerosis., *JAMA*, 282, 2035-2042, 1999.

[55] Fukumoto, Y., et al., Localized elevation of shear stress is related to coronary plaque rupture: a 3- dimensional intravascular ultrasound study with *in vivo* color mapping of shear stress distribution, *J. Am. Coll. Cardiol*, 51, 6, 645-50, 2008.

[56] Gijsen, F.J., et al., Strain distribution over plaques in human coronary arteries relates to shear stress, *Am. J. Physiol Heart Circ Physiol*, 295, 4, H1608- 14, 2008.

[57] Malek, A.M., Alper, S.L., Izumo, S., Hemodynamic shear stress and its role in atherosclerosis, *JAMA*, 282, 21, 2035-42, 1999.

[58] Wootton, D.M., Ku, D.N., Fluid mechanics of vascular systems, diseases, and thrombosis, *Annu Rev Biomed Eng*, 1, 299-329, 1999.

[59] Y. Haik, V. Pai, and C. J. Chen, Biomagnetic fluid dynamics, *Fluid Dynamics at Interfaces*, edited by W. Shyy and R. Narayanan (Cambridge University Press, Cambridge, 1999), pp. 439–452.

[60] P.A. Voltairas, D.I. Fotiadis, L.K. Michalis, Hydrodynamics of magnetic drug targeting, *J. Biomech.*, 35, 813–821, 2002.

[61] W. Arnold, R. J. Klein, C. Alexiou, Loco regional cancer treatment with magnetic drug targeting, *Cancer Research*, 6641–6648, 2000.

[62] C. Alexiou, R. Jurgons, R. J. Schmid, C. Bergemann, J. Henke, W. Erhardt, , E. Huenges, F. Parak, Magnetic drug targeting bio distribution of the magnetic carrier and the chemotherapeutic agent mitoxantrone after loco regional cancer treatment, *Journal of Drug Targeting*, 11 (3), 139–149, 2003.

[63] Schenck J. F., Dumoulin C. L., Redington R. W., Kressel H. Y., Elliot R. T., McDougall I. L., Human exposure to 4.0-Tesla magnetic fields in a whole-body scanner, *Medical Physics*, 19, 1089–1098, 2003.

[64] Yamamoto T., Nagayama Y., Tamura M., A blood-oxygenation-dependent increase in blood viscosity due to a static magnetic field, *Physics in Medicine and Biology*, 49, 3267–3277, 2004.

[65] Sud V. K. and Sekhon G. S., Blood flow through human arterial system in the presence of a steady magnetic field, *Physics in Medicine and Biology*, 34 (7), 795–805, 1989.

[66] Kinouchi Y., Yamaguchi H., Tenforde T. S., Theoretical analysis of magnetic field interactions with aortic blood flow, *Bioelectromagnetics*, 17, 21–32, 1996.

[67] Bali R. and Awasthi U., Effect of a magnetic field on the resistance to blood flow through stenotic artery, *Applied Mathematics and Computation*, 188, 1635–1641, 2007.

[68] Haik Y., Pai V. and Chen C. J., Apparent viscosity of human blood in a high static magnetic field, *Journal of Magnetism and Magnetic Materials*, 225, 180–186, 2001.

[69] Khashan S. A. and Haik Y., Numerical simulation of biomagnetic fluid downstream an eccentric stenotic orifice, *Physics of Fluids*, 18 (11), 113601, 2006.

[70] Papadopoulos, P.K., Tzirtzilakis, E.E., Biomagnetic flow in a curved square duct under influence of an applied magnetic field, Physics of Fluids, 2004, 16 (8), 2952–2962.

[71] Tzirtzilakis E. E., A mathematical model for blood flow in magnetic field, *Physics of Fluids*, 17, 1–15, 2005, Art. No: 077103.

[72] B. Berkovski and V. Bashtovoy, Magnetic Fluids and Applications Handbook, *Begell House Inc.*, New York, 1996.

[73] P. A. Davidson, An Introduction to Magnetohydrodynamics, *Cambridge University Press*, 2001.

[74] R. Ganguly, A. P. Gaind, S. Sen, I. K. Puri, Analyzing ferrofluid transport for magnetic drug targeting, *J. Magn. Magn. Mater.* 289, 331–334, 2005.

[75] V. Loukopoulos, E. Tzirtzilakis, Biomagnetic channel flow in spatially varying magnetic field, *Int. J. Engrg. Sci.*, 42, 571–590, 2004.

[76] V. C. Loukopoulos, G. A. Katsiaris, G. T. Karahalios, A steady-state solver for the simulation of Taylor vortices in spherical annular flow, *Comput. Methods Appl. Mech. Engrg.* 192, 2993–3003, 2003.

[77] E. E. Tzirtzilakis, A simple numerical methodology for BFD problems using stream function vorticity formulation, *Comm. Numer. Methods Engrg.*, 24, 683–700, early view, Published Online: 11 Jan 2007, doi:10.1002/cnm.981.

[78] Zhao S., Xu X., Collins M., The numerical analysis of fluid-solid interactions for blood flow in arterial structures Part 2: development of coupled fluid-solid algorithms, Proceedings of the Institution of Mechanical Engineers, *Part H: Journal of Engineering in Medicine*, 212(4):241-252, 1998.

[79] Tang D., Yang C., Kobayashi S. and Ku D. N., Generalized finite difference method for 3-D viscous flow in stenotic rubes with large wall deformation and collapse, *Applied Numerical Mathematics*, 38, 49-68, 2001

[80] Chan W, Ding Y, Tu J, Modeling of non-Newtonian blood flow through a stenosed artery incorporating fluid-structure interaction, *ANZIAM Journal*, 47:C507-C523, 2007.

[81] Oscuii H. N., Shadpour M. T., Ghalichi F, Flow Characteristics in Elastic Arteries Using a Fluid-Structure Interaction Model, *American Journal of Applied Sciences*, 4, 8, 516, 2007.

[82] McCord B. M. and Ku D. N., Mechanical rupture of the atherosclerotic plaque fibrous cap, Proceedings of 1993 Bioengineering Conference, Colorado, BED-24, 324, 327, 1993

[83] Ohja M., Cobbold R. S. C., Johnston K.W. and Hummel R. L. Pulsatile flow through constricted tubes: an experimental investigation using photo chromic tracer methods, *Journal of Fluid Mechanics*, 203, 173-197, 1989

[84] Chakravaty S. and Mandal P. K., Two-dimensional blood flow through tapered arteries under stenotic conditions, *International Journal of Non-Linear Mechanics*, 35, 779-793, 2000

[85] Zendehbudi G. R. and Moayeri M. S., Comparison of physiological and simple pulsatile flows through stenosed arteries, *Journal of Biomechanics*, 32, 959-965, 1999

[86] Deplano V. and Siouffi M., Experimental and numerical study of pulsatile flows through stenoses: Wall shear stress analysis, *Journal of Biomechanics*, 32, 1081-1090, 1999

[87] Li Z. and Kleinstreuer C., Blood flow and structure interactions in a stented abdominal aortic aneurysm model, *Medical Engineering & Physics*, 27, 369-382, 2005

[88] M. M. Cross, Journal of Colloid Science, 20, 417–437, 1965.

[89] S. S. Varghese and S. H. Frankel, Numerical Modeling of Pulsatile Turbulent Flow in Stenotic Vessels, *J. Biomech*, Vol. 125, pp. 445-460, 2003.

[90] M. R. Habibi, M. Ghasemi, Numerical study of magnetic nanoparticles concentration in biofluid (blood) under influence of high gradient magnetic field, *Journal of Magnetism and Magnetic Materials*, 323, 32–38, 2011.

[91] A. Alshare, B. Tashtoush, Simulations of Magnetohemodynamics in Stenosed Arteries in Diabetic or Anemic Models, *Computational and*

Mathematical Methods in Medicine, Article ID 8123930, 13 pages, 2016, doi.org/10.1155/2016/8123930.

[92] Purves W. K., Sadava D., Orians G. H. and Heller C. H., Life: The Science of Biology, W. H. Freeman and Company, 6th Edition, 2003

[93] Ohja M., Cobbold R. S. C., Johnston K.W. and Hummel R. L., Pulsatile flow through constricted tubes: an experimental investigation using photochromic tracer methods, *Journal of Fluid Mechanics*, 203, 173-197, 1989

[94] Finol E. A., Amon C. H., Flow Dynamics in Anatomical Models of Abdominal Aortic Aneurysms: Computational Analysis of Pulsatile Flow, *Acta Científica Venezolana*, 54, 43-49, 2003.

[95] ENCYCLOPEDIA BRITANNICA, *White blood cell*, May 27, 2020, https://www.britannica.com/science/white-blood-cell

[96] WIKIPEDIA, *Ascending aorta*, 11 January 2020, https://en.wikipedia.org/wiki/Ascending_aorta

[97] AIBOLITA, *Blood Vessel Tunics*, https://aibolita.com/sundries/12808-blood-vessel-tunics.html

[98] WIKIMEDIA COMMONS, *File:Heart diagram-en.svg*, 12 June 2020, https://commons.wikimedia.org/wiki/File:Heart_diagram-en.svg

[99] WIKIMEDIA COMMONS, *File:2101 Blood Flow through the Heart.jpg*, 20 April 2019, https://commons.wikimedia.org/wiki/File:2101_Blood_Flow_Through_the_Heart.jpg

[100] M. Gordon, *Heart and vessels,* http://www.studyblue.com/notes/note/n/heart-and-vessels/deck/6409908. 2013. 11

[101] Weng Yew Chan, 'simulation of arterial stenosis incorporating fluid-structural interaction and non-Newtonian blood flow', March 2006, Thesis of Masters, Mechanical and Manufacturing Engineering RMIT University, Australia.

[102] M. X. Li, J. J. Beech-Brandt, L. R. John, P. R. Hoskins, and W. J. Easson, "Numerical analysis of pulsatile blood flow and vessel wall mechanics in different degrees of stenoses," *Journal of Biomechanics*, vol. 40, no. 16, pp. 3715–3724, 2007.

[103] D. V. Boger, "Demonstration of upper and lower Newtonian fluid behaviour in a pseudoplastic fluid," *Nature*, vol. 265, no. 5590, pp. 126–128, 1977.

[104] M. G. Rabby, A. Razzak, M. M. Molla, Pulsatile non-Newtonian blood flow through a model of arterial stenosis, *Procedia Engineering* 56 (2013) 225–231.

[105] S. P. Shupti, M. G. Rabby, and M. M. Molla, Rheological Behavior of Physiological Pulsatile Flow through a Model Arterial Stenosis with Moving Wall, *Journal of Fluids*, Volume 2015, Article ID 546716, 22 pages, http://dx.doi.org/10.1155/2015/546716

Appendix

Appendix 1:

Table 1: Stenotic severity, eccentricity, non-dimensional length and flow spirality data for 120 observations.

n	Severity (%)	Eccentricity	Length	Spirality (c)	n	Severity (%)	Eccentricity	Length	Spirality (c)
1	25	0	1	0	61	62	0.3	1	0.015
2	35	0	1.5	0.083	62	60	0.3	1.5	0.098
3	30	0	2	0.167	63	57	0.3	2	0.152
4	33	0	2.5	0.25	64	65	0.3	2.5	0.235
5	35	0.2	3	0.001	65	65	0.5	3	0.016
6	28	0.2	1	0.084	66	57	0.5	1	0.099
7	33	0.2	1.5	0.166	67	60	0.5	1.5	0.151
8	25	0.2	2	0.249	68	62	0.5	2	0.234
9	30	0.4	2.5	0.002	69	60	0.7	2.5	0.017
10	28	0.4	3	0.085	70	65	0.7	3	0.02
11	35	0.4	1	0.165	71	57	0.7	1	0.15
12	25	0.4	1.5	0.248	72	62	0.7	1.5	0.233
13	25	0.6	2	0.003	73	65	0.4	2	0.018
14	28	0.6	2.5	0.086	74	60	0.4	2.5	0.021
15	33	0.6	3	0.164	75	57	0.4	3	0.149
16	35	0.6	1	0.247	76	62	0.4	1	0.232
17	35	0.5	1.5	0.004	77	62	0.1	1.5	0.019

18	33	0.5	2	0.087	78	65	0.1	2	0.022
19	30	0.5	2.5	0.163	79	57	0.1	2.5	0.148
20	25	0.5	3	0.246	80	60	0.1	3	0.231
21	42	0.1	1	0.005	81	67	0.9	1	0.02
22	37	0.1	1.5	0.088	82	73	0.9	1.5	0.023
23	40	0.1	2	0.162	83	70	0.9	2	0.147
24	45	0.1	2.5	0.245	84	75	0.9	2.5	0.23
25	42	0.3	3	0.006	85	73	0.6	3	0.021
26	40	0.3	1	0.089	86	67	0.6	1	0.024
27	37	0.3	1.5	0.161	87	75	0.6	1.5	0.146
28	45	0.3	2	0.244	88	70	0.6	2	0.229
29	45	0.5	2.5	0.007	89	67	0.8	2.5	0.022
30	40	0.5	3	0.09	90	70	0.8	3	0.025
31	37	0.5	1	0.16	91	73	0.8	1	0.145
32	42	0.5	1.5	0.243	92	75	0.8	1.5	0.228
33	40	0.7	2	0.008	93	67	0	2	0.023
34	45	0.7	2.5	0.091	94	75	0	2.5	0.026
35	42	0.7	3	0.159	95	70	0	3	0.144
36	37	0.7	1	0.242	96	73	0	1	0.227
37	37	0.4	1.5	0.009	97	75	0.2	1.5	0.024
38	45	0.4	2	0.092	98	67	0.2	2	0.027
39	42	0.4	2.5	0.158	99	70	0.2	2.5	0.143
40	40	0.4	3	0.241	100	73	0.2	3	0.226
41	50	0.2	1	0.01	101	82	0.8	1	0.025
42	53	0.2	1.5	0.093	102	76	0.8	1.5	0.028

43	48	0.2	2	0.157	103	80	0.8	2	0.142
44	55	0.2	2.5	0.24	104	85	0.8	2.5	0.225
45	48	0.4	3	0.011	105	82	0.7	3	0.026
46	50	0.4	1	0.094	106	80	0.7	1	0.029
47	53	0.4	1.5	0.156	107	76	0.7	1.5	0.141
48	55	0.4	2	0.239	108	85	0.7	2	0.224
49	50	0.6	2.5	0.012	109	80	0.9	2.5	0.027
50	55	0.6	3	0.095	110	85	0.9	3	0.03
51	48	0.6	1	0.155	111	76	0.9	1	0.14
52	53	0.6	1.5	0.238	112	82	0.9	1.5	0.223
53	55	0.5	2	0.013	113	85	0.1	2	0.028
54	48	0.5	2.5	0.096	114	82	0.1	2.5	0.031
55	53	0.5	3	0.154	115	80	0.1	3	0.139
56	50	0.5	1	0.237	116	76	0.1	1	0.222
57	48	0	1.5	0.014	117	76	0.3	1.5	0.029
58	55	0	2	0.097	118	82	0.3	2	0.032
59	53	0	2.5	0.153	119	80	0.3	2.5	0.138
60	50	0	3	0.236	120	85	0.3	3	0.221

Appendix 2:

User defined function: user defined function has been written in C++ programming language to demonstrate the boundary conditions and fluid properties. It has been presented by the following code.

```
#include "udf.h"
DEFINE_PROPERTY(user_power_law,c,t)
{
real visc_dyn_min=0.00345;
real visc_dyn_max=0.0364;
real index_n=1.45;
real k=2.63;
real mu_app;
real mu_temp;
mu_temp=0.00345+(0.0364-
0.00345)*pow((1+pow((C_STRAIN_RATE_MAG(c,t)/2.63),index_n)),-1);
/*if (N_ITER<1)
```

```
mu_app=k;

if ((mu_temp > visc_dyn_min) && (mu_temp < visc_dyn_max))

mu_app=mu_temp;

else if ((mu_temp >= visc_dyn_max))

mu_app=visc_dyn_max;

else if ((mu_temp <= visc_dyn_min))

mu_app=visc_dyn_min;

return mu_app;*/

return mu_temp;

}

/* DEFINE_PROFILE(inlet_x_velocity, thread, position)

{

real x[ND_ND];

real y, h, z, u, v;

face_t f;

real t = CURRENT_TIME;

h = 0.003;
```

```
begin_f_loop(f,thread)
{
F_CENTROID(x, f, thread);
y = x[0];
z = x[1];
u = 0.38888 + 0.27777 * sin ( 7.662421106 * t);
v = 12 * u * ( h / ( sqrt ( y * y + z * z ) ) );
F_PROFILE(f, thread, position) = v * ( 1 - ( y * y + z * z ) / ( h * h ) );
}
end_f_loop(f, thread)
}
DEFINE_PROFILE(outlet_pressure, thread, position)
{
real x[ND_ND];
real y, h, z, p;
face_t f;
real t = CURRENT_TIME;
```

```
h = 0.003;

begin_f_loop(f,thread)

{

F_CENTROID(x, f, thread);

y = x[0];

z = x[1];

p = 13332.2368 + 2666.44737 * sin ( 7.662421106 *t);

F_PROFILE(f, thread, position) = p;

}

end_f_loop(f, thread)

}*/

DEFINE_PROFILE(inlet_x_axial_velocity, thread, position)

{

real x[ND_ND];

real y, h, z, u;

face_t f;

real t = CURRENT_TIME;
```

```
h = 0.003;
begin_f_loop(f,thread)
{
F_CENTROID(x, f, thread);
y = x[0];
z = x[1];
u=(1- 0.2264*cos(7.66*t)+0.591*sin(7.66*t)-
0.6183*cos(2*7.66*t)+0.07234*sin(2*7.66*t)
+0.04647*cos(3*7.66*t)-0.4058*sin(3*7.66*t)+0.1555*cos(4*7.66*t)-
0.1639*sin(4*7.66*t)
+0.2239*cos(5*7.66*t)+0.1471*sin(5*7.66*t)-
0.1041*cos(6*7.66*t)+0.1149*sin(6*7.66*t)
-0.03886*cos(7*7.66*t)+0.01257*sin(7*7.66*t)-0.06137*cos(8*7.66*t)-
0.04677*sin(8*7.66*t)
+0.05177*cos(9*7.66*t)-
0.03975*sin(9*7.66*t)+0.0136*cos(10*7.66*t)+0.0109*sin(10*7.66*t)
+0.03434*cos(11*7.66*t)+0.02011*sin(11*7.66*t)-
0.02045*cos(12*7.66*t)+0.03278*sin(12*7.66*t)
```

```
-0.01162*cos(13*7.66*t)+0.002044*sin(13*7.66*t)-0.01869*cos(14*7.66*t)-
0.001022*sin(14*7.66*t)
+0.0009446*cos(15*7.66*t)-
0.01793*sin(15*7.66*t)+0.009188*cos(16*7.66*t)+0.001358*sin(16*7.66*t))/6;
F_PROFILE(f, thread, position) = u * ( 1 - ( y * y + z * z ) / ( h * h ) );
}
end_f_loop(f, thread)
}
DEFINE_PROFILE(inlet_x_tangetial_velocity, thread, position)
{
real x[ND_ND];
real y, h, z, u;
face_t f;
real t = CURRENT_TIME;
h = 0.003;
begin_f_loop(f,thread)
{
```

```
F_CENTROID(x, f, thread);

y = x[0];

z = x[1];

u=(1- 0.2264*cos(7.66*t)+0.591*sin(7.66*t)-
0.6183*cos(2*7.66*t)+0.07234*sin(2*7.66*t)+0.04647*cos(3*7.66*t)-
0.4058*sin(3*7.66*t)+0.1555*cos(4*7.66*t)-
0.1639*sin(4*7.66*t)+0.2239*cos(5*7.66*t)+0.1471*sin(5*7.66*t)-
0.1041*cos(6*7.66*t)+0.1149*sin(6*7.66*t)-
0.03886*cos(7*7.66*t)+0.01257*sin(7*7.66*t)-0.06137*cos(8*7.66*t)-
0.04677*sin(8*7.66*t)+0.05177*cos(9*7.66*t)-
0.03975*sin(9*7.66*t)+0.0136*cos(10*7.66*t)+0.0109*sin(10*7.66*t)+0.03434*c
os(11*7.66*t)+0.02011*sin(11*7.66*t)-
0.02045*cos(12*7.66*t)+0.03278*sin(12*7.66*t)-
0.01162*cos(13*7.66*t)+0.002044*sin(13*7.66*t)-0.01869*cos(14*7.66*t)-
0.001022*sin(14*7.66*t)+0.0009446*cos(15*7.66*t)-
0.01793*sin(15*7.66*t)+0.009188*cos(16*7.66*t)+0.001358*sin(16*7.66*t))/6;

F_PROFILE(f, thread, position) = u * 0.5 * 0.0 *  pow(( y * y + z * z ),0.5)/h;

}

end_f_loop(f, thread)
```

```
}

DEFINE_PROFILE(outlet_pressure, thread, position)

{

real x[ND_ND];

real y, h, z, p;

face_t f;

real t = CURRENT_TIME;

h = 0.003;

begin_f_loop(f,thread)

{

F_CENTROID(x, f, thread);

y = x[0];

z = x[1];

p = (90+(-0.2264*cos(7.66*t)+0.591*sin(7.66*t)-

0.6183*cos(2*7.66*t)+0.07234*sin(2*7.66*t) +0.04647*cos(3*7.66*t)-

0.4058*sin(3*7.66*t)+0.1555*cos(4*7.66*t)-0.1639*sin(4*7.66*t)

+0.2239*cos(5*7.66*t)+0.1471*sin(5*7.66*t)-

0.1041*cos(6*7.66*t)+0.1149*sin(6*7.66*t)-
```

```
0.03886*cos(7*7.66*t)+0.01257*sin(7*7.66*t)-0.06137*cos(8*7.66*t)-
0.04677*sin(8*7.66*t) +0.05177*cos(9*7.66*t)-
0.03975*sin(9*7.66*t)+0.0136*cos(10*7.66*t)+0.0109*sin(10*7.66*t)+0.03434*c
os(11*7.66*t)+0.02011*sin(11*7.66*t)-
0.02045*cos(12*7.66*t)+0.03278*sin(12*7.66*t)-
0.01162*cos(13*7.66*t)+0.002044*sin(13*7.66*t)-0.01869*cos(14*7.66*t)-
0.001022*sin(14*7.66*t) +0.0009446*cos(15*7.66*t)-
0.01793*sin(15*7.66*t)+0.009188*cos(16*7.66*t)+0.001358*sin(16*7.66*t))*14)
*133.322;
F_PROFILE(f, thread, position) = p;
}
end_f_loop(f, thread)
}
```